The Influence of Test Conditions on the Results of Pedestrian Headform Impact Tests

Daniel Jeffrey Searson

Centre for Automotive Safety Research
University of Adelaide

April 2012

Contents

Abstract

Pedestrian headform impact tests are used to assess the relative level of danger that a vehicle poses to the head of a struck pedestrian. The tests are conducted using a dummy headform that is launched at specific locations on the front of a stationary vehicle. The conditions of the test are specified in the relevant test protocol, and include the mass of the headform, the impact speed, and the impact angle. There are test protocols for vehicle design regulations and for new car assessment programs, each of which may specify different test conditions.

Previous studies have not examined in detail the influence of the test conditions on the result of the test, as measured via the Head Injury Criterion (HIC). HIC is proportional to the duration and magnitude of the acceleration of the headform during the impact. In this thesis, a theoretical model of a linear spring is used to examine, in the simplest case, the influence that headform mass and impact speed have on HIC and peak dynamic displacement.

These relationships were also studied empirically using real test data. The empirical effect of impact speed on HIC was found to be similar to that predicted by the linear spring model, and the influence of headform mass was found to be slightly weaker than what was predicted theoretically. An effect of headform diameter was also found in the test data. In summary: HIC was found to increase with impact speed, and was found to decrease with increasing headform mass and diameter. Increasing the impact speed, headform mass or diameter resulted in higher peak displacements, leading to a higher likelihood of contact with harder structures beneath the outer vehicle surface.

These relationships were used to predict the compliance of sixty vehicles with the Global Technical Regulation on pedestrian safety, based on their results under the European New Car Assessment Program pedestrian testing protocol. The relationship between HIC and impact speed was also used to compare the performance of theoretical structures that meet different test criteria, across a published distribution of real crash speeds. An injury risk function for HIC was used to demonstrate how test performance at a single crash speed can be related to an overall real world injury risk.

The results presented in this thesis show that HIC and peak displacement can be extrapolated or interpolated from a single test to apply to a wider range of test conditions. This methodology, in its simplest application, can be used to predict how a tested structure performs under different test protocols. A more complex application of this methodology might be a new method for assessing vehicle performance, based on its performance across the full range of conditions encountered in real world pedestrian crashes.

Statement of originality

This work contains no material which has been accepted for the award of any other degree or diploma in any university or other tertiary institution to Daniel Searson and, to the best of my knowledge and belief, contains no material previously published or written by another person, except where due reference has been made in the text.

I give consent to this copy of my thesis when deposited in the University Library, being made available for loan and photocopying, subject to the provisions of the Copyright Act 1968.

The author acknowledges that copyright of published works contained within this thesis (as listed below) resides with the copyright holder(s) of those works.

I also give permission for the digital version of my thesis to be made available on the web, via the University's digital research repository, the Library catalogue, the Australasian Digital Theses Program (ADTP) and also through web search engines, unless permission has been granted by the University to restrict access for a period of time.

Daniel Searson

List of publications

- Searson, D. and Anderson, R. (2008). Pedestrian impact testing: modelling the effect of head-form mass and speed. In *Proceedings of the 2008 Australasian Road Safety Research, Policing and Education Conference*, Adelaide, Australia. Department for Transport, Energy and Infrastructure.

- Searson, D. and Anderson, R. (2009). Predicting vehicle performance under the Global Technical Regulation on pedestrian protection using ANCAP test results. In *Proceedings of the 2009 Australasian Road Safety Research, Policing and Education Conference*, Sydney, Australia. Road Traffic Authority of New South Wales.

- Searson, D., Anderson, R., Ponte, G., and van den Berg, A. (2009). Headform impact test performance of vehicles under the GTR on pedestrian safety. CASR Report CASR072, Centre for Automotive Safety Research, University of Adelaide, Adelaide, Australia.

- Searson, D. and Anderson, R. (2010). Implications of easing head impact criteria in pedestrian crash standards. CASR Report CASR083, Centre for Automotive Safety Research, University of Adelaide, Adelaide, Australia.

- Searson, D. and Anderson, R. (2011). The Global Technical Regulation on pedestrian safety: Likely effects on vehicle design. In *Proceedings of the 2011 Australasian Road Safety Research, Policing and Education Conference*, Perth Australia. Government of Western Australia.

Acknowledgements

First and foremost I would like to thank my two supervisors, Robert Anderson and Paul Hutchinson. Their guidance and expertise has been invaluable.

Several organisations have contributed financial or inkind support to this project, and I thank them for their support and for supporting pedestrian safety research. These organisations include the Australian Department for Infrastructure and Transport, the Australasian New Car Assessment Program (ANCAP), Toyota Motor Corporation, General Motors Holden and Hyundai Motors Australia.

I would like to thank my colleagues at the Centre for Automotive Safety Research for making it a great place to work and study. In particular I would like to thank Andrew van den Berg and Giulio Ponte from the impact laboratory and Jaime Royals, the CASR librarian. I would also like to thank fellow student Jeffrey Dutschke for many productive (and unproductive) discussions.

Finally I would like to thank my friends and family, who will probably be greatly surprised to hear that this is all done.

Chapter 1

Introduction

Pedestrian impact testing is a means of assessing the relative level of danger posed by a particular vehicle model to a pedestrian in the event of a collision. To understand how and why this testing is conducted, consider the unfortunate event of a pedestrian being struck by a typical passenger vehicle. In such a collision, the pedestrian can be best described as being 'run under'. The legs of the pedestrian are swept out from under them, and the head is flung downwards, typically being struck by either the bonnet or the windscreen of the vehicle. The resulting head impact may have consequences ranging from minor injury to death.

With appropriate vehicle design, the level of injury sustained by the pedestrian in such a collision can be reduced. A typical approach might be to reduce the structural stiffness of the vehicle surface, while ensuring that there is sufficient free space beneath the surface for it to deform and absorb the energy of the impact, without coming into contact with a harder structure underneath.

Different vehicles, and different areas on a vehicle's front surface, may be more or less dangerous to a pedestrian in the event of a collision and this can assessed by measuring their performance in pedestrian impact tests. Pedestrian impact testing is used to rank a vehicle's overall performance against others, or to mandate a minimum level of performance that must be met before the vehicle is able to be sold. The tests are also used as part of research that attempts to reconstruct real pedestrian crashes.

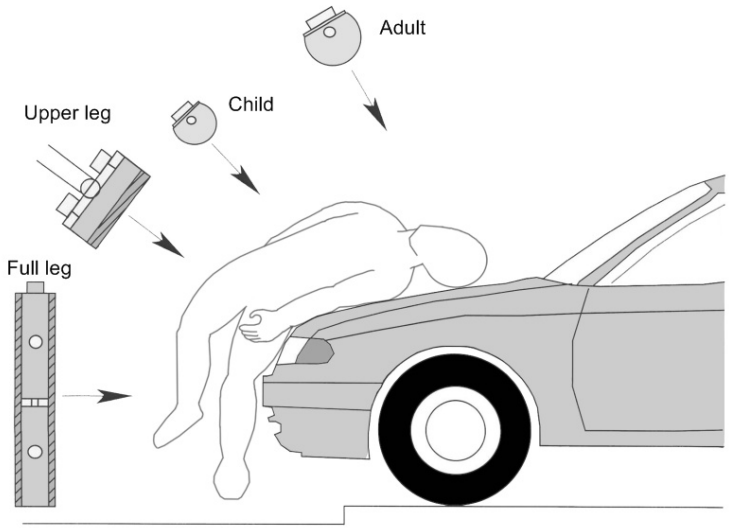

Figure 1.1: Pedestrian subsystem impactors and their relation to a struck pedestrian.

Pedestrian impact testing is conducted using 'subsystem' impactors, each of which represents a different part of the pedestrian's body. The subsystem impactors include a full legform that strikes the bumper of the vehicle, an upper legform that strikes the leading edge of the vehicle, a child sized headform that strikes the front area of the bonnet surface, and an adult sized headfrom that strikes the rear area of the bonnet and lower area of the windscreen (see Figure 1.1). Each of these impactors is equipped with different sensors that are used to measure the severity of the impact.

The focus of this thesis is on the headform impact tests. In these tests, the acceleration of the head is measured and is used to calculate the Head Injury Criterion, or HIC, which is a measure of the relative risk of head injury in a particular impact. A HIC below 1000 is generally considered 'safe'. The headform mass, impact angle and impact speed may vary, and these values are specified as part of the written protocol for the testing being conducted.

Each of these test conditions will have some effect on the severity of the impact. For example, it is reasonable to expect that the impact would be more severe for higher speeds. Conversely, the impact severity would be expected to decrease with increasing headform mass; for a higher mass, the

headform would experience less acceleration and would thus score a lower HIC value. In the case of impact angle, the closer that the angle is towards being perpendicular to the vehicle surface, the greater the expected severity of the impact. The selection of test conditions also has implications for the possiblity of 'bottoming out' occurring, in which the outer surface of the vehicle deforms sufficiently that it comes into contact with a much harder structure beneath.

During the past 20 years, various pedestrian impact testing protocols have been developed to measure the relative level of safety of a vehicle. The test conditions for the headform tests have differed between protocols. For example, test protocols have included impact speeds of 30, 32, 35 or 40 km/h, and the range of headforms used have included masses of 2.5, 3.5, 4.5 and 4.8 kg. The selection of test conditions has generally been based on an attempt to replicate the conditions of a real crash, along with some consideration of how feasible it is for a vehicle to pass the test.

This variation in test conditions has implications for interpreting the results of a pedestrian headform test. A HIC value obtained under one set of test conditions cannot be immediately compared with that obtained under another set of conditions. For example, a vehicle surface rated as 'safe' at 35 km/h by one test may not necessarily be considered 'safe' based on another protocol with a test speed of 40 km/h.

This leads to several questions: What effect does the difference in test conditions have on the measured severity of a particular test location? What implications does this have for the performance of an entire vehicle? What are the effects on real-world safety? These are the questions that this thesis sets out to answer.

Chapter 2 begins with a brief history of how existing pedestrian testing protocols were developed, and how the test conditions in those protocols were selected. Three pedestrian headform testing protocols are described in detail due to their relevance in Australia. Finally, a review is given of previous studies that have somehow quantified the effect of headform test conditions on HIC.

Chapter 3 examines two theoretical models that can be used to predict the influence of test conditions on HIC and peak dynamic displacement. The

first model is of a simple linear spring, and the second is a more complex model based on Hertz contact theory, with a damping component.

Chapter 4 describes how the headform test data were obtained for later chapters. The experimental setup and headform testing process is explained, along with a method of estimating peak displacement from the acceleration measurements. A summary is given of the datasets used for later chapters.

Chapter 5 compares the theoretical models to the empirical data, using a regression analysis. The results presented in this chapter are used as a basis for predicting the change in HIC and peak displacement under two different sets of test conditions.

Chapter 6 examines two specific test protocols: the European New Car Assessment Program (Euro NCAP) pedestrian testing protocol and the Global Technical Regulation (GTR) on pedestrian safety. The results from the previous chapter, as well as further test data, are used to predict the differences in HIC for tests conducted under these two protocols.

Chapter 7 continues the comparison of the Euro NCAP and GTR protocols, but for overall vehicle performance. Existing results from tests performed under the Euro NCAP protocol are used to estimate vehicle compliance with the GTR, for sixty cars tested in Australia.

Chapter 8 is focused on the selection of impact speed in pedestrian testing protocols. A comparison of different test protocols is made in the context of a real world pedestrian crash speed distribution. The results of this chapter illustrate the strong effect of speed on impact severity, and demonstrate a method for comparing the severity of test protocols in terms of real world injury.

Chapter 9 provides a summary and discussion of the results, and suggestions for future work.

Chapter 2

Background

Pedestrian impact testing has a history dating back to the 1960s, and the current test protocols have been under development for the last two decades. The first section of this chapter gives a brief history of the development of pedestrian impact testing and the evolution of the current test protocols.

In the second section, three pedestrian testing protocols are described in detail. These protocols are those that are relevant to Australia, the first two of which are also arguably the most important in an international context.

The third section is an examination of existing literature that relates to the influence of test conditions on the results of pedestrian headform tests. While there exists a great number of studies related to pedestrian testing, there are few studies that have directly investigated the effect of the test conditions on test outcomes.

The final section of this chapter contains a summary of the background information, and describes the research goals of the thesis.

2.1 Brief history of pedestrian testing protocols and regulations

Pedestrian impact testing has only been conducted regularly for the last decade or so, but has a history that dates back almost fifty years.

In the 1960s, the role of vehicle design in the safety of pedestrians became apparent. Ryan and McLean (1965) described the typical pedestrian

accident as a process of being 'run under' rather than 'run over', which at the time was a relatively new notion. The authors also suggested that the design of a vehicle could affect the severity of injury experienced by the pedestrian. According to McLean (2005), the commonly held view at the time was that "the typical impact was too great to be modified by any practicable change in vehicle design". Around the same time, the first pedestrian impact tests took place using instrumented dummies, which also demonstrated the typical sequence of events in a pedestrian crash (Severy, 1963; Severy and Brink, 1966). This sort of testing continued in the 1970s. Harris (1976) performed testing using adult and child dummies, and discussed the aspects of vehicle design that needed to be modified for pedestrian protection, including "matching the collapse characteristics of the front of the car to the appropriate human tolerance loads".

The European Experimental Vehicle Committee (EEVC) started an ad hoc working group in 1980 to examine how vehicle design was related to pedestrian safety in European countries. The EEVC is an organisation that was started to facilitate collaboration on vehicle safety research[1]. The first EEVC pedestrian safety working group was later referred to as 'Working Group 7' (EEVC, 1985). In the first report of this working group (EEVC, 1982), it was noted that the 50th percentile of impact speeds for pedestrian crashes was somewhere in the range of 16–36 km/h and that the 90th percentile was in the range of 44–58 km/h. This was based on a sample of pedestrian crash data from European countries. This suggested testing to represent an impact speed of around 40 km/h would cover more than 50% of crash speeds.

In 1988, a new working group known as 'Working Group 10' (WG10) was established by the EEVC to develop a method for testing passenger cars for pedestrian protection. This method was specified as a series of subsystem tests to the bumper, the bonnet leading edge and the bonnet top (Harris, 1989). The EEVC test procedures developed by WG10 were used as the basis for the first Euro NCAP pedestrian tests, and the subsystem tests designed by WG10 have generally formed the basis of the other test protocols discussed in this section. Subsystem tests are limited in that they

[1]EEVC website: http://www.eevc.org

do not replicate all of the forces on each body part, for example there is no force on the test headform that replicates the force that would be exerted by the neck. However, the main advantages of the subsystem tests are the ability to precisely fire each body part at the most injurious locations on the vehicle, as well as the lower cost and reduced validation requirements (Simms and Wood, 2009, Chapter 6).

A head impact speed of 40 km/h was selected by WG10 as it covered a significant range of pedestrian crash speeds (based on the findings of WG7) and it was also a speed that was seen to be practical to design for (Lawrence and Hardy, 1998).

The headforms proposed by WG10 were 2.5 kg and 4.8 kg and were chosen to represent a six-year-old child and an adult pedestrian (Lawrence et al., 2006). These masses were meant to represent the 'effective mass' of the head while striking the bonnet, which is the headform mass that best represents the mass of the head in a collision with a pedestrian, including an allowance for the rest of the body via a force acting through the neck. If this neck force is tensile, then the effective mass is lower than the static, or cut-off, mass of the head. The opposite is true if the force through the neck is compressive. Different methods have been proposed to calculate the effective mass, either by averaging the force on the head divided by its acceleration (Mizuno, 2003) or by energy equivalence (Janssen and Nieboer, 1990). Glaeser (1991, Table 4) contains a summary of the headform masses and effective mass estimates from various studies conducted prior to WG10. This summary shows a range of cadaver head masses from 3.5 to 5.3 kg, and headform masses from 4.4 to 7.1 kg. The results of computer simulations conducted by Janssen and Nieboer (1990) are consistent with the masses used by EEVC WG10 and show an effective mass of around 2.5 kg for a six year old child, around 3.5 kg for a 5th percentile female, and around 4.5 to 5.5 kg for a 50th percentile male depending on the geometry of the front of the vehicle.

The severity measurement specified in the protocol developed by WG10 was the Head Injury Criterion, or HIC. The HIC was developed by Versace (1971), and is based on the acceleration experienced by the headform during the impact. The formula for calculating HIC from the recorded head

acceleration $a(t)$ is:

$$\text{HIC} = max \left[(t_2 - t_1) \left(\frac{\int_{t_1}^{t_2} a(t)\,\mathrm{d}t}{(t_2 - t_1)} \right)^{2.5} \right] \tag{2.1}$$

The values of t_1 and t_2 are chosen to maximise the value inside the square brackets. Every pedestrian protocol discussed in the remainder of this section has also used HIC as the measurement of the risk of head injury. Alternatives to HIC exist (Marjoux et al., 2008), but have not been taken up in pedestrian testing protocols.

The use of HIC has limitations and has been criticised, most notably by Newman (1980). Among Newman's criticisms are that headform kinematics alone are a poor predictor of injury and that there is little correlation between measured head injury severity and HIC. Another limitation of measuring HIC with a solid headform is that it does not distinguish between contact with a flat surface or a sharp surface if the measured acceleration is the same. In reality, the sharp surface will be more prone to causing skull fracture or puncture wounds (Melvin and Evans, 1971).

Despite these criticisms and limitations, later studies have shown a positive correlation between HIC and real world injury risk (Anderson et al., 2003; Pellman et al., 2003), and the relationship between HIC and real world injury risk has been examined in studies published after Newman (1980). The relationship between HIC and Mild Traumatic Brain Injury (MTBI) has been investigated by equipping American Football player's helmets with accelerometers (Funk et al., 2007). The resulting injury risk curve suggested a 100% risk of MTBI at a HIC of 1000, and as such is of limited applicability to pedestrian impacts, in which HIC values routinely exceed 1000 and the emphasis is on preventing more severe head injuries. A similar curve for the risk of concussion with HIC was presented by Newman et al. (2000), but this suffers from the same limitations as the MTBI curve published by Funk et al..

Marjoux et al. (2008) derived HIC injury risk curves from a combination of 12 motorcycle accidents, 22 football player impacts and 27 pedestrian accidents that were all reconstructed using Hybrid III dummy heads. The

resulting curves showed the risk of four different types of injury: moderate and severe neurological injuries, subdural haematoma and skull fracture. At a HIC of 1000, the risk of moderate neurological injury and skull fracture was 100%, with an approximate 50% risk of severe neurological injury and 5% risk of subdural haematoma. At a HIC of 2000, the risk of all four types of injury was virtually 100%.

The present industry standard for more severe impacts is based on the work of Prasad and Mertz (1985), who used cadaver test data from three separate studies to predict the relationship between HIC and AIS 4+ head injury risk, as well as HIC and skull fracture risk. The resulting risk curves are the most frequently referenced today and imply an AIS 4+ head injury risk of 16% for a HIC of 1000. The skull fracture risk curve derived by Prasad and Mertz is very close to the AIS 4+ curve, and predicts a much lower risk of skull fracture than what was later shown by Marjoux et al. (2008). The Prasad and Mertz curves were also extended to other AIS levels by the National Highway Traffic Safety Administration (NHTSA, 1995).

Around the same time that EEVC WG10 were developing a pedestrian testing protocol, a similar working group was formed by the International Standards Organisation (ISO) Technical Committee on Road Vehicles. The ISO working group was tasked with developing a similar test method for assessing the front end of passenger cars for their relative risk towards a struck pedestrian, and met for the first time in 1988. The ISO working group had similar membership to the EEVC working groups and thus arrived at similar recommendations (McLean, 2005).

One key difference between the ISO and EEVC procedures was that the ISO headforms were both 165 mm diameter and had masses of 4.5 kg and 3.5 kg for the adult and child, respectively. The mass of these headforms were also meant to represent effective mass, but computer simulations performed by ISO indicated that the effective mass was equal to the static mass (Mizuno and Ishikawa, 2001).

The ISO working group was superseded by a pedestrian safety working group formed under the International Harmonized Research Activities (IHRA) program, in 1996. The IHRA working group developed test procedures that were also similar to the EEVC procedures but using the ISO

headforms. One notable feature of the IHRA test procedures was that the test speed and impact angle would vary based on the shape of the vehicle (Mizuno, 2003). Simulations performed by IHRA showed that for a vehicle crash speed of 40 km/h, the bonnet top of a sedan would strike a child head at 30.0 ± 4.0 km/h and an adult head at 30.4 ± 7.2 km/h (Mizuno, 2003).

The reasons for the variation in head impact speed with car shape and pedestrian size are complex. When the vehicle strikes the legs of the pedestrian, the body of the pedestrian is accelerated and the head begins to move downwards towards the bonnet or windscreen. The interaction between the vehicle bumper and the body, the height of the bonnet, the lead of the bonnet and the length of the bonnet will all play a part in determining the final head impact speed (Simms and Wood, 2009, Chapter 10). The results presented by Mizuno (2003) suggest that contact with the windscreen results in higher normal (perpendicular to surface) head impact speeds than contact with the bonnet. The results also suggest that adults struck by SUVs experience slightly higher normal head impact speeds than sedans, and that adults struck by vans result in speeds that are slightly lower. This result for SUVs was confirmed in a later study by Anderson and Doecke (2011), but it was shown that despite the lower normal impact speed the SUVs caused more severe impacts. For children, Mizuno's results suggest that the normal head impact speeds are much closer across vehicle types, but sedans resulted in slightly higher impact speeds. These results illustrate the complexity of modelling head impact speeds and support the methodology that was proposed by IHRA, but such a system was never adopted in working protocols.

In 1997, 'Working Group 17' (WG17) was formed by the EEVC. The goals of WG17 were to review the WG10 test methods and propose changes based on new research (EEVC, 1998). There were no major changes to the headform test conditions brought about by WG17, however there were changes made to the material of the headform skin, the certification procedure, and the testing zone definition. The headform test speed remained at 40 km/h and the headform masses remained the same as they were under the original WG10 protocol.

A study performed under WG10 showed that for a vehicle impact speed

of 40 km/h, the head impact speed could vary from 32 km/h for a 5th percentile adult female, to 55 km/h for a 50th percentile adult male and 60 km/h for a 95th percentile adult male. Other work performed by WG17 confirmed that the head impact speed may be higher or lower than the vehicle impact speed, depending on the pedestrian's size and the shape of the vehicle. The end conclusion of WG17 was that the test speed should remain at 40 km/h, for simplicity and feasibility (Lawrence et al., 2006).

The EEVC test procedures were implemented as part of the European New Car Assessment Programme (Euro NCAP) pedestrian testing procedure. Euro NCAP is an organisation that performs crash testing of vehicles for consumer information purposes, typically through assigning each vehicle a star rating for its relative level of safety. Euro NCAP pedestrian testing was based on the EEVC test procedure and began in the late 1990s (Hobbs and McDonough, 1998; Lawrence and Hardy, 1998). This test protocol was also adopted by the Australian New Car Assessment Program (ANCAP), and testing began in Australia in 2000. The Euro NCAP pedestrian testing protocol is discussed in greater detail in Section 2.2.1.

The testing conducted by Euro NCAP and ANCAP is not mandatory, and poor performance does not stop the vehicle from being sold. However, compulsory vehicle design regulation for Europe was planned in two phases beginning in the mid-2000s. Phase 1 was introduced in October 2005. In order to pass the Phase 1 regulations, vehicles had to undergo a test procedure similar to that used by Euro NCAP but with different test conditions. The Phase 1 test was conducted at 35 km/h using a 3.5 kg headform and testing only the bonnet top. The HIC limit was 1000 for at least two thirds of the bonnet test area, and 2000 for up to one third of the bonnet test area. Phase 2 was originally planned to be introduced in 2010, and the original form of Phase 2 was based on the test methods developed by EEVC. That is, the headforms used were 2.5 kg and 4.8 kg, with a test speed of 40 km/h and a HIC limit of 1000 for all test locations. However, with the development of the Global Technical Regulation (GTR) on pedestrian safety (discussed shortly), the originally planned Phase 2 of the European regulation was not adopted in 2010. Instead, the European regulation was harmonised with the GTR test procedure (European Parliament, 2009).

At around the same time as the introduction of Phase 1 of the European regulations, a standard for vehicle designs in Japan also came into effect, starting in September 2005 and applicable to all new car designs. This standard was designed by the Japan Ministry of Land, Infrastructure and Transport (MLIT) and was called the 'Technical Standard for Protection of Heads of Pedestrians' (MLIT, 2004). The MLIT standard was based on the test method proposed by IHRA, using the ISO headforms of 3.5 kg and 4.5 kg. The test speed in the Japanese standard was 32 km/h, with the impact angle dependent on the shape of the front of the car. The lower impact speed was based on taking the average value of head impact speeds from simulations performed with a crash speed of 40 km/h (Lawrence et al., 2006). According to Lawrence et al. (2006), this average was skewed by the presence of some very low velocities, and the test speed of 32 km/h would represent less than 50% of accidents.

As mentioned, a more recent development in pedestrian safety testing is the development of a Global Technical Regulation (GTR) on pedestrian safety. The GTR was developed by an informal working group on pedestrian safety under the Working Party on Passive Safety in the United Nations Economic Commission for Europe (UNECE). Global Technical Regulations developed by the UNECE are developed under the so-called '1998 Agreement', which compels member countries to consider harmonising their vehicle design regulations with GTRs (UNECE, 1998). The GTR on pedestrian safety is also known as GTR number 9 and for the remainder of this thesis will generally be referred to as simply the GTR.

The GTR test procedures began development in 2002, and were finalised in 2009. The headforms used in the GTR are those developed by ISO, with adult and child masses of 4.5 kg and 3.5 kg, respectively. The GTR was designed for a vehicle impact speed of 40 km/h, but the working group eventually adopted a lower headform test speed of 35 km/h. The lower speed was justified on the basis of the IHRA simulations that suggested a ratio of head impact speed to vehicle impact speed of 0.8 (UNECE, 2003). The ratio of 0.8 would imply a head impact speed of 32 km/h to represent a vehicle impact speed of 40 km/h, and this was the speed proposed in the 2004 working draft of the GTR (UNECE, 2004). However, in 2005, the

speed was agreed upon as 35 km/h in order to harmonise with the European regulations that were being adopted that year (UNECE, 2005).

In late 2010, Vehicle Safety Standards Australia issued a Regulation Impact Statement on the adoption of the GTR as an Australian Design Rule (ADR). However, the statement was later retracted for reasons connected with bull bars (King, 2011).

The details of the Euro NCAP/ANCAP protocol and the GTR testing protocol are given in greater detail in the next section. These are the two test protocols of most relevance for passenger vehicles in Australia.

2.2 Current pedestrian testing protocols of relevance in Australia

Headform testing is currently used as part of three pedestrian testing protocols that have relevance in Australia. The first of these is the Euro NCAP protocol, which is used by the Australasian New Car Assessment Program (ANCAP), the second is the Global Technical Regulation (GTR) on pedestrian safety, and the third is the Australian Standard for bull bars, AS 4876.1 'Motor vehicle frontal protection systems'.

2.2.1 Euro NCAP protocol

For the last 10 years, the Australasian New Car Assessment Program (ANCAP) have conducted pedestrian impact testing on selected new vehicles. The test protocol used by ANCAP is the same as that used by the European New Car Assessment Programme (Euro NCAP, 2009). The protocol includes sub-system tests using a full-length legform, an upper legform, and adult and child headforms.

The headform testing component of the Euro NCAP protocol focuses on the areas of the vehicle that are most likely to strike a pedestrian's head – that is, the bonnet and windscreen. All tests are performed at 11.1 m/s (40 km/h), with either a child headform or the heavier adult headform. Whether a child or adult headform is used depends on the wrap around distance (WAD) measurement to the location being tested. The WAD is

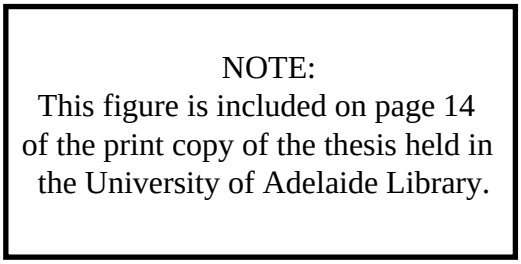

Figure 2.1: Wrap around distance (WAD) measurement (Euro NCAP, 2009).

the distance measured from the ground in front of the vehicle, along the vehicle surface, to the location in question (Figure 2.1).

In 2010, Euro NCAP released and adopted Version 5 of the pedestrian testing protocol (Euro NCAP, 2009), which differs significantly from Version 4 (Euro NCAP, 2008). ANCAP also began conducting pedestrian testing under the new Version 5 protocol in 2010. Under Version 4, the EEVC headforms are used: the child headform had a mass of 2.5 kg and a diameter of 130 mm, and the adult headform had a mass of 4.8 kg and a diameter of 165 mm. Under the newer Version 5 protocol, the ISO headforms are used: both headforms have a diameter of 165 mm, the child headform is heavier with a mass of 3.5 kg and the adult headform is slightly lighter with a mass of 4.5 kg. The majority of the work in this thesis refers to Version 4 of the protocol, as it was the effective protocol while the research was being conducted. Version 3 of the protocol was similar to Version 4, and their results can be compared with one another. A greater volume of ANCAP test results presently exist for Versions 3 and 4 than for Version 5.

Under both Versions 4 and 5 of the protocol, the child headform is used for WADs between 1000 mm and 1500 mm, and is fired at an angle of 50° to

the ground. The adult headform is generally used for WADs between 1500 mm and 2100 mm, and is fired at an angle of 65° to the ground. However, under the newer Version 5 protocol, in the WAD range of 1500 mm to 1700 mm, any tests on the bonnet top are performed using the child headform instead of the adult headform. Tests in this range that are on the windscreen are still conducted with the adult headform.

Prior to 2010, ANCAP awarded each vehicle a pedestrian star rating (separate to the occupant star rating), between zero and four stars. From 2010, ANCAP award the vehicle a worded rating, with 'Poor' corresponding to one star, 'Marginal' to two stars, 'Acceptable' to three stars, and 'Good' to four stars. The star and word ratings are based on a points system, with a maximum of 36 points available, 24 of which are from the headform testing component of the test program. The HIC obtained from each child or adult headform test is used to determine how many points are awarded for that test location. The system for deciding how many points are available for each location is somewhat complicated, and is described below.

The child and adult test areas are each split into six numbered zones across the width of the test area. Each zone is then split into four smaller subzones, lettered A to D (see Figure 2.2). Within each zone, ANCAP (or Euro NCAP) selects what is thought to be the most potentially harmful test location. The vehicle manufacturer is then given the option to nominate one or more of the subzones, except that which contains the ANCAP nominated location, for an additional test. ANCAP (or Euro NCAP) then selects the worst location in the nominated subzones. For example: if the most harmful location is chosen in subzone A, the manufacturer might choose subzones C and D for an additional test. One extra test location is then selected, in either subzone C or D. The advantage for the manufacturer is that the new location in subzone C or D would be expected to perform better than the location in subzone A, hence scoring more points towards the star rating of the vehicle.

Each zone is worth a maximum of two points, which contribute toward the star rating of the vehicle. If the manufacturer does not nominate an additional test, then the original test location counts for the maximum two points. Otherwise, the two points available are shared between the two

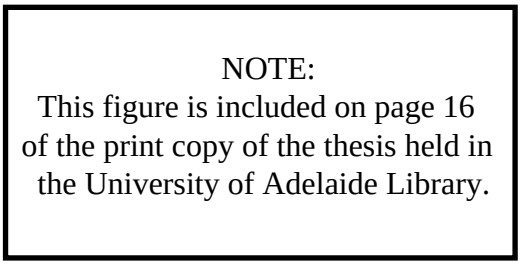

Figure 2.2: Euro NCAP/ANCAP zone divisions (Euro NCAP, 2009).

test locations depending on how many subzones the manufacturer has nominated. Each subzone nominated by the manufacturer counts for up to half a point. For example: if the manufacturer has only nominated one subzone, then the manufacturer's test location counts for a maximum of 0.5 points, and the original for a maximum of 1.5. If two subzones are nominated then there is one point available for each location. If three subzones are nominated, then there are 1.5 points available to the manufacturer location and 0.5 available for the original.

The proportion of the maximum points available that is scored by a particular location depends on the HIC obtained during the test. If the HIC at the test location is less than 1000, then the maximum points are awarded for that location. If the HIC exceeds 1350, then zero points are awarded. If the HIC is between 1000 and 1350 then the points score is linearly scaled – e.g. for a HIC of 1175, half of the maximum points are awarded.

2.2.2 Global Technical Regulation on pedestrian safety

A more recent development in pedestrian impact testing is the Global Technical Regulation (GTR) on pedestrian safety (UNECE, 2009), developed under the United Nations Economic Commission for Europe (UNECE). This regulation describes a series of tests, similar to those used by Euro NCAP, that are used to assess whether a vehicle meets an acceptable level of pedestrian protection prior to it being sold.

Under the GTR, headform testing is conducted in a similar manner to Euro NCAP testing, with some differences. The similarity is that both protocols use the same style of headform testing, and are focused on testing the worst, or most injurious, locations on the vehicle surface. The most significant difference is that the impact speed for GTR tests is 9.7 m/s, or 35 km/h. The GTR uses the ISO headforms, so the child headform mass is 3.5 kg, and the adult headform mass is 4.5 kg, as for Version 5 of the Euro NCAP testing protocol (Euro NCAP, 2009). Both headforms are 165mm in diameter.

The dividing line between the GTR child and adult headform test areas differs slightly to that used by ANCAP. Under the GTR, the child headform is used for all WAD values between 1000 mm and 1700 mm (instead of 1500 mm), and is fired at an angle of 50° to the ground. The adult headform is used for WAD values between 1700 mm and 2100 mm, and is fired at an angle of 65° to the ground. The GTR excludes the windscreen from any testing – the headform test area is bounded at the rear by the rear edge of the bonnet (or the WAD 2100 mm line, whichever comes first, which in practice is most likely to be the rear edge of the bonnet).

If the HIC obtained in a GTR test is less than 1000, that test location passes the requirements. However, the vehicle manufacturer may also nominate a 'relaxation' zone, in which the test HIC may be up to 1700 and still pass. The relaxation zone may be defined in any way, and may consist of several non-continuous sections. The GTR does not use a structured concept of zones and subzones in the way that Euro NCAP does, the area of the relaxation zone is measured by plotting on a computer. The relaxation zone may consist of up to 1/3 of the total test area, and may be no more

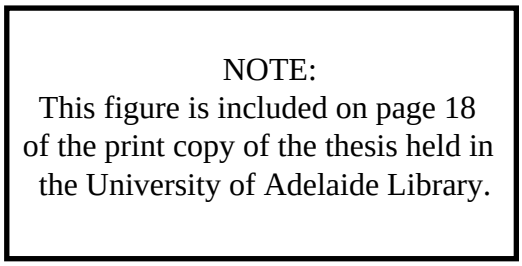

Figure 2.3: Example of the GTR relaxation zone (UNECE, 2009).

than 1/2 of the child test area. Figure 2.3 shows an example of relaxation zone selection.

2.2.3 AS 4876.1 Motor vehicle frontal protection systems (bull bars)

Finally, another pedestrian headform testing protocol of relevance in Australia is the test specified as part of Australian Standard 4876.1 'Motor Vehicle Frontal Protection Systems Part 1: Road User Protection' (Standards Australia, 2002). The standard specifies a single test, conducted with a 2.5 kg child headform. The test is conducted at what is judged to be the most potentially injurious location lying above a height of 1000 mm when the bull bar is mounted on a vehicle. The impact speed is 30 km/h, and the headform is fired horizontally into the bullbar. The standard requires that the HIC from the impact test is less than 1500.

At the time of writing, compliance with AS 4876.1 is not compulsory for bull bars sold in Australia. Failing to pass the standard does not prevent a bull bar from being sold.

2.3 Previous studies on the influence of test conditions

A variety of procedures have been developed for pedestrian impact testing. Each of the procedures are based on the similar concept of using a headform in free flight, fired into the bonnet and sometimes the windscreen of the vehicle. However, the test procedures differ in the specification of the test conditions: specifically the impact speed and headform mass, and in some cases the impact angle and headform diameter.

There would appear to be little existing published research that examines how the selection of test conditions affects the HIC in a pedestrian headform test. The selection of test conditions has, in the past, been based on biofidelity. That is, the tests have been designed to attempt to replicate the conditions of a real pedestrian accident. The selection of speed has been based on compromises between the feasibility of passing the tests and covering a substantial proportion of real crash speeds. However, no systematic consideration has been given to how the HIC may vary with test condition selection, and the implications for safety.

The following section examines previous published research which, directly or indirectly, considers the influence of impact speed on the results of a headform test. Following this is are similar discussions on the influence of impact angle and headform mass.

2.3.1 The effect of impact speed on HIC

As mentioned previously, it is reasonable to expect that HIC would increase with increasing impact speed. An increase in impact speed leads to an increase in headform energy prior to impact. In order to absorb this energy, longer duration and/or higher forces are required, which implies longer duration and/or higher accelerations. Since HIC is related to the magnitude and duration of the acceleration experienced by the head, it is thus positively related to the impact speed (in the simplest sense).

As such, if two tests are performed on a given structure, but at different test speeds, then we would expect the faster test to produce a higher HIC

value. Ideally, we would be able to predict the difference in HIC values by some theoretical or empirical relationship that is independent of the structure's properties. The literature was searched for existing studies that presented such a relationship and these are discussed below. In some of these studies, data were presented that related HIC to the test speed; in these cases a power function was fitted to the published data (see Appendix B for plots).

Theoretical studies

Two analytical studies of HIC and impact speed (Lim et al., 1995; Mizuno and Kajzer, 2000) have shown that a relationship between HIC and impact speed has the following form:

$$\text{HIC} = CS^{-1.5}V^4 \tag{2.2}$$

In this form, C is a constant that is dependent on pulse shape, S is the peak dynamic displacement and V is the impact speed. Lim et al. (1995) used this form for acceleration pulses in the shape of a square wave, sine wave and haversine wave. Mizuno and Kajzer (2000) derived this form for a quadratic acceleration pulse.

At first glance, this might suggest that HIC is proportional to impact speed to the power of four. However, this would only be true for fixed values of peak dynamic displacement. In reality, S and V are not independent variables. That is, if two tests were performed on the same structure but at different impact speeds, then the peak displacement would likely be higher for the faster speed. Since HIC is inversely related to S, the increased peak displacement would cause a reduction in HIC that would cancel out some of the effect of the increase in impact speed. If the relationship between S and V were known, then this dependence could be resolved.

Liu et al. (2002)

Liu et al. (2002) used MADYMO[2] multibody simulation software to simulate a vehicle striking a pedestrian. They used vehicle crash speeds ranging from

[2]TASS, Delft, The Netherlands

20 km/h to 50 km/h, in 10 km/h increments, and found that HIC increased with crash speed, as would be expected. The hood stiffness was varied from 200–800 N/mm on the edges, and 75–300 N/mm on the top. The force-deformation characteristic of the hood was taken from impactor tests but no further details are given. In the simulations, the ratio of head impact speed to vehicle crash speed varied from 0.72 up to 1.04. As such, no explicit relationship was derived between head impact speed and HIC, or vehicle crash speed and HIC.

The data presented by Liu et al. (2002) were fitted to a power function using Microsoft Excel[3] (see Figure B.1 in Appendix B). Since multiple impacts were simulated at each crash speed, the mean HIC values were taken from the graph. The resulting power function had an exponent of 1.68 ($R^2 = 0.99$), implying that HIC was proportional to vehicle impact speed raised to the power 1.68.

A major limitation of this study in its applicability to pedestrian headform tests is that it is based on a MADYMO model of a full body dummy being struck by a vehicle, and not of a freeflight pedestrian headform test. Thus, it is not possible to make any definite conclusions from this study regarding the relationship between HIC and headform impact speed.

Svoboda et al. (2003)

A similar MADYMO study was performed by Svoboda et al. (2003) using a model of a car striking either a 50% Hybrid II adult dummy, or a 6th-year-old dummy. The resulting HIC values were plotted against the vehicle impact speeds, which varied from 10 km/h to 80 km/h, in 10 km/h increments. The results suggested a great increase in HIC with impact speed, and while the authors showed a line of best fit through the data points, the equation of the line of best fit was not revealed.

Again, Microsoft Excel was used to fit a power function to the data presented by Svoboda et al. (2003). The resulting power function had an exponent of 1.80 ($R^2 = 0.90$). When only speeds of 10–60 km/h were considered, this exponent was 1.39 ($R^2 = 0.96$) and the fit was improved

[3]Version 11, Microsoft Corporation, Redmond, USA

(by visual inspection). Figure B.2 in Appendix B shows the data and fitted functions.

This study is limited in applicability in the same way as Liu et al. (2002), in that the simulations were performed using full body dummies, and not a headform in freeflight.

Oh et al. (2008)

Another MADYMO study by Oh et al. (2008) compared vehicle impact speed with the resulting HIC values in both adult and child pedestrian dummies. This study used vehicle impact speeds ranging from 10–100 km/h and six types of vehicle model. The results of the many simulations were fit to two different statistical models, a power function and an exponential function. The relationships were presented as follows:

$$\mathrm{HIC} = 0.053\, V_c^{2.284} \tag{2.3}$$

$$\mathrm{HIC} = 15.107\, \exp(0.055\, V_c) \tag{2.4}$$

Oh et al. used the second model (Equation 2.4) for further work, as the value of 0.053 in Equation 2.3 was not found to be statistically signficant (the value of 2.284 was, however).

One difficulty in applying the results of Oh et al. (2008) to pedestrian impact testing is that only vehicle impact speed was considered (noted above as V_c, in km/h). The head impact speed may have differed from this. Additionally, the use of a full body pedestrian dummy may influence the effective head mass and impact angle, which may also affect the HIC.

Liu et al. (2010)

Liu et al. (2010) used a finite-element model of a headform striking a windscreen, with the mechanical properties of the windscreen being derived from physical testing. They performed simulations at impact speeds ranging from 5–25 m/s (18–90 km/h). The results showed a clear increase in HIC with impact speed, but again, no explicit relationship was derived by the au-

thors. The data presented by Liu et al. (2010) was read off and fitted to a power function using Microsoft Excel (see Figure B.3 in Appendix B). The resulting power function had an exponent of 1.71 ($R^2 = 0.87$).

By visual inspection, the power function was not an appropriate fit to the data presented by Liu et al. (2010). The data exhibited a sharp increased in HIC at 90 km/h, which was not matched by the fitted power function. A limitation of this study was that it was specifically based on windscreen impacts, which have significant mechanical differences to impacts with structures made of sheet metal (e.g. bonnets).

Youn et al. (2005)

This limitation was not present in a study by Youn et al. (2005), who used a finite-element model to simulate headform-to-bonnet impacts. The results showed an increase in the relative HIC values with an increase in impact speed. Three impact speeds were considered: 32, 35 and 40 km/h. The simulations were conducted using two different headform masses (2.5 and 3.5 kg) and three different impact angles (50, 65 and 90°). The authors presented the results as ratios of the HIC obtained at 40 km/h, using a 2.5 kg headform, at a 50° impact angle. The authors did not attempt to find a generalised relationship for HIC and impact speed, or any of the the other test conditions.

To see if the data presented by Youn et al. (2005) imply a generalised relationship, the results were used to fit a power function in Microsoft Excel. This was done for each headform mass separately. There were nine simulation results for each headform mass. Two different methods were used to fit the function. The first was to use the total headform impact speed V (in km/h) and the second was to calculate the approximate 'normal', or perpendicular, component of the impact speed using the impact angle, θ:

$$V_n = V \sin(\theta) \tag{2.5}$$

The resulting power functions are shown in Table 2.1, and can be seen along with the data in Figures B.5 and B.6 in Appendix B. Each power function suggests that the relative HIC was proportional to the impact speed

NOTE:
This table is included on page 24
of the print copy of the thesis held in
the University of Adelaide Library.

Table 2.1: Fitted power law functions for data presented in Youn et al. (2005).

raised to the power of an exponent somewhere between 1.6 and 2. When normal impact speed was used, the exponent was lower in magnitude and the power function was a better fit (as indicated visually and by the values of R^2).

Amori et al. (1995)

Amori et al. (1995) performed headform testing on vehicle interiors, a type of test that differs from pedestrian impact testing, but also uses a headform in free flight and uses HIC as a measure of impact severity. The tests utilise a 4.55 kg headform fired at around 25 km/h. The authors looked at different aspects of the test including impact speed, headform calibration and impact angle. The study found that impact speed was the highest contributor towards variations in HIC. The authors did not quantify how the HIC was affected by the impact speed nor present any data, as the study was only looking at what parameters affected HIC, and not the extent of the effects.

Mizuno and Kajzer (2000)

Mizuno and Kajzer (2000) performed pedestrian headform testing at different impact speeds at two different locations, one on the bonnet and one on the windscreen of a passenger vehicle. The tests were performed at speeds of 30, 40 and 50 km/h. The HIC values obtained from the tests were relatively low – between 400 and 1200 for the bonnet tests and lower for the windscreen. The results showed a linear increase in HIC with impact speed, implying a power function exponent of one, which contrasts to what was suggested by other studies.

Pereira (2010)

In a more recent headform testing study, Pereira (2010) performed pedestrian headform tests on a vehicle at two different test speeds - the Euro NCAP test speed of 40 km/h and the GTR test speed of 35 km/h. A total of eight locations were tested, five using the ISO 3.5 kg child headform, and three using the ISO 4.5 kg adult headform.

Pereira (2010) plotted the HIC values obtained at each test speed against each other, and found a line of best fit for both the child and adult headforms. A linear line of best fit was given, as well as a polynomial line. However, there would appear to be no clear reason for the polynomial line, as the study shows that the linear and polynomial regression equations give almost identical results.

The linear line of best of fit for the child headform tests was

$$\mathrm{HIC}_{C,35} = 0.8756\,\mathrm{HIC}_{C,40} - 118.49 \tag{2.6}$$

For the adult headform tests it was:

$$\mathrm{HIC}_{A,35} = 0.644\,\mathrm{HIC}_{A,40} + 66.048 \tag{2.7}$$

These two equations were used by Pereira (2010) to predict what the equivalent HIC values would be under the GTR, for tests that achieve HIC values in the Euro NCAP tests of 1000 and 1350. One problem with these equations is that they do not have a zero intercept. This implies that if the HIC at 40 km/h were zero, then the HIC at 35 km/h would be non-zero.

The HIC values published by Pereira were analysed in Microsoft Excel. To confirm that the data had been entered correctly, the results published in the paper were successfully reproduced using lines of best fit with a non-zero intercept. The lines of best fit were then changed to have a fixed zero intercept; the slope of the child line became 0.789 ($R^2 = 0.97$) and the slope of the adult line became 0.678 ($R^2 = 0.999$). The child and adult results were also plotted together and a line of best fit with a zero intercept gave a slope of 0.729 ($R^2 = 0.94$), implying that the HIC obtained at 35 km/h would be 0.729 multiplied by the HIC obtained at 40 km/h. See Figure B.4

in Appendix B for the data and fitted line.

If a power law relationship between HIC and impact speed were assumed, then the combined slope of 0.729 implies an exponent of 2.37 for impact speed.

Kahane and Tarbet (2006)

Kahane and Tarbet (2006) performed head impact testing on vehicle interiors that were designed before and after changes were introduced to the US standard FMVSS 201. The ideal test speed was 24 km/h, but the actual test speeds varied from this. In order to compare their results directly, the HIC values from each test were adjusted to match the desired impact speed. The adjustment formula used by Kahane and Tarbet (2006) was as follows:

$$HIC_{adjusted} = HIC_{measured} \left(\frac{24}{v_{measured}} \right)^{2.5} \tag{2.8}$$

In Equation 2.8, $v_{measured}$ was set to the measured impact speed in km/h. Thus, the HIC was adjusted using the ratio of speeds, raised to the power 2.5. The reference for this procedure was given by Kahane and Tarbet (2006) as personal communication.

Summary of HIC and impact speed

In summary, the existing research shows that HIC is positively related to head impact speed and vehicle impact speed, as would be expected. A few studies have directly compared HIC and impact speed, but have not systematically investigated or attempted to give a general relationship. There is some suggestion that the relationship might be in the form of a power law, with HIC being proportional to head impact speed raised to the power of some exponent. The value of that exponent is not clear, as different studies have implied different values.

Table 2.2 summarises the power law exponents suggested by different studies. These exponents have either been presented directly in the study, or estimated from the data using the power law trendline function in Microsoft Excel. The value of N in the table is the number of data points used to derive the power function. Some studies only looked at vehicle impact speed,

Study	Exponent	R^2	N	Method
Liu et al. (2002)	1.68[1]	0.99	4	MADYMO, full body
Svoboda et al. (2003)	1.39[1]	0.96	6	MADYMO, pedestrian dummy
Oh et al. (2008)	2.28[1]	0.63	60	MADYMO, pedestrian dummy
Liu et al. (2010)	1.64	0.85	4	FEA, headform to windshield
Youn et al. (2005)	1.77[2]	0.98	9	FEA, 2.5 kg headform to bonnet
	1.63[2]	0.97	9	FEA, 3.5 kg headform to bonnet
Mizuno and Kajzer (2000)	1	-	3	Headform tests to bonnet/windshield
Pereira (2010)	2.37	0.94	8	Headform tests to bonnet
Kahane and Tarbet (2006)	2.5	-	-	HIC adjustment equation

[1] Estimated using vehicle impact speed.
[2] Estimated using normal impact speed.

Table 2.2: Power function exponents for HIC versus speed, as implied by different studies.

not head impact speed. In those cases, the power law would only hold true if the head impact speed were equal to the vehicle impact speed.

A theoretical relationship between HIC and impact speed may also be used. If a relationship between impact speed and peak displacement were known, or assumed, then Equation 2.2 could be used to derive a theoretical relationship between impact speed and HIC.

2.3.2 The effect of impact angle

In both the Euro NCAP and GTR headform test protocols, the impact angle is specified as the angle between the trajectory of the headform and the horizontal plane. In both protocols, adult headform tests are conducted with an impact angle of 65° and child headform tests with an angle of 50°.

The selection of the impact angle is important because it determines the speed of the headform in the direction perpendicular to the surface of the vehicle. The headform experiences far more resistance in the normal direction compared with the tangential direction (Liu et al., 2009), and so a more perpendicular impact is likely to be more severe.

A positive relationship between impact angle and HIC was shown by Stammen and Saul (2001), in headform tests conducted on multiple locations on two vehicles at 40 km/h. Impact angles of 53°, 65° and 90° (perpendicular) were considered. All locations exhibited an increase in HIC with impact angle. For each impact location, a line of best fit was given, relating impact angle and HIC. The fitting method used was a logarithmic fit, and

the fit parameters were not consistent for each test location. One reason for this might be that some locations were chosen due to the presence of a harder structure beneath the bonnet surface, and some were chosen in 'clear' areas. The locations with harder structures beneath may have been more likely to experience interference with those harder structures at higher impact angles.

One difficulty in generalising the results of Stammen and Saul is that different headforms were used for each impact angle: a 4.5 kg ISO headform for the 53° test, a 4.8 kg EEVC headform for the 65° test and a 4.5 kg NTHSA headform for the perpendicular test. The NHTSA headform was also a guided impactor test, in that the headform was fixed to a particular axis and was not in free flight. These inconsistencies make it difficult to draw any conclusions about the general relationship between impact angle and HIC in repeated tests on the same location.

A positive effect of impact angle on HIC was also demonstrated by Youn et al. (2005) who, as mentioned the previous section, performed finite element simulations of bonnet-to-headform impacts. When comparing the relative HIC values for different impact angles, the jump from 50° to 65° resulted in a large jump in HIC, however the jump from 65° to 90° (perpendicular) resulted in a relatively small jump in HIC. As shown in Table 2.1, the normal impact speed, calculated using the impact angle, was a better predictor for HIC than the total impact speed.

2.3.3 The effect of headform mass

To the author's knowledge, there has not been any previously published research that has looked directly at the relationship between headform mass and HIC. Most existing research related to headform mass has focused on replicating the conditions of a real pedestrian crash through the calculation of the 'effective head mass' (e.g. Lawrence et al. (2006)).

The effective mass is highly dependent on the shape of the front of the vehicle as well as the age and size of the pedestrian being modelled (Janssen and Nieboer, 1990; Okamoto and Kikuchi, 2006). For example, Lawrence et al. (2006) suggests that the effective mass in the child test area would be

around 2.5 kg at the front of the child zone, corresponding to the shortest child pedestrians, but up to 3.7 kg at the rear of the child zone, corresponding to those who are taller and to a 5th percentile adult female (Robbins, 1983). Thus, existing test headform masses are inherently a compromise that are chosen to best represent the average effective mass in a collision.

As mentioned previously, one study has compared the relative HIC values for tests performed using different headform masses on the same location. Youn et al. (2005) used a finite-element model of a child headform striking a bonnet, and compared the relative HIC values for 2.5 kg and 3.5 kg impactors. These relative HIC values were taken across a range of impact angles (50, 65 and 90°) and a range of impact speeds (32, 35 and 40 km/h). Taking all of these impact angles and speeds into account, there were nine pairs of relative HIC values that could be compared against each of other for the two headform masses. On average, the ratio of the 3.5 kg HIC values to the 2.5 kg HIC values was 0.80, with a maximum of 0.83 and a minimum of 0.78. This implies that if a location were tested with a 2.5 kg headform, then tested with a 3.5 kg afterwards at the same impact angle and speed, the second test would produce a HIC value about 20% lower than the first. If this were generalised to a power law, it would imply that the ratio of HIC values was inversely proportional to the ratio of headform masses raised to the power 0.66.

It is worth noting that while an increased headform mass may reduce the potential for head injury due to the decreased acceleration, it may increase the potential for a skull fracture if a constant skull strength is assumed. Thus, while a change in headform mass may have a positive or negative effect on the test HIC, the implications for real world injury may not be as clear.

2.4 Summary and research goals

The idea of testing vehicles for their level of pedestrian protection originated in the 1960s, but it was not until the late 1980s that serious efforts were made to design a usable testing procedure. The procedure developed by the EEVC was eventually used as part of the European New Car Assessment

Program (Euro NCAP) in the late 1990s, and this was in turn adopted by the Australasian New Car Assessment Program (ANCAP). A similar test procedure was also adapted for the Global Technical Regulation (GTR) on pedestrian safety.

The test speed used in the EEVC procedure, and by the Euro NCAP protocol, is 40 km/h. This appears to have been selected on the basis of the feasibility of passing such tests, and to replicate a crash speed greater than a large proportion of real world pedestrian accidents. The original headforms used by Euro NCAP were 2.5 kg and 4.8 kg for the child and adult, respectively. However, in recent times, the Euro NCAP protocol has adopted the ISO headforms, which are 3.5 and 4.5 kg. The ISO headforms are also used for the GTR, but at a lower test speed of 35 km/h.

There is limited existing research that examines the relationship between HIC and the conditions of a headform test, namely the impact speed, headform mass and impact angle. Some studies have presented results for HIC versus impact speed, but none have performed a thorough investigation of this relationship. The existing work suggests that HIC is positively related to impact speed as would be expected, and that a power law relationship might be appropriate. Previous studies have shown a positive relationship between HIC and impact angle. To the author's knowledge, there have not been any published studies that have directly examined the influence of headform mass on HIC in a pedestrian headform test, however one study has presented results that a suggest an inverse relationship between HIC and headform mass.

Given the difference in test conditions between different test protocols, it would be useful to be able to convert a result obtained under one set of test conditions to an equivalent result under a different set of test conditions. An example would be a test result that has been obtained in a Euro NCAP pedestrian headform test. If this test scored a HIC value of 1500, which is awarded zero points under Euro NCAP, what HIC value would we expect the same test location to score under the GTR test protocol?

Thus, the primary goal of this thesis is to investigate the relationship between HIC and the test conditions, that is, the impact speed, headform mass and impact angle. This enables the severity of different testing protocols to

be compared against each other.

This primary goal will be achieved by firstly examining theoretical models for headform impacts, which give a general form for the relationship between HIC and test conditions. Following this, a series of back-to-back test results will be used to compare the theoretical relationships with those implied by experimental data. The data are obtained from headform tests that were performed on multiple vehicles.

The second goal of this thesis is to predict the performance of vehicles under the GTR based on their ANCAP test result. A large number of vehicles have been tested by ANCAP in Australia, mainly under Versions 3 and 4 of the Euro NCAP pedestrian testing protocol. The new GTR on pedestrian safety may become a regulation in Australia but at present there have not been any vehicles tested under the GTR. Using a relationship developed for converting HIC values under different sets of test conditions, it is possible to take ANCAP test results and predict equivalent test results under the GTR. This enables some estimate to made of the impact of the GTR on vehicle design, and to compare the relative demands of performance under each test protocol.

The comparison of the protocols must take into account the different methods used to compile individual test results into an overall vehicle result. The test zones and other rules have an affect on the overall result, that may modulate the effect of the differences in test conditions.

The final goal of this thesis is to use real pedestrian crash speeds to examine different selections of test speed and HIC limits used in pedestrian testing protocols. By taking a real crash speed distribution, it is possible to calculate an equivalent HIC distribution if we assume that a structure meets the requirements of a particular protocol. This HIC distribution may also be related to head injury risk in a struck pedestrian. This enables multiple test protocols to be compared against each other in terms of potential real world crash outcomes.

Chapter 3

Theoretical models

In a headform test, both the HIC and the peak displacement are affected by the headform mass and impact speed. Increasing the impact speed generally leads to an increase in both HIC and peak displacement. A higher headform mass generally leads to a decrease in acceleration, and as a result, a decrease in HIC. An increase in headform mass also generally results in an increase in peak displacement.

As discussed in the previous chapter, the effect of changes in headform mass and impact speed on HIC and peak displacement are not well known and have not been systematically investigated in previous studies.

This chapter describes two theoretical contact models that were used to develop relationships for predicting the differences in HIC and peak displacement under two sets of test conditions.

Each model represents the normal component of the headform impact. Examination of test data has shown that the normal component of acceleration is generally higher in magnitude compared with the tangential component of acceleration. When added together geometrically, the normal component is dominant and has a much stronger effect on the HIC.

The contact models described in this chapter give an equation for the normal force F, as a function of normal displacement x, and the normal velocity $\dot{x}$. Figure 3.1 is a graphical representation of these values.

The first contact model is a simple linear spring model, in which the headform impact is represented by a mass impacting upon a spring with

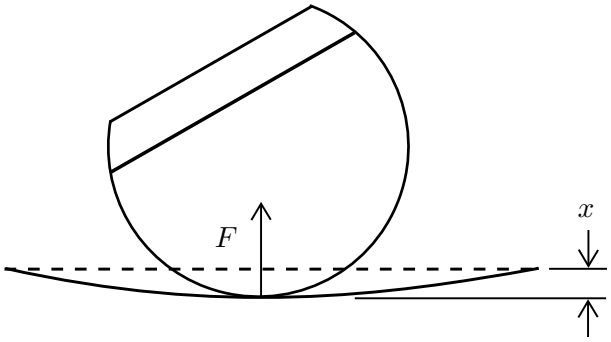

Figure 3.1: Schematic of headform impact showing the normal force F and normal displacement x.

constant stiffness. The contact force is given by $F = kx$. Using the results from Chou and Nyquist (1974), a relationship was derived analytically for the change in HIC with impact speed and headform mass. The relationship for the change in peak displacement was derived analytically from an energy balance.

The second contact model is a more general contact model based on Hertz contact theory, with a damping component added as per Hunt and Crossley (1975). The contact force in this model is given by $F = kx^n(1+c\dot{x})$. Due to the nonlinearity in this equation, a simple analytical solution cannot be found and so a numerical method was used to simulate impacts using this model. The results of the simulated impacts were used to examine the change in HIC and peak displacement between two sets of test conditions. The model was first considered with the damping factor c set to zero, and the influence of n was considered in isolation. The damping factor c was then introduced.

3.1 Linear spring model

Consider the impact of the headform against the tested structure to be represented by a lumped mass m, impacting upon a linear spring with stiffness k. For a linear spring, the force on the headform is given by $F = kx$. If $\ddot{x}$ is the acceleration of the headform, and x is the displacement from its initial position, then the equation of motion for this contact model is:

$$m\ddot{x} = -kx \tag{3.1}$$

Equation 3.1 is a differential equation that has a solution of the form:

$$\ddot{x} = A\sin(\omega t) \tag{3.2}$$

Thus, the acceleration pulse for this model has a half-sine shape, rising to a maximum acceleration of A. The pulse ends when $\ddot{x} < 0$, as this can only occur if the theoretical spring were in tension, at which point the headform will separate from the structure.

Chou and Nyquist (1974) analysed many different impact pulse shapes, and derived analytical expressions for HIC and peak displacement. This included a half-sine acceleration pulse, which was specified by its peak acceleration value A and its duration, T.

Chou and Nyquist derived the following expression for HIC (which is applicable to a half-sine pulse, a triangular pulse and a square pulse):

$$\text{HIC} = C_1(\Delta V)A^{3/2} \tag{3.3}$$

In this equation, ΔV is the change in velocity and C_1 is a constant dependent on the pulse shape. An expression was also derived by Chou and Nyquist for peak displacement, S. This applies to a half-sine pulse, but can also be used for a triangular pulse or a square pulse. The relationship is:

$$S = C_2\frac{(\Delta V)^2}{A} \tag{3.4}$$

Similarly, C_2 is a constant dependent on the pulse shape. If we rearrange Equation 3.4 for A and substitute this into Equation 3.3, then we obtain an expression for HIC in terms of velocity change and peak displacement:

$$\text{HIC} = C_1C_2^{3/2}\frac{(\Delta V)^4}{S^{3/2}} \tag{3.5}$$

The form of Equation 3.5 is the same as that obtained by Mizuno and Kajzer (2000) for a quadratic acceleration pulse, and also by Lim et al. (1995) for a half-sine, haver-sine and square wave. This form was not presented

by Chou and Nyquist (1974), but as shown, it can easily be derived by rearranging their results.

Next, we can consider the energy balance when the headform reaches its peak displacement, S. At this point the velocity of the headform will be zero, and the work done on the structure will be equal to the initial kinetic energy of the headform. The initial kinetic energy is equal to $\frac{1}{2}mv_0^2$, where v_0 is the initial velocity of the headform.

In order to give an expression for the work done on the structure, we must consider the specific case of the linear spring, which produces a half-sine acceleration pulse. In the case of a linear spring, the work done on the structure at the time of peak displacement will be equal to $\frac{1}{2}kS^2$. The energy balance at the time of peak displacement is then given by:

$$\frac{1}{2}kS^2 = \frac{1}{2}mv_0^2 \tag{3.6}$$

Simplifying Equation 3.6 and rearranging, we obtain:

$$S = \sqrt{\frac{m}{k}}\, v_0 \tag{3.7}$$

An impact with a linear spring is purely elastic, as the kinetic energy of the headform is the same before and after the impact takes place. As such, the final velocity of the headform will be the negative of its original velocity. Hence, the change in velocity ΔV is simply twice the initial velocity v_0. Recognising this, and substituting Equation 3.7 into Equation 3.5, we arrive at:

$$\text{HIC} = 16C_1C_2^{3/2}k^{3/4}m^{-3/4}v_0^{5/2} \tag{3.8}$$

In Equation 3.8, the applicable values of C_1 and C_2 are the values corresponding to the half-sine pulse in Chou and Nyquist (1974). While the initial equations in this section were applicable to other pulse shapes, this equation is specific to the half-sine pulse, as it has been derived using the energy balance for a linear spring (Equation 3.6).

Finally, we can consider two theoretical impacts on the same structure, under different test conditions. In this case the structure is represented by k,

which remains constant between both tests. The first test is with headform mass m_1 and initial velocity v_1, and the second set is with headform mass m_2 and initial velocity v_2. The HICs from each test are HIC_1 and HIC_2. If we take the ratio of HIC_1 and HIC_2 using Equation 3.8, then we obtain the following relation:

$$\frac{\text{HIC}_1}{\text{HIC}_2} = \left(\frac{m_1}{m_2}\right)^{-3/4} \left(\frac{v_1}{v_2}\right)^{5/2} \tag{3.9}$$

Similarly, Equation 3.6 can be rearranged, and the following relationship is obtained for changes in peak displacement, S:

$$\frac{S_1}{S_2} = \left(\frac{m_1}{m_2}\right)^{1/2} \left(\frac{v_1}{v_2}\right) \tag{3.10}$$

These two equations give us a theoretical relationship between the results of two tests on a given structure, with different test conditions, based on a linear spring contact model.

3.1.1 Other derivations for HIC

Equation 3.9 can also be derived from results presented in previous studies. Bicchi and Tonietti (2004) used a model of two masses colliding on a linear spring, to model a robot arm striking a human head. This model can be applied to the situation of a headform striking a vehicle, if one of the masses is assumed to be very large in comparison to the other. When this assumption is made, the model presented by Bicchi and Tonietti (2004) can be simplified to give the same result as Equation 3.9.

Martin (1990) modelled impacts with a playing field surface, using a half-sine shaped acceleration pulse. The impact severity was expressed using the Gadd Severity Index, or GSI, a measure for head impact severity that predates HIC (Versace, 1971). Equation 17 in Martin (1990) can be simplified to read:

$$\text{GSI} = \left(\frac{Bq}{pmh^{p-1}}\right)^{3/2p} H^{(4p-3)/2p} \tag{3.11}$$

In this formula, B is the surface area, q is a constant, p is one plus the

exponent of displacement in the force-displacement equation, m is the mass of the headform, h is the thickness of the surface being tested and H is the height that the headform is dropped from. If we assume a linear spring relationship, then the exponent of displacement in the force-displacement equation is one, and hence p is equal to two. Thus, Equation 3.11 can be simplified to read the following, with D_1 being constant for a given test surface:

$$\text{GSI} = D_1 m^{3/4} H^{5/4} \tag{3.12}$$

We can now make two more changes to this formula. Firstly, from an energy balance, we can recognise that the drop height H is proportional to the impact velocity squared. Secondly, Chou and Nyquist (1974) showed that for simple pulse shapes (including half-sine), GSI and HIC are related similarly to the pulse characteristics, the only difference being the magnitude of the scaling constant. Thus, we can substitute HIC for GSI in Equation 3.12, and v^2 for H. When such substitutes are made, the result is identical to Equation 3.9.

3.2 Hertz contact model with damping

The linear spring model has two characteristics which are not true of real impacts: the force is linearly proportional to displacement and the impact is perfectly elastic. The damped Hertz model analysed in this section does not have these characteristics and as such may be more representative of real impacts. The aim of this analysis was to determine whether the damped Hertz model would predict similar relationships for HIC and peak displacement to the simple linear spring model.

3.2.1 Description of the model

This contact model is based on Hertz contact theory, which gives an equation for the contact force between a sphere and an elastic plane. A generalised version of the Hertz contact model is given by:

$$F = kx^n \tag{3.13}$$

In classical Hertz theory, the value of n is 3/2, and k is dependent on the radius of the sphere as well as the mechanical properties of the sphere and the elastic plane (Johnson, 1985).

Hunt and Crossley (1975) used the generalised Hertz model as a basis, and added a velocity dependent damping component. In this contact model, the contact force is given by:

$$F = kx^n(1 + c\dot{x}) \tag{3.14}$$

The value of c is representative of the level of damping. If this is the decelerating force on the headform, then the equation of motion becomes:

$$m\ddot{x} = -kx^n(1 + c\dot{x}) \tag{3.15}$$

Note that when $n = 1$ and $c = 0$, the equation of motion is the same as that of the linear spring model. For $n \neq 1$ or $c > 0$, this relationship is nonlinear and there is no simple analytic solution for x. Because of this, the change in HIC and peak displacement was examined by numerically simulating impacts under different test conditions.

3.2.2 Overview of simulation

The method for numerically simulating the impacts is described fully in Appendix C. The simulation was used to generate values of acceleration, velocity and displacement for an impact with certain test conditions and impact parameters. From these results, the HIC and peak displacement could be calculated. The test conditions were the headform mass and initial velocity. The impact parameters were the values of k, n and c in Equation 3.14. The simulation was implemented in Matlab Version 7.5[1].

In the previous section, the linear spring model gave power law relationships for the change in HIC (Equation 3.9) and for the change in peak displacement (Equation 3.10). These power laws can be generalised so that

[1]The Mathworks, Natick, Massachusetts

the exponents are given by values a and b for the HIC relationship, and α and β for the peak displacement relationship. The generalised relationships are as follows:

$$\frac{\mathrm{HIC}_1}{\mathrm{HIC}_2} = \left(\frac{m_1}{m_2}\right)^a \left(\frac{v_1}{v_2}\right)^b \tag{3.16}$$

$$\frac{S_1}{S_2} = \left(\frac{m_1}{m_2}\right)^\alpha \left(\frac{v_1}{v_2}\right)^\beta \tag{3.17}$$

The headform mass in the simulated impacts was varied in order to calculate values of a and α. Two impacts were simulated, with the same impact parameters and a constant impact speed. A headform mass of m_1 was used to produce HIC_1, and a mass of m_2 was used to produce HIC_2. From these results, the value of a was calculated by rearranging Equation 3.16 into the following form:

$$a = \frac{\log(\mathrm{HIC}_1) - \log(\mathrm{HIC}_2)}{\log(m_1) - \log(m_2)} \tag{3.18}$$

Similarly, the value of α was calculated from the values of peak displacement in the two simulated impacts, S_1 and S_2.:

$$\alpha = \frac{\log(S_1) - \log(S_2)}{\log(m_1) - \log(m_2)} \tag{3.19}$$

A similar process was used to calculate values of b and β by varying the impact speed. Two impacts were simulated with the same impact parameters, and a constant headform mass. An impact speed of v_1 was used to produce HIC_1, and an impact speed of v_2 was used to produce HIC_2. These results were used to calculate b as follows:

$$b = \frac{\log(\mathrm{HIC}_1) - \log(\mathrm{HIC}_2)}{\log(v_1) - \log(v_2)} \tag{3.20}$$

Similarly, the value of β was calculated from the values of peak displacement, S_1 and S_2:

$$\beta = \frac{\log(S_1) - \log(S_2)}{\log(v_1) - \log(v_2)} \tag{3.21}$$

Thus, for a given set of impact parameters (k, n and c) and a given change in test conditions (m_1, m_2, v_1 and v_2), it was possible to calculate the corresponding values of the exponents a, b, α and β, from the simulation results.

The influence of each impact parameter on the values of the exponents was investigated by varying them individually. These results are discussed in the next three sub-sections.

The range of values of the impact parameters k, n and c were chosen to produce HIC values in a similar range to those obtained in real pedestrian impact tests. The values used for m_1 and m_2 were 2.5 kg and 4.8 kg. This is representative of the range of headform masses used in real pedestrian impact testing. The values used for v_1 and v_2 were 9.7 m/s and 11.1 m/s, which correspond to the GTR and Euro NCAP impact speeds. Again, this is representative of the range of impacts speeds used in real pedestrian impact testing.

The intent of this analysis was not to estimate specific values of the exponents using the damped-Hertz contact model, but to suggest how the values of the exponents predicted by the linear spring model might change if the power law relationships are applied to a more complex contact characteristic.

3.2.3 Influence of stiffness k

Figure 3.2 shows the influence of k on the shape of the acceleration pulse, with n and c held constant. As k increases, the peak acceleration increases and the pulse becomes narrower.

The effect of k on the values of the exponents was examined. The values of n and c were held constant at 1.5 and 0.2 s/m respectively, and the stiffness value k was varied between 100 kN/m$^{3/2}$ and 200 kN/m$^{3/2}$ at intervals of 5 kN/m$^{3/2}$. Multiple impacts were simulated using increasing values of k between these two values. The resulting values of HIC and peak displacement in the simulations were in the range of what might be expected in a real pedestrian headform test.

The value of k was found to have no effect on the values of the exponents. That is, the values of a, b, α and β were constant for all values of k, when

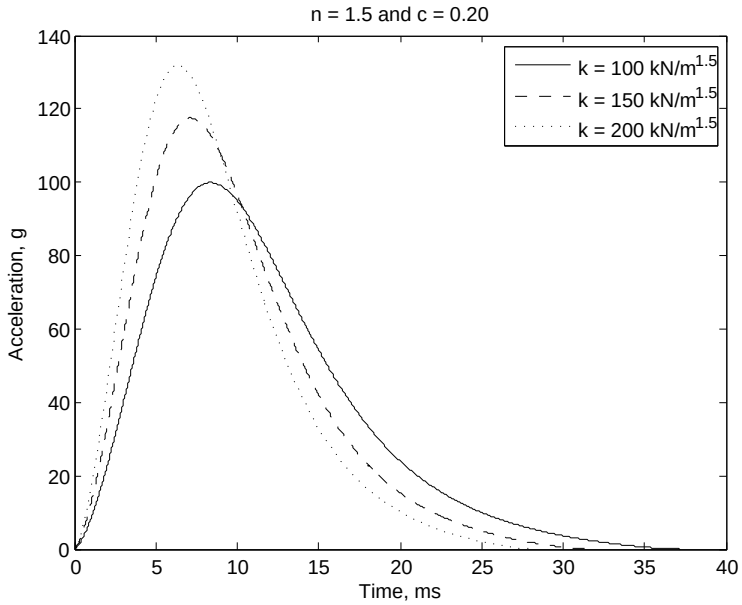

Figure 3.2: Influence of k on the acceleration pulse shape (n = 1.5, c = 0.2).

the values of c and n were held constant.

This implies that the power law relationships for predicting changes in HIC and peak displacement were not affected by differing values of stiffness in the damped Hertz model.

3.2.4 Influence of n with zero damping

The case of zero damping was considered by setting c to zero in the simulation. In this case, the decelerating force on the headform was given by $F = kx^n$. Having established that k has no effect on the values of the exponents, k was set to a fixed value of 100 kN/m^n. The value of n was varied between 1 and 3, at increments of 0.1.

The resulting values of HIC and peak displacement in the simulations were generally in the range of what might be expected in a real pedestrian headform test. At higher values of n, the peak displacement values increased above what might be expected, indicating that those values might not be appropriate choices.

Values of n less than one were not considered. Hertz contact theory is

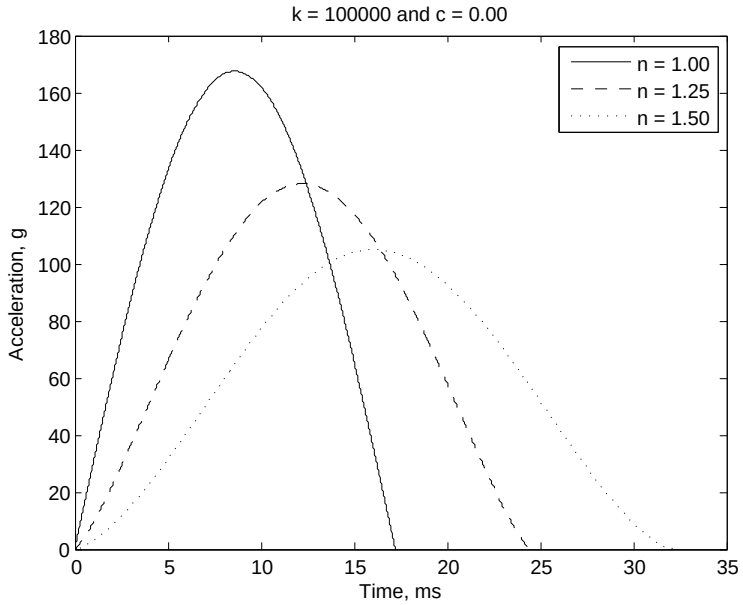

Figure 3.3: Influence of n on the acceleration pulse shape (k = 100 kN/m^n, c = 0).

based on an expanding area of contact between two surfaces, which implies a value of $n > 1$ (Johnson, 1985).

Figure 3.3 shows the influence of n on the acceleration pulse shape. As n is increased, the pulse becomes significantly longer, with a reduced peak acceleration. Additionally, the shape of the pulse changes. At $n = 1$, the pulse is a pure sine-wave, at higher values of n, the edges of the pulse are curved inwards. This trend continues for higher values of n, but values up to 1.5 are shown in the figure to better illustrate the changes in pulse shape.

For each value of n, the values of the exponents a, b, α and β were calculated from simulated impact results.

Figure 3.4 shows the change in the values of the exponents, for increasing values of n. As expected, when n was equal to 1, the values of the exponents were the same as what was derived for the linear mass-spring model ($a = -0.75$, $b = 2.5$, $\alpha = 0.5$ and $\beta = 1.0$).

Note that in Figure 3.3, the value of k is 100 kN/m^n and as such its units change with n. Thus, the three pulses in this figure cannot be compared to each other as if they had equivalent stiffness. The magnitude of k can

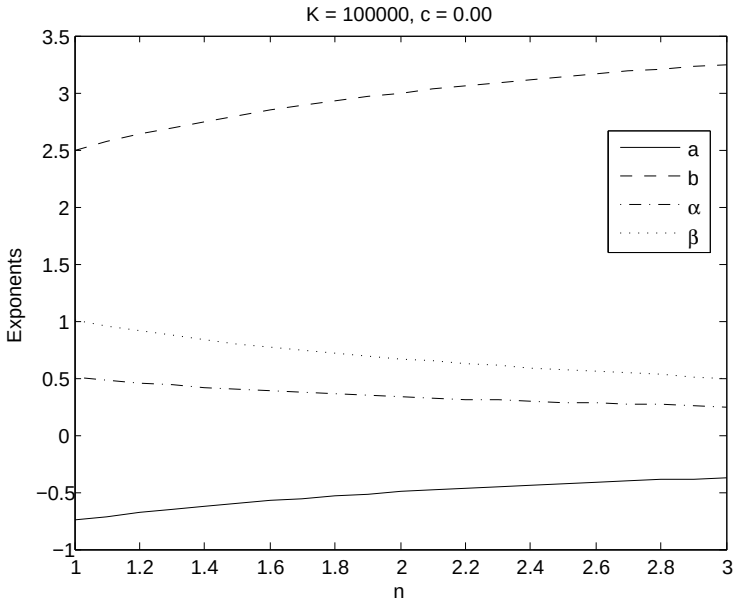

Figure 3.4: Influence of n on the values of exponents (k=100 kN/m^n, c=0).

only be meaningfully compared when n is constant. This does not affect the results in Figure 3.4, as it has been established in Section 3.2.3 that the magnitude of k does not affect the values of a, b, α or β. To verify this, the simulations were run again with randomly selected values of k for each value of n, and Figure 3.4 was unchanged.

The value of n was found to affect all of the exponents. As n was increased:

- The value of a decreased in magnitude, implying that the effect of mass on HIC became weaker.
- The value of b increased, implying that the effect of impact speed on HIC became stronger.
- The value of α decreased, implying that the effect of mass on peak displacement became weaker.
- The value of β decreased, implying that the effect of impact speed on peak displacement became weaker.

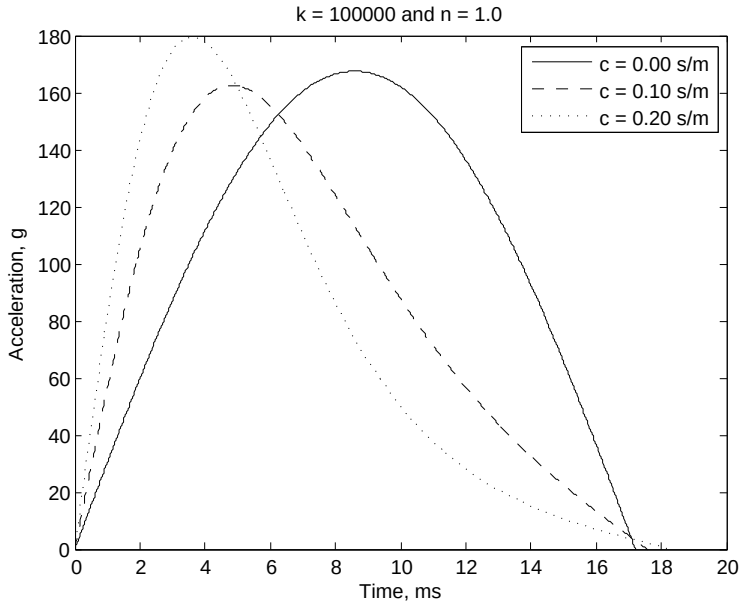

Figure 3.5: Influence of c on the acceleration pulse shape (k = 100 kN/m, n=1).

3.2.5 Influence of damping factor c

Finally, damping was introduced by considering values of c greater than zero. Figure 3.5 shows the influence of c on the shape of the acceleration pulse. For non-zero values of c, the pulse becomes non-symmetrical, as the impact is no longer elastic. The effect of damping is to increase the acceleration in the early part of the impact when the velocity is highest, and this can be seen by the shifting of the acceleration peak to the left as c increases.

To consider the effect of damping on the exponents, n was set to 1 and k was also held constant at 100 kN/m. The value of c was varied between 0 and 0.4 s/m, at increments of 0.02 s/m. An examination of test data showed that these values would produce appropriate pulse shapes, judged by visual inspection, and HIC values within reasonable limits (over 100 and under 10,000) for the given headform masses and test speeds.

For each value of c, simulation results were used to calculate values of the exponents. Figure 3.6 shows the variation of the exponents with increasing values of c.

In this case, the effect of c was limited to the exponents of impact speed:

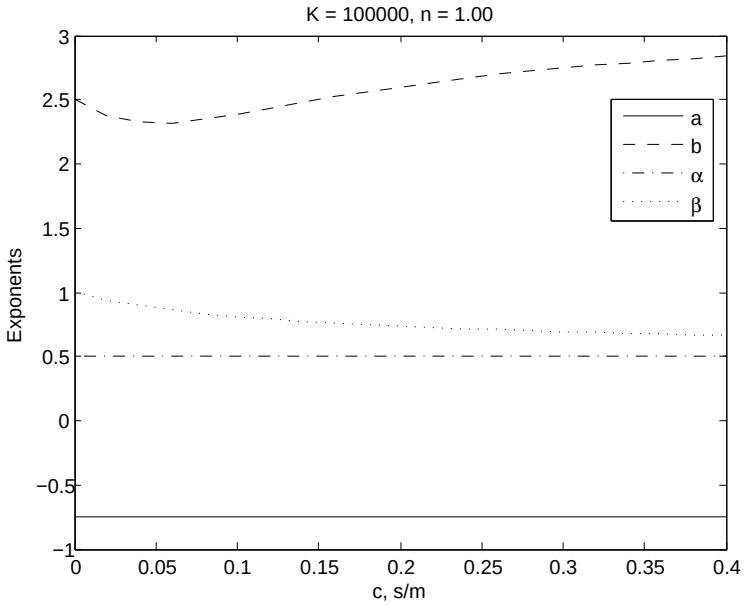

Figure 3.6: Influence of c on the values of exponents (k=100 kN/m, n=1).

b and β. The value of b was seen to initially decrease, and then increase with c, implying a lesser or greater effect of impact speed on HIC depending on the value of c. The value of β was seen to decrease with an increase in c, implying a weaker effect of impact speed on peak displacement with increased damping.

The exponents of mass, a and α, were not affected by the change in c. This implies that the level of damping did not change the effect of the headform mass on either HIC or peak displacement.

3.3 Summary of the theoretical models

In the simplest case, the impact was modelled as a mass and a linear spring. In this case, the decelerating force on the headform was given by $F = kx$. The following relationships were found for the change in HIC and the change in peak displacement between two impacts with different test conditions:

$$\frac{\mathrm{HIC}_1}{\mathrm{HIC}_2} = \left(\frac{m_1}{m_2}\right)^a \left(\frac{v_1}{v_2}\right)^b$$

$$\frac{S_1}{S_2} = \left(\frac{m_1}{m_2}\right)^{\alpha} \left(\frac{v_1}{v_2}\right)^{\beta}$$

In the case of the linear spring model, the exponents had the following values: $a = -0.75$, $b = 2.5$, $\alpha = 0.5$ and $\beta = 1.0$. These exponents may be more widely applicable, if they are unaffected by the complexities of a real impact.

Using these values for the exponents, we can calculate how test results may vary for a change in test conditions. For example, consider the two test protocols discussed in Section 2.2: The Euro NCAP pedestrian testing protocol (as used by ANCAP) and the Global Technical Regulation (GTR). Under Version 4 of the Euro NCAP protocol, the child headform weighs 2.5 kg, and the test speed is 40 km/h. The same test area would be tested under the GTR using a 3.5 kg headform and a test speed of 35 km/h.

Using these two test conditions as an example, the linear spring model implies that the ratio of HIC values would be 0.556. This suggests that if the same child head test location were tested under the GTR and Version 4 of the Euro NCAP test protocol, the HIC obtained in the GTR test would be approximately 56% of the HIC obtained in the Euro NCAP test. Similarly, the linear spring model implies that the peak displacement in the GTR test would be 4% higher than the Euro NCAP test.

A more complicated contact model was then considered: a Hertz contact model with damping, as presented by Hunt and Crossley (1975) and also used by Anderson et al. (2009). The decelerating force on the headform in this case was given by $F = kx^n(1 + c\dot{x})$. The impact parameters k, n and c were varied to see if the exponents in the HIC and peak displacement relationships would be affected. The results showed that the values of the exponents were not affected by changes in the stiffness parameter k. The case of zero damping was considered by setting c to zero, and n was varied. The value of n was found to affect all four parameters: a decreased in magnitude, b increased, and α and β decreased. Finally, the effect of damping was introduced and c was varied. The value of c had no effect on the mass exponents a and α. However, an increase in c lead to a general increase in the value of b (after an initial decrease), and a decrease in the value of β.

One factor that may reduce the applicability of both models is that they do not account for any discontinuity in the structure undergoing impact. These discontinuities may be present in a real test. For example, the bonnet of the vehicle may deform sufficiently that it comes into contact with a stiffer structure beneath (for example, the engine or suspension tower). This particular problem is often referred to as 'bottoming out'. A theoretical model for bottoming out was outside the scope of this thesis.

Another limiter of applicability for both models is that their acceleration pulse shapes do not closely match typical acceleration pulses from real impacts. Figure 3.7 shows an acceleration pulse obtained from a test where bottoming out did not occur, along with acceleration pulses generated using the linear spring and damped Hertz contact models. The theoretical models only produce the normal acceleration in the impact (as illustrated in Figure 3.1). The total acceleration for the real test is shown, but in this case, and in most cases, the total acceleration was very close to the normal acceleration.

The normal force is also plotted against the normal displacement for the real test (the method for estimating these values is described in the next chapter), and these are compared with the force and displacement obtained using the theoretical models. The initial speed in the contact models was matched to the normal impact speed in the real test, and the parameters of the models were chosen such that the peak normal displacement values were similar. Despite matching the initial speed and peak displacement, the HIC values produced by these pulses are quite different: 1225 from the real test, 4166 using the linear spring model and 1654 from the damped Hertz model.

As shown in Figure 3.7, real impacts often result in acceleration pulses with multiple peaks, even when bottoming out does not occur. It is unclear whether these multiple peaks are a structural characteristic, or are due to mechanical vibration during the impact. The theoretical contact models do not mimic these multiple peaks. Furthermore, the force-versus-displacement relationships are very different for the theoretical models, compared with the real impact. These factors make it difficult to fit either of the models to existing data.

Thus, the level of applicability of either contact model to a real headform test is not known. It is clear that a real headform test tends to produce a

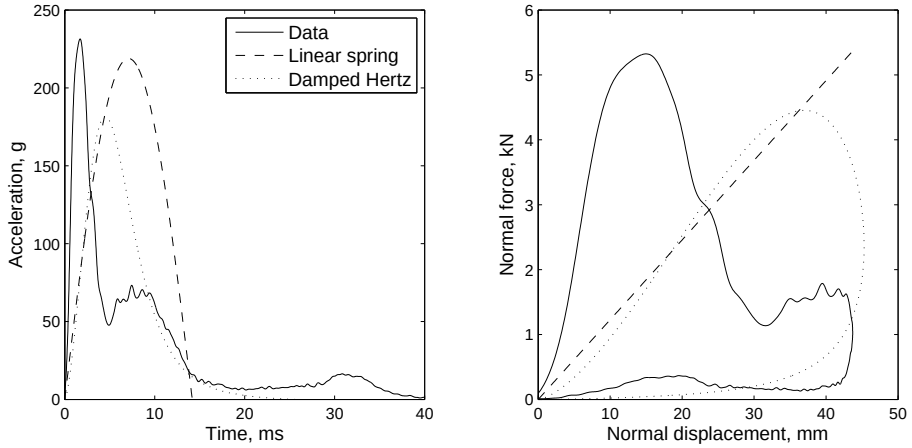

Figure 3.7: Real test data compared to theoretical contact models.

much more complex acceleration pulse than either of these theoretical models. The theoretical models considered in this Chapter are not sufficiently complex to capture the intricacies of the real impact data. However, the goal of this work is not to accurately model individual pulses, the goal is to predict the changes in HIC and peak displacement that occur due to a change in impact speed and headform mass.

As such, despite the differences in pulse shape, real tests may still conform to the same relationships for predicting changes in HIC and peak displacement to those predicted by the theoretical models. This possiblity was examined using results from real pedestrian impact tests. The next chapter describes these tests in detail, and the resulting data that were used for this analysis in later chapters.

Chapter 4

Test method and data

This chapter describes the method used for performing headform tests, and gives an overview of the test data used later in this thesis. The headform testing was performed at the impact laboratory of the Centre for Automotive Safety Research (CASR) in Adelaide, Australia. The method used to perform the tests is described in Section 4.1.

For each headform test, the acceleration of the headform was measured, and was used to calculate the HIC. The acceleration data was also used to estimate the peak normal displacement of the vehicle surface during the test. The method of estimation is described in Section 4.2.

The test results were split into four sets, described in Section 4.3. The first two sets contained test results relating to the general influence of impact speed and headform mass on HIC and peak displacement. The third and fourth sets contained test results relating to the specific relationship between the ANCAP and GTR test protocols. The data from each of these sets is used in subsequent chapters.

This chapter concludes with a discussion of the potential sources of error when comparing repeated tests on the same location.

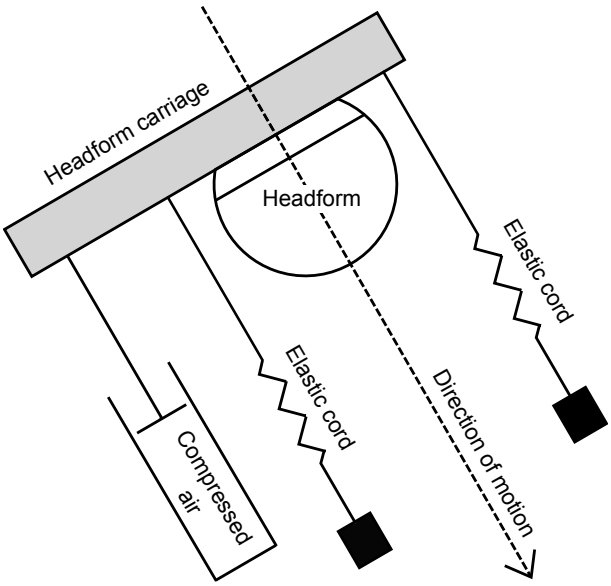

Figure 4.1: Schematic of the headform launching machine 'B1'.

4.1 Headform testing method

4.1.1 Test equipment

The headform tests used for this project were conducted in the CASR impact laboratory. A schematic diagram of the launching machine (B1) is given in Figure 4.1. The headform is mounted to a carriage, which is drawn back using compressed air. The carriage is released and the elastic cords, which are in tension, accelerate the headform. The height of B1 is adjustable to account for the height of the test location.

Test results were used from tests conducted in the laboratory as part of regular pedestrian testing for the Australasian New Car Assessment Program (ANCAP). Additional tests were conducted specifically for this project and other results were drawn from tests conducted by CASR for research projects. All of the headform tests were conducted on the bonnet (hood) of the vehicle.

A new bonnet was used for every test conducted for ANCAP. Multiple tests were sometimes conducted on the same bonnet for the non-ANCAP tests, but only when the test locations were sufficiently far apart that there was no obvious structural interference between the two.

Mass	Diameter	Specification	Certification
2.5 kg	130 mm	WG17	1 kg impact test: Euro NCAP (2008)
3.5 kg	165 mm	ACEA	Drop test: UNECE (2009) Annex 6, Sec 3
3.5 kg	165 mm	ISO	Drop test: UNECE (2009) Annex 6, Sec 3
4.5 kg	165 mm	ISO	Drop test: UNECE (2009) Annex 6, Sec 3
4.8 kg	165 mm	WG17	1 kg impact test: Euro NCAP (2008)

Table 4.1: Headforms and certification procedure used.

Five different headform types were used, representing four different headform masses. These were the 2.5 kg and 4.8 kg WG17 headforms (EEVC, 2002), a 3.5 kg ACEA headform and 3.5 kg and 4.5 kg ISO headforms. The headforms and their certification procedures are summarised in Table 4.1.

The 2.5 kg and 4.8 kg WG17 headforms were certified using the headform certification procedure detailed in the Euro NCAP testing protocol (Euro NCAP, 2008). This procedure involves striking the stationary headform with a 1 kg cylindrical mass. The peak acceleration experienced by the headform must fall within a certain range for the headform to pass the test. The test is repeated three times.

The 3.5 kg and 4.5 kg headforms were certified using the headform certification procedure detailed in Annex 6, Sec 3 of the GTR (UNECE, 2009). This procedure involves dropping the headform from a certain height (dependent on mass) onto a flat steel plate. Again, the peak acceleration must fall within a certain range, and the test is repeated three times on different areas of the headform.

Three different accelerometer types were used during the course of the testing. Early testing used an undamped triaxial Endevco accelerometer block. Later testing used a damped Kyowa accelerometer block or a damped Endevco accelerometer block. All accelerometers had been calibrated within the required interval and were checked as part of the certification procedures outlined above.

Data was acquired at 50 kHz through an Endevco 136 3-channel DC amplifier, and a United Electronic Industries UEI-30 acquisition board. The amplifier was calibrated at the time of testing. A 10 kHz filter was used in the amplifier.

During all testing, the laboratory temperature was maintained at $20 \pm 4°C$.

4.1.2 Test process

The testing followed a standard procedure, which was common to both the ANCAP and non-ANCAP tests.

Before each test, a new bonnet was fitted to the vehicle if necessary. A new bonnet was always used for ANCAP tests. Where possible, the insulator sheet was fitted to the underside of the bonnet. This is typically a thin sheet of insulating material, for sound and heat insulation. Any other fittings such as rubber stoppers and rubber 'weather strips' were fitted.

The test location was marked onto the bonnet and the angle of the bonnet at that point was measured. The test location was defined as the first point of contact of the headform to the bonnet. The trajectory of the headform was set to ensure that the point of first contact conincided with the intended test location. Following each test, high-speed film was consulted to ensure that this had occurred.

The speed of the headform was measured by recording the time taken for it to cross two parallel laser beams.

During each test, the accelerometer data was recorded using a PC-based data acquistion system, and afterwards the data was processed using a Matlab[1] script. The script applied a CFC1000 filter to the acceleration data and calculated the HIC, using a maximum time window of 15ms.

This process was performed for each test. The end result was a data file containing the acceleration of the headform on three axes. This file was later processed to estimate the peak displacement, the method for doing so is described in the next section.

4.2 Estimation of peak displacement

This section describes a method that was developed to estimate the displacement of the headform during the test. The reason for doing this was to examine the relationship between peak displacement and the test conditions. As discussed in Chapter 3, the peak displacement has implications for the measured severity of a test, in that bottoming out may be more likely

[1]The Mathworks, Natick, Massachusetts

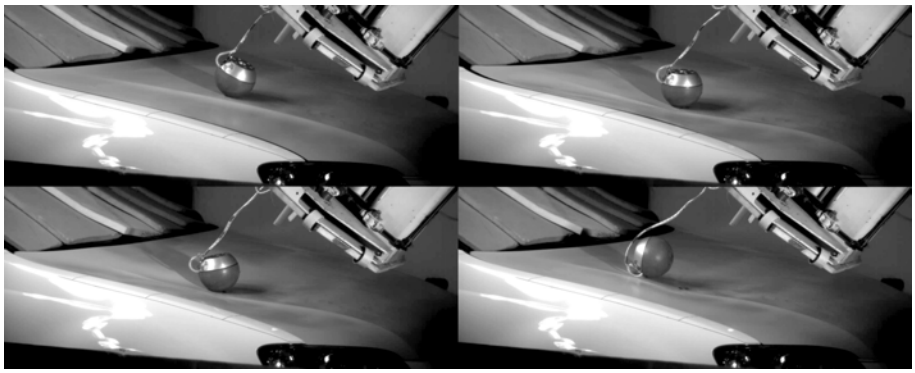

Figure 4.2: High speed video capture of a typical headform test.

to occur when the peak displacement is higher.

If the impact were one-dimensional, then the peak displacement could be calculated by double-integration of the measured acceleration. However, a real pedestrian headform test is not one-dimensional. The headform (most often) strikes the bonnet at an angle and as such a rolling motion is induced, as shown in Figure 4.2. The peak displacement in the normal direction only is required, and this cannot be easily obtained when the orientation of the accelerometers changes throughout the impact.

Thus, the peak displacement was estimated by firstly estimating the orientation of the headform throughout the impact, using a theoretical model of the headform kinematics. This model relies upon knowing the orientation of the accelerometers relative to the headform, and the intitial orientation of the headform relative to the vehicle surface. The method was validated using a MADYMO model of a headform impacting a flat surface.

4.2.1 Description of method

The method for estimating peak displacement is described below, in two sections. The first describes a method for transforming the accelerometer measurements into a normal and tangential component, and the second describes how the normal and tangential components were calculated throughout the duration of the impact.

Transformation of accelerometer measurements

The accelerometer measurements taken in the CASR laboratory were transformed into a normal and tangential component, based on the orientation of the headform.

There were three mutually perpendicular measurement axes of the accelerometer block: X, Y, and Z. When the headform was loaded into the launching machine, the accelerometers were orientated such that Z-axis was aligned with the initial direction of motion of the headform. The X and Y axes were in the plane perpendicular to the Z-axis. This is shown graphically in Figure 4.3.

There are three additional axes shown in Figure 4.3, shown as dotted lines. The initial direction of motion is the travelling axis of the headform before it strikes the bonnet. The horizontal axis perpendicular to the initial direction of motion is shown. The R-axis is perpendicular to the initial direction of motion and to the horizontal axis.

The angle ϕ in Figure 4.3 is the angle between the Y-axis and the R-axis. In the CASR laboratory, the ideal alignment was for $\phi = 45°$. However, this is an approximation of how the headform was typically loaded before each test: there was no mechanism on the launching machine to ensure that this was always an exact 45° angle.

It was assumed that the impact was two-dimensional. That is, the acceleration along the horizontal axis was assumed to be zero. As a result, there were two acceleration components considered: the Z-axis, and the R-axis. The Z-axis acceleration was measured directly during the test by the Z-axis accelerometer. The R-axis acceleration was a combination of the X and Y-axes accelerometer measurements.

The X and Y-axes accelerations were projected onto the R-axis using the approximately known value of ϕ. The value of a_r was calculated using the following formula, with $\phi = 45°$:

$$a_r = a_x \sin(\phi) - a_y \cos(\phi) \tag{4.1}$$

The R-axis acceleration a_r, and the Z-axis acceleration a_z were then known. These values were measured relative to the headform. In order to

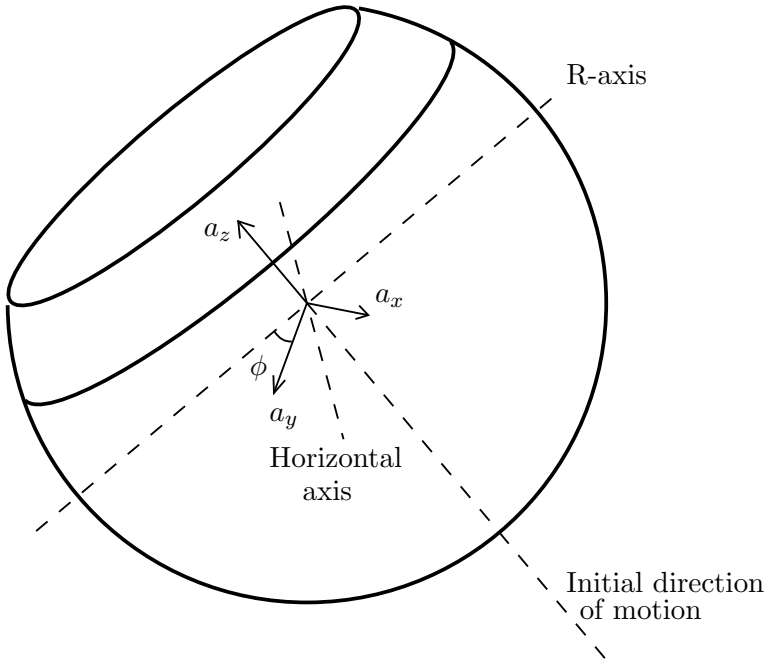

Figure 4.3: Alignment of the accelerometer measurement axes.

be useful, they had to be transformed into measurements that were relative to the struck surface: i.e. the normal and tangential acceleration values.

The angle between the Z-axis and the struck surface, θ, was used to transform a_r and a_z into normal and tangential components. Figure 4.4 shows these acceleration measurements. The following equations were used to resolve the normal and tangential acceleration components:

$$a_n = a_z \sin(\theta) + a_r \cos(\theta) \tag{4.2}$$

$$a_t = a_z \cos(\theta) - a_r \sin(\theta) \tag{4.3}$$

Thus, if θ was known, the normal and tangential acceleration components could be calculated from the measured X, Y and Z acceleration values, using Equations 4.1, 4.2 and 4.3.

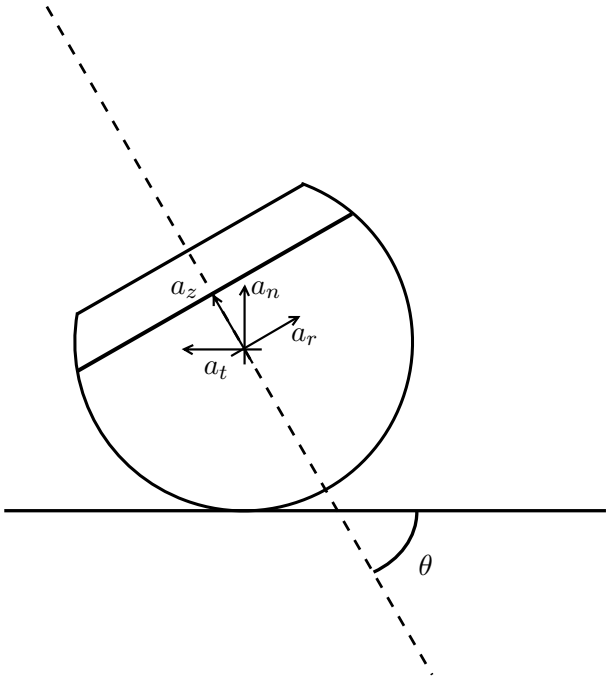

Figure 4.4: Headform impacting a flat surface, showing R-axis and Z-axis acceleration components.

Calculation of θ during the impact

As shown above, in order to calculate the values of a_n and a_t throughout the duration of the impact, it was necessary to estimate θ throughout the duration of the impact.

The initial angle θ_0 was measured before the test, so the acceleration components at the beginning of the impact, $a_{n,0}$ and $a_{t,0}$ could be calculated.

An assumption was made that the headform rolls along the surface of the bonnet with no slippage. The acceleration was measured in discrete time-steps. For the ith time-step, starting at $i = 0$, the angular acceleration $\dot{\omega}_i$ was calculated:

$$\dot{\omega}_i = \frac{a_{t,i}}{r} \tag{4.4}$$

where r is the radius of the headform. The resulting angular velocity ω_i and the angle θ_i were calculated for time-steps $i > 0$ with time difference Δt:

$$\omega_i = \omega_{i-1} + \dot{\omega}_i \Delta t \tag{4.5}$$

$$\theta_i = \theta_{i-1} + \omega_i \Delta t \tag{4.6}$$

Thus, by stepping through each time-step of the recorded acceleration data, θ_i could be calculated, along with the normal and tangential acceleration components. Numerical integration was then used to estimate the normal velocity and normal displacement. The peak displacement was estimated by finding the maximum value of the normal displacement.

A Matlab[2] script based on this methodology was developed to post-process the test results for this project. This script was also used to process the results of a MADYMO simulation, described in the next section.

4.2.2 Validation using MADYMO

The method for estimating peak displacement was tested using the results of a computer simulated model of an impact. The simulation was performed using the multi-body simulation package MADYMO[3].

The analysis of the results was performed by the author, however the simulation was performed by a colleague.

Method

In the MADYMO simulation, a child headform was impacted upon a flat surface. The headform was represented by a validated finite element model of an EEVC child headform[4]. The contact characteristic between the headform and the surface was defined using a damped Hertz contact model, similar to that described in Section 3.2, but with permanent deformation as per Anderson et al. (2009). A dynamic friction coefficient of 0.4 was used. The conditions of the MADYMO model are summarised in Table 4.2.

In the MADYMO simulation, the acceleration was measured using three virtual 'accelerometers' mounted within the headform. These corresponded

[2]The Mathworks, Natick, Massachusetts
[3]Version 6.4, TASS, Delft, The Netherlands
[4]MADYMO Finite Element EEVC child headform impactor model, Version 3.1

Condition	Value	Comments
Diameter	130 mm	As for Euro NCAP child headform
Mass	2.5 kg	As for Euro NCAP child headform
Moment of inertia	0.0036 kg m^2	As for Euro NCAP child headform
Velocity	11.1 m/s	Euro NCAP head test velocity (40 km/h)
Angle to horizontal	65°	As for Euro NCAP adult head test
Surface angle	10.6°	Typical bonnet angle

Table 4.2: Test conditions used for the MADYMO simulation.

to the accelerometers used in a real headform test. The orientation of the accelerometers was similar to that shown in Figure 4.3, however in the MADYMO model the X-axis was aligned with the R-axis, and the Y-axis was aligned with the horizontal axis. Thus, $\phi = 90°$.

The X, Y and Z-axes acceleration measurements from the simulation were used to estimate the peak normal displacement with the Matlab script based the method outlined in the previous section. In other words, the simulation results were processed in exactly the same way as if the acceleration measurements had come from a real headform test.

In the MADYMO simulation, the normal displacement of the headform relative to the surface and the normal force on the headform were also measured directly. These values could be compared to the estimated values, which were derived from the virtual X, Y and Z accelerometer readings.

Results

Figure 4.5 shows a comparison of the estimated displacement and the actual displacement given by MADYMO, as well as a similar comparison for the force vs. displacement curves. The estimated peak displacement was 45.14 mm, and the peak displacement given from the simulation results was 44.90 mm.

This analysis suggests that for a simulated impact on a flat surface, the peak displacement can be accurately estimated using the method described in the previous section. In a real impact with a bonnet, the surface is almost certainly not flat, and the force-displacement relationship is not likely to be as clear as that shown in Figure 4.5. However, this analysis shows that the method produces a valid estimate for a simplified impact. Any departures

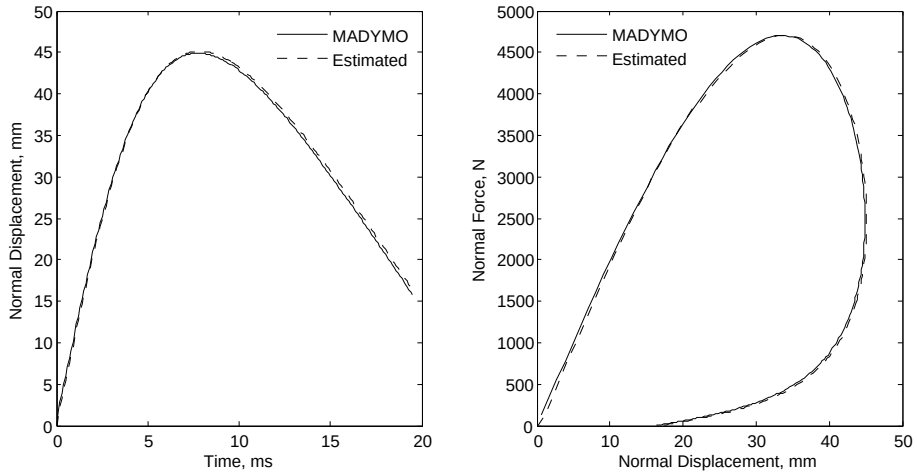

Figure 4.5: Comparison of the estimated force and displacement with that calculated directly by MADYMO.

from these simplifications may affect the validity of the results.

The assumption of 'no-slip' was not true for the MADYMO simulation. In fact, the results showed that the headform experienced dynamic friction before the rolling motion was induced. Despite this, the estimation still provided an accurate estimate of the peak displacement, suggesting that the accuracy of the results are not overly affected by the assumption of no-slip.

4.2.3 Summary and potential sources of error in the estimation of peak displacement

In summary, the peak displacement was estimated using the following methodology:

1. During the test, the triaxial accelerometers recorded three values for each time step: a_x, a_y and a_z.

2. The value of a_r was calculated using Equation 4.1 for each time-step.

3. The initial value of θ was known from measurements, and was used to calculate the initial normal and tangential acceleration (Equations 4.2 and 4.3).

4. The initial angular acceleration was calculated from the tangential acceleration (Equation 4.4).

5. The angular velocity and the angle were calculated for the next time-step, based on the angular acceleration (Equations 4.5 and 4.6).

6. Steps 3 – 5 were repeated for all time-steps.

7. The normal acceleration was double integrated to obtain a normal displacement for each time-step.

8. The maximum value of the normal displacement was found.

This method was validated using a MADYMO simulation of a headform impacting upon a flat surface. The simulation results indicated that the method gave an appropriate estimation of peak displacement, for an impact with a flat surface.

This method was used to estimate the peak displacement in each headform test used in this thesis. Using these estimated values, the relationship between test conditions and peak displacement could be further investigated.

There were several potential sources of error in this method, which are discussed in further detail below.

Flat surface assumption

The first potential source of error in the method for estimating peak displacement is the assumption that the impact occurs on a flat surface. This assumption implies that the headform does not experience any signficant sideways rotation, and that the angle of the bonnet surface to the ground does not change with position. The impacts used in this study were mostly performed on relatively flat sections of the bonnet surfaces, however this assumption may affect the validity of the results.

Angle of accelerometers

Another source of error was that the angle ϕ between the X and Y axes of the accelerometer block were assumed to be exactly 45° to the horizontal axis (see Figure 4.3). In reality, the headform was only loaded into the launching

machine with an approximate 45° angle, and this may have varied from test to test.

To check how this assumption may affect the test results, ten headform tests were selected at random. The peak displacement was estimated for these tests using the assumed value of $\phi = 45°$, and also using values for ϕ of 30° and 60°. The difference in the estimated peak displacement values was less than 1 mm in all cases, and did not exceed 2% of the original $\phi = 45°$ value.

Thus, the effect of this source of error on the test results is likely to be very small. The reason for this is that the value of ϕ was only used to calculate the R-axis acceleration, which depends only on the X and Y-axes measurements. In the majority of impacts, the X and Y-axes acceleration measurements were relatively small compared with the Z-axis measurement, and thus did not have a significant effect on the overall result.

Assumption of no-slip

Another source of error is that the calculation of peak displacement relies on the assumption of 'no slip'. That is, it was assumed that the headform rolls perfectly along the surface of the bonnet, with all linear movement being matched by a rotation of the headform. If linear movement occurred without rotation, then the headform would be 'slipping' along the surface.

This assumption was made on the basis of viewing high speed footage of headform impact tests, in which the headform appears to roll along the surface without slipping. It is likely that some slipping does occur in the impact, which would lead to an underestimate of the angular motion of the headform. This would lead to some inaccuracy in the estimation of peak normal displacement.

To test the effect of this assumption, the peak displacement was estimated for ten randomnly selected tests, assuming that some slippage did occur. Slip was accounted for by introducing a slip ratio η, which would be equal to zero for no slip, and equal to one for total slip (no rotation of the headform). Equation 4.4 was modified to the following:

$$\dot{\omega}_i = \frac{(1-\eta)a_{t,i}}{r} \tag{4.7}$$

For each of the ten tests, the peak displacement was estimated using the original assumption of no slip ($\eta = 0$), and then using values of 0.25 and 0.5 for η. The results indicated that when slip was introduced, the estimated peak displacement was slightly higher. In nine of the ten cases with $\eta = 0.5$, the estimated peak displacement rose by less than 1mm, or less than 2%. In one of the cases, the estimated peak displacement was approximately 2mm (3%) higher when $\eta = 0.5$.

This implies that if the assumption of no slip were incorrect, then there may be a small effect on the accuracy of the estimated peak displacement.

4.3 Compilation of headform test data

The headform test data used in this thesis was a collection of results compiled from ANCAP tests and testing conducted for the purposes of this project. The test results span several years. Five different vehicle models were used, and in some cases there was more than one physical vehicle used in the representation of that vehicle model. These vehicles are detailed in Section 4.3.1.

There were a total of 95 headform test results used in this thesis. These tests were split into four sets of test results, labelled A, B, C and D. Each data set was used to research a particular topic:

A: The influence of impact speed on HIC and peak displacement.

B: The influence of headform mass and diameter on HIC and peak displacement.

C: The difference in HIC between Euro NCAP child and GTR child headform tests.

D: The difference in HIC between Euro NCAP adult and GTR child headform tests.

	Set A	Set B	Set C	Set D
Number of tests	29	39	28	6
Number of locations	7	15	14	3
On each location:				
Speed varied?	Y	N	Y	Y
Mass varied?	N	Y	Y	Y
Diameter varied?	N	Y	Y	N

Table 4.3: Summary of four data sets: A, B, C and D.

In data sets A and B, tests were repeated on the same locations using different headforms and a range of impact speeds. One parameter was held constant while the other was varied across several tests.

In data sets C and D, tests were conducted under the GTR test conditions, on locations and vehicles previously tested by ANCAP (under Versions 3 and 4 of the Euro NCAP protocol). This allowed a direct comparison to be made of the two test protocols.

Table 4.3 summarises the four data sets. The number of tests and the number of different locations are listed. The variation of each parameter within each data set is also shown. Note that the variation applies to multiple tests on a given location. For example, in Set B, the normal impact speed varied between test locations, but was as constant as practicable for every test on the same location.

Note that some test results and locations were included in more than one of the four sets. Thus, the sum of tests in each set is greater than the total number of tests (95).

4.3.1 Test vehicles

Five different vehicle models are represented in the test results. However, the testing took place using 11 physical vehicles.

The reason for this spread is that the test results were compiled from a mix of ANCAP tests and tests conducted for the purposes of this project. The distributions of locations and tests across each vehicle are listed in Table 4.4. The year given is the year of manufacture represented – i.e. the year that the original vehicle was manufactured.

Make/model	Year	Vehicles	Locations	Tests
Mazda3	2004	2	7	14
Toyota Camry	2006	3	7	14
Holden Commodore	2006	3	5	16
Toyota Kluger	2007	2	12	39
Hyundai ix35	2009	1	2	12

Table 4.4: Vehicles used in this project.

Each vehicle model and the vehicles used to represent that model are described below.

Figure 4.6 shows the underside of each vehicle model's bonnet. Every bonnet was made of steel and was designed to hinge at the rear. The bonnet structures share some common characteristics: each has a bulky section at front and rear, where it comes into contact with the supporting structure, and the outer skin of the bonnet is supported in the middle by some form of stiffening structure. The layout of this stiffening structure differed between bonnet designs.

Mazda3 (2004)

The Mazda3 was represented by two physical vehicles. The first was tested by ANCAP in April 2004, and the second was tested in June 2009. The Mazda3 is classified as a small car by ANCAP. The underside of the bonnet was similar to many vehicles that have not been optimised for pedestrian protection, with large stiffening ribs running diagonally across the inner surface.

Toyota Camry (2006)

The Toyota Camry was represented by three physical vehicles: a Toyota Camry tested by ANCAP in December 2006, a Toyota Aurion tested by ANCAP in February 2007, and a Toyota Camry tested in June 2009.

The Aurion model was based on the Camry and the bonnet design was found to be sufficiently similar that the results could be directly compared. A total of three test results were taken from ANCAP testing on the Toyota Aurion, and were compared with results from the later testing on a Toyota

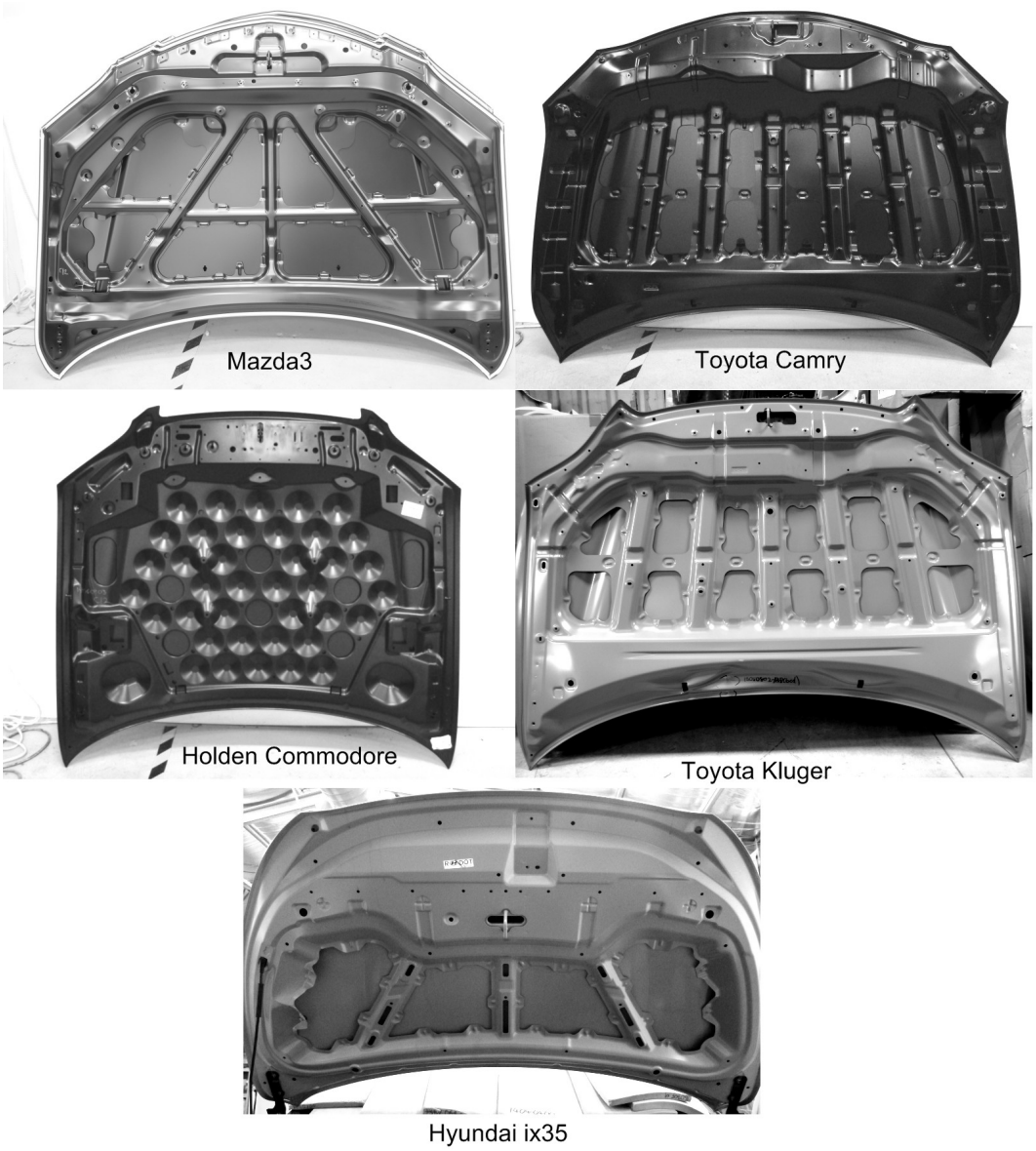

Figure 4.6: Underside of the bonnets for each vehicle.

Camry. These results were included in Set C.

The Toyota Camry and Toyota Aurion are classified as large cars by ANCAP. The underside of the bonnet appears to have been optimised for pedestrian protection, with multiple stiffening ribs that run the length of the bonnet between the front and rear bulkier sections.

Holden Commodore (2006)

The Holden Commodore was represented by three physical vehicles. The first was tested by ANCAP in December 2006, the second in June 2009, and the third in April 2010. The Holden Commodore is classified as a large car by ANCAP. The underside of the Commodore bonnet is a design common to General Motors vehicles (Kerkeling et al., 2005). The middle of the bonnet is supported by a second layer, which has been molded into a series of conical indentations.

The hinge mounting system for the Commodore also appears to have been modified for pedestrian protection, with the hinge mounting bolts entering the bonnet from the side. The more common, and more potentially dangerous, method is for the bolts to be directed upwards.

Toyota Kluger (2007)

The Toyota Kluger was represented by two physical vehicles. The first was tested by ANCAP in October 2007, and the second was tested in May 2008. The Toyota Kluger is classified as a large four wheel drive (4WD) by ANCAP. The underside of the bonnet is similar to that of the Toyota Camry.

Hyundai ix35 (2009)

The Hyundai ix35 was represented by one physical vehicle, tested in April 2010. The Hyundai ix35 is classified as a compact 4WD by ANCAP. The underside of the bonnet is similar to the Mazda3, however it has a much larger frontal bulkhead section. The stiffening ribs have sections removed along their length, which may act to reduce their stiffness.

4.3.2 Set A: Varying impact speeds

Set A contained results from 29 impact tests in which the impact speed was varied for tests using the same headform. There were seven locations tested, across three vehicle models: the Toyota Kluger (four locations), Holden Commodore (one location) and Hyundai ix35 (two locations). The full listing of tests in Set A can be found in Appendix A, Table A.1.

For every test in Set A, a headform weighing 3.5 kg with a diameter of 165 mm was used. This was either the ACEA 3.5 kg headform or the ISO 3.5 kg headform, as described in Section 4.1.1. All of the test locations in Set A were tested with at least three different speeds. In some cases the same speed was used more than once for the same location, these were included to give some idea of repeatability.

The test speeds used were in the range normally used for pedestrian impact testing, the lowest being 9.3 m/s (33.5 km/h) and the highest being 13.9 m/s (50.0 km/h). The impact angle for almost every test was 50° to the horizontal, the bonnet angle varied between test locations. The exception to this were three tests that were performed at a perpendicular impact angle. The reason for including these tests was so that the influence of impact angle could be also be captured in the results.

None of the tests in Set A were identified as involving bottoming out (contact between the bonnet and a harder structure below).

4.3.3 Set B: Different headforms

Set B contained results from 39 tests in which a constant impact speed was used for each location (within 0.2 m/s), but different headforms were used between tests. There were a total of 15 locations tested, across three vehicle models: the Toyota Kluger (12 locations), Holden Commodore (one location) and Hyundai ix35 (two locations). The full listing of tests in Set B can be found in Appendix A, Table A.2.

The impact speed for each test in Set B was approximately 11.1 m/s (40 km/h), with a minimum speed of 10.9 m/s and a maximum of 11.2 m/s. The normal component of the impact speed was also approximately constant (within 0.2 m/s) for each test location. However, the normal component of

the impact speed varied more across all of the test locations, with a minimum of 9.4 m/s and maximum of 11.2 m/s.

For each test on the same location, different headforms were used – this meant that there were differences in headform mass, but in some cases there was also a difference in headform diameter. The 2.5 kg headform had a diameter of 130 mm, while all of the other headforms had a diameter of 165 mm. There was also a difference in the moment of inertia between each headform.

One test location in Set B, with two tests, was identified as involving bottoming out. These two tests were conducted at 11.1 m/s on Location ID 9 (see Appendix A). The HIC values for these two tests were relatively low (848 and 834), so even though bottoming out occurred, it was assumed that it had little effect on the results.

4.3.4 Set C: Comparison between Euro NCAP and GTR child headform tests

Set C contained results from locations where two tests were conducted. The first test was conducted as a Euro NCAP Version 4 child headform test – i.e. a 2.5 kg headform, with an impact speed of 11.1 ± 0.2 m/s (40 km/h). The second test was conducted as a GTR child headform test – i.e. a 3.5 kg headform, with an impact speed of 9.7 ± 0.2 m/s (35 km/h). The impact angle was 50° for both tests.

There were a total of 28 tests included in Set C, across 14 different locations on three vehicle models. The vehicle models used were the Toyota Camry (five locations), Holden Commodore (three locations) and Mazda3 (six locations). The full listing of tests in Set C can be found in Appendix A, Table A.3.

None of the tests in Set C were identified as involving bottoming out.

4.3.5 Set D: Comparison between Euro NCAP adult and GTR child headform tests

Set D also contained results from locations where two tests were conducted. The first test was conducted as a Euro NCAP Version 4 adult headform test

– i.e. a 4.8 kg headform, with an impact speed of 11.1 ± 0.2 m/s (40 km/h). The second test was conducted as a GTR child headform test – i.e. a 3.5 kg headform, with an impact speed of 9.7 ± 0.2 m/s (35 km/h). The impact angle was 65° for the Euro NCAP test and 50° for the GTR test.

The reason for this comparison was that selected locations were tested with an adult headform under the Euro NCAP procedure, but would be tested with a child headform under the GTR. These are the locations that lie between wrap-around-distance values of 1500 and 1700 mm (see Section 2.2).

There were a total of six tests included in Set D, across three different locations, each on a different vehicle model. The vehicle models used were the Toyota Camry, Holden Commodore and Mazda3. The full listing of tests in Set D can be found in Appendix A, Table A.4.

None of the tests in Set D were identified as involving bottoming out.

4.4 Potential sources of error when comparing repeated tests

This section discusses sources of error that may be present when comparing two test results that were performed on the same location. There were no known important sources of systematic error, but there were various sources of error that may lead to variability in such a comparison.

The test setup and the nature of the testing make it difficult to eliminate all of these sources of error. Some attention is given to why each error may be minimal or how it has been reduced.

4.4.1 Aiming error

There is some level of inaccuracy in the aiming of the headform. The headform may not strike the exact same location twice. The accepted error in the Euro NCAP protocol, used by ANCAP, is 10 mm in any direction, and the CASR headform launching machine (B1) has been used extensively for this sort of testing. For this reason, it was considered reasonable to assume that the aiming error was within ±10 mm for each test location.

4.4.2 Potential structural differences

Tests were sometimes considered to be on the same location, where they had been performed symmetically on opposite sides of the bonnet. For example, if the first test had been performed on the left side of the bonnet, then the symmetrical location on the right hand side of the bonnet may have been used for the second test. This was done only when the structure of the bonnet was symmetrical (by visual inspection) and the bonnet was not contacting anything underneath during the impact. Despite this check, there may have been some structural differences between the left and right hand sides of the bonnet that were not apparent.

Another potential structural difference may have arisen from tests that were performed on a bonnet that was already damaged from a previous test. This was only done when the damage from the first test was not predicted to affect the location of the second test. This was judged by examining the area of bonnet that the first test affected, and comparing this to the area of the bonnet that the second test would be likey to affect. If those two areas did not intersect, then the second test was carried out. Again, despite this check, there may have been some structural differences between a test performed on a fresh bonnet and one performed on a previously damaged bonnet.

4.4.3 Differences in test equipment

As mentioned in Section 4.1.1, there were three different types of accelerometer used for the tests included in this study. Additionally, there were two different 3.5 kg headforms that were used. Some differences may have existed in the results produced by these pieces of equipment.

To address this problem, every headform and accelerometer combination was certified using the relevant certification procedure, either from the Euro NCAP or GTR test protocol. The accelerometers were all calibrated by their respective manufacturers at regular intervals, as a matter of standard laboratory procedure.

4.4.4 Repeatability

Finally, it is important to consider how the test results may vary even if the test conditions were not different between two tests on the same location. These differences may arise even if the structural differences are minimised (e.g. by using a fresh bonnet for both tests) and the exact same equipment is used.

For two tests conducted with the same headform, at the same speed, on the same location, some variation in the HIC and peak displacement could be expected. The calculation of HIC, in particular, can be very sensitive, and large variations may be possible for a relatively small variation in peak acceleration or pulse duration.

4.5 Summary

This chapter has described the method that was used for performing all of the headform tests used in this thesis. An elastic-powered launching device was used to fire the headform into the bonnet of the vehicle. This method was common to tests performed under the ANCAP and GTR test protocols, and for tests performed specifically for this thesis.

Following this was a description of the method used to estimate the peak displacement in each test. This method was based upon an assumption that the headform rolls along the surface of the bonnet. The linear accelerometer measurements were transformed into a normal and tangential component, and the normal acceleration was numerically integrated to find the normal displacement. The method was validated using a MADYMO simulation of a headform striking a flat surface.

Test data were described and were split into four different sets. Each of these data sets will be used in further chapters. Set A and Set B contained test results relating to the changes in HIC and peak displacement with either impact speed or headform mass. These results can be analysed to test the theoretical relationships presented in Chapter 3. This analysis is performed in the next chapter (Chapter 5). Set C and Set D contained test results that can be used compare the Euro NCAP and GTR test protocols. These

test results may also be compared to what is predicted by the theoretical relationships in Chapter 3. This analysis is performed later in Chapter 6.

Finally, a discussion is given on the potential sources of error that may exist when comparing two tests performed on the same location. There were no known systematic errors, but those listed may introduce some variability in the test results.

Chapter 5

Analysis of test data

In Chapter 3, two theoretical models were used to develop relationships that predicted the differences in HIC and peak displacement as a result of different test conditions. Chapter 4 described the data that was obtained from real headform tests. This chapter contains an analysis of that test data, the results of which are compared with the relationships predicted by the theoretical models.

The theoretical power law relationships for HIC and peak displacement were firstly linearised in terms of their exponents. A linear regression was then used to determine values of the exponents from the test results, which are then compared with the theoretical values.

The results of this chapter form a basis for predicting changes in HIC and peak displacement, for a given change in test conditions. These results are used in later chapters for comparing different test protocols.

5.1 Method

Data from real impact tests were used to examine the relevance and applicability of the theoretical models developed in Chapter 3. This section describes the method for analysing this data. The goal of the analysis was to use multiple linear regression to calculate values of the exponents a, b, α and β. These values could then be compared to those predicted by the theoretical models.

The software used to perform all regression analysis was SPSS Version 17.0[1].

5.1.1 General regression model

A general regression model was firstly developed for analysing the data.

Recall, from earlier, Equation 3.8:

$$\text{HIC} = 16 C_1 C_2^{3/2} k^{3/4} m^{-3/4} v_0^{5/2}$$

The above equation was written in a generalised form using the exponents a and b for mass and impact speed. The constants C_1 and C_2, as well as the location dependent stiffness k, were grouped into a single location dependent constant L.

$$\text{HIC} = L m^a v^b \tag{5.1}$$

Taking the logarithm of each side gives

$$\log(\text{HIC}) = \log(L) + a \log(m) + b \log(v) \tag{5.2}$$

This equation is in a linear form, for the unknown exponents a and b. The HIC, and the values of m and v were known for each test. The location-dependent component, $\log(L)$, was unknown.

The term $\log(L)$ was replaced with a linear combination of dummy variables representing each location. The dummy variables L_j were introduced, with j ranging from one to the number of locations in the data set. For a given test, each dummy variable was set to zero, unless it corresponded to the location for that test, in which case it was set to one. This system of dummy variables was used to prevent tests on different locations from being compared against each other in the regression.

Additionally, the 2.5 kg headform was smaller in diameter (130 mm) than the three other headforms used (165 mm). It was possible that the headform diameter had some effect on the test results that was not captured in the theoretical models. For this reason, an additional dummy variable

[1] SPSS, an IBM Company, Chicago, USA

was introduced to account for headform diameter in the regression: D_{165} was set to zero for the 2.5 kg headform impacts, and one otherwise.

Thus, the final form of the equation was as follows:

$$\log(\text{HIC}) = a\log(m) + b\log(v) + d_{165}D_{165} + l_1L_1 + l_2L_2 + \cdots \tag{5.3}$$

In this form, multiple regression could be used to find empirical values for a, b, d_{165} and l_j. If the real impact tests behaved similarly to the linear spring model, then the exponents a and b would be expected to equal -0.75 and 2.5, respectively.

The results from simulations using the damped Hertz model give some indication of how these exponents might vary from those predicted in the linear spring model. The damped Hertz model suggests a normal force $F = kx^n(1 + c\dot{x})$. For values of n greater than one, the value of a decreased and b increased. For values of the damping factor c greater than zero, a was unaffected, but the value of b initially decreased, and then increased for values of c greater than about 0.05.

A similar regression was used to estimate values for the exponents in the equation for peak displacement. Recall Equation 3.7:

$$S = \sqrt{\frac{m}{k}}v_0$$

This equation was rewritten in a more general form:

$$S = \Lambda m^{\alpha}v^{\beta} \tag{5.4}$$

Again, the stiffness term was replaced with a general constant Λ, which was dependent upon the location being tested. The exponents of mass and velocity were replaced with α and β.

After taking the logarithm of both sides, this becomes:

$$\log(S) = \log(\Lambda) + \alpha\log(m) + \beta\log(v) \tag{5.5}$$

Again, m and v were known for each test, and S had been estimated from the measured acceleration data (see Chapter 4, Section 4.2).

D_{165} and L_j were used to account for headform diameter and location, as in Equation 5.3. Thus, the final equation for peak displacement had the following form:

$$\log(S) = \alpha \log(m) + \beta \log(v) + \delta_{165} D_{165} + \lambda_1 L_1 + \lambda_2 L_2 + \cdots \tag{5.6}$$

Multiple regression was used to find empirical values for α, β, δ_{165} and λ_j. If the linear spring model were an appropriate way to describe the behaviour of real tested structures, then the exponents α and β would be expected to equal 0.5 and 1.0, respectively.

Again, the results from simulations using the damped Hertz model gives some indication of how these exponents might vary: with increasing values of n, both α and β decreased. With increasing values of c, β decreased and α was unaffected.

5.1.2 Regression model for impact speed only

The regression model was used for multiple tests on the same locations, in which the same headform was used, but the impact speed was varied.

For these cases, the mass m was constant for each test on a given location, and the value of D_{165} was also constant for each location. In effect, these variables became part of the location dependent components (L_i) of the regression equation.

Thus, the mass and diameter terms could be eliminated from the regression equation and the regression equation for HIC became:

$$\log(\text{HIC}) = b \log(v) + l_1 L_1 + l_2 L_2 + \cdots \tag{5.7}$$

And for displacement:

$$\log(S) = \beta \log(v) + \lambda_1 L_1 + \lambda_2 L_2 + \cdots \tag{5.8}$$

These two equations were used to estimate values for b and β from the test data.

The value of v was taken from the normal component of the measured impact speed, v_{n0}.

The normal component was calculated using the known angle between the initial trajectory of the headform and bonnet surface, θ_0. The normal component of the impact speed was calculated as follows:

$$v_{n0} = v_0 \sin(\theta_0) \tag{5.9}$$

The normal impact speed was used in the regression, as the acceleration in the normal direction was found to be dominant compared with tangential component. It is reasonable to expect that the effect of impact speed on HIC would be mainly determined by the forces acting in the normal direction.

This was confirmed by the inclusion of tests that were conducted perpendicular to the bonnet surface, with their test speed matching the normal impact speed of a previous test. These tests produced similar HIC values to the original, non-perpendicular tests.

5.1.3 Regression model for headform mass and diameter

The general regression model was also used for multiple tests on the same location, in which different headforms were used, but the impact speed remained relatively constant. The general model was simplified to remove the influence of impact speed.

Ideally the impact speeds would be identical for all tests used in such a regression, however in practice the test equipment has some variation. This variation in impact speed was minimised between tests, usually within 0.1 m/s, or 0.2 m/s at the most. Despite this relatively small tolerance this may mean a significant change in HIC, compared with the desired impact speed. For example, at a test speed of 10 m/s, a difference of 0.2 m/s in impact speeds is a 2% difference, which implies a 5% change in HIC via the linear spring model.

These relatively small variations in impact speed were corrected for by adjusting the HIC values for each test. This was done by choosing an adjusted impact speed, v_{adj}, for all tests performed on a given location. Although in theory any speed could be used, the average impact speed for the

tests on that location was used to minimise the error in this process.

The linear spring model implies that an adjusted HIC value can be calculated using the following relation:

$$\mathrm{HIC}_{adj} = \mathrm{HIC}_0 \left(\frac{v_{adj}}{v_0} \right)^{2.5} \tag{5.10}$$

In this equation, HIC_0 and v_0 are the original HIC value and impact speed. The adjusted HIC values are representative of what would be likely to occur if exactly the same impact speed was achieved for each test on a given location.

Similarly, peak displacement was adjusted as follows:

$$S_{adj} = S_0 \left(\frac{v_{adj}}{v_0} \right) \tag{5.11}$$

If these adjusted values were used in the regression, then for tests on the same location, the effective impact speeds were all the same value (v_{adj}). Thus, the impact speed term effectively became part of the location dependent part of the equation, and could be removed.

Thus, the regression equation for HIC was:

$$\log(\mathrm{HIC}_{adj}) = a \log(m) + d_{165} D_{165} + l_1 L_1 + l_2 L_2 + \cdots \tag{5.12}$$

And for peak displacement:

$$\log(S_{adj}) = \alpha \log(m) + \delta_{165} D_{165} + \lambda_1 L_1 + \lambda_2 L_2 + \cdots \tag{5.13}$$

These two regression equations were used to estimate values for a and α from the test data. Values for d_{165} and δ_{165} were also estimated.

5.2 Results

This section describes the results of analysing the test data using the regression method described in the previous section. The test data was analysed in order to estimate values for the exponents a, b, α and β. The values of

these exponents were compared to what was predicted by the theoretical models in Chapter 3.

The logarithm used for all plots in this section was base 10.

5.2.1 Effect of normal impact speed on HIC

Figure 5.1 shows the dependence of HIC on normal impact speed for each test location in Set A. The logarithm of HIC is plotted against the logarithm of normal impact speed. For each impact location, a linear trendline was generated using Microsoft Excel[2] and is displayed on the figure. The coefficient of x in each trendline equation was the effective estimate for b in the impact model for that location.

Figure 5.2 shows the same data, but on a linear scale. In this case, a power function trendline has been fitted to the results on each impact location. The exponent of x in each trendline equation are the estimates for b, and correspond to the coefficients shown in Figure 5.1. The linear scale plot also demonstrates a good fit between the power functions and the data.

The coefficients for x in Figure 5.1 varied from 1.61 to 3.04. However, on average, the coefficients were close to 2.5. The test results for each location exhibited strong linearity on the logarithmic scale, which is supported by the R^2 values being close to 1. This would seem to confirm that a power relationship is appropriate for relating HIC and normal impact speed. Although, due to the relatively small variation in impact speed, this linearity may be exaggerated.

The two locations producing the lowest and highest slopes in Figure 5.1 were locations 1 and 4. These locations also produced the highest HIC values. Both of these locations were on the front edge of the bonnet of the Toyota Kluger, which in this area was resting against a strong support rail. These locations were different to most of the other impacts, which were conducted in a more central, unsupported area of the bonnet. This difference in structure may explain why the relationship of HIC to impact speed was different for these locations.

The data in Set A were also used in a multiple regression based on

[2]Version 11, Microsoft Corporation, Redmond, USA

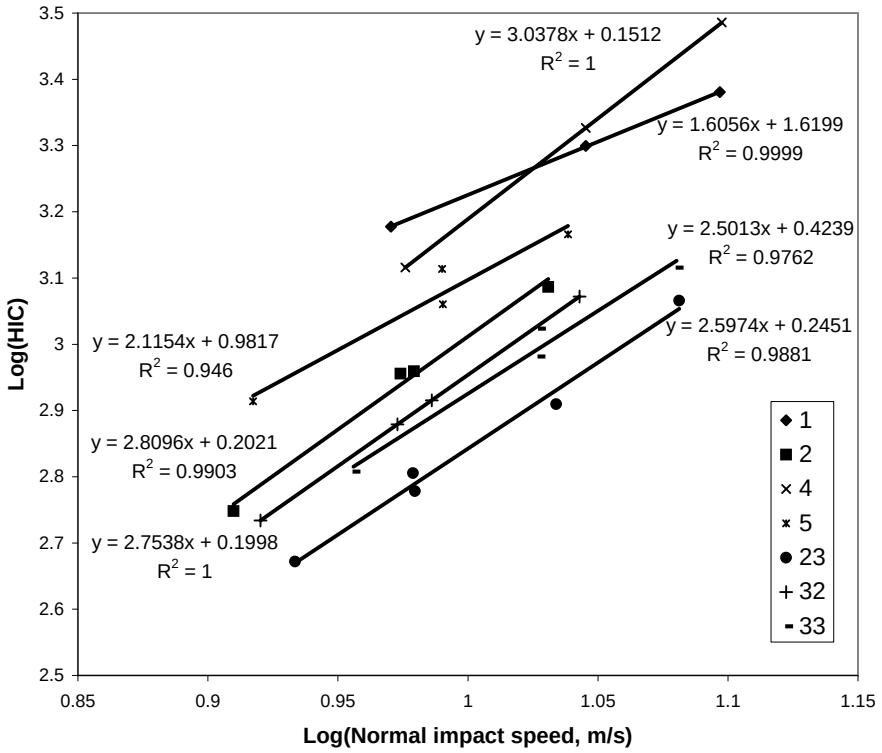

Figure 5.1: HIC versus normal impact speed for test locations in Set A, logarithmic scale.

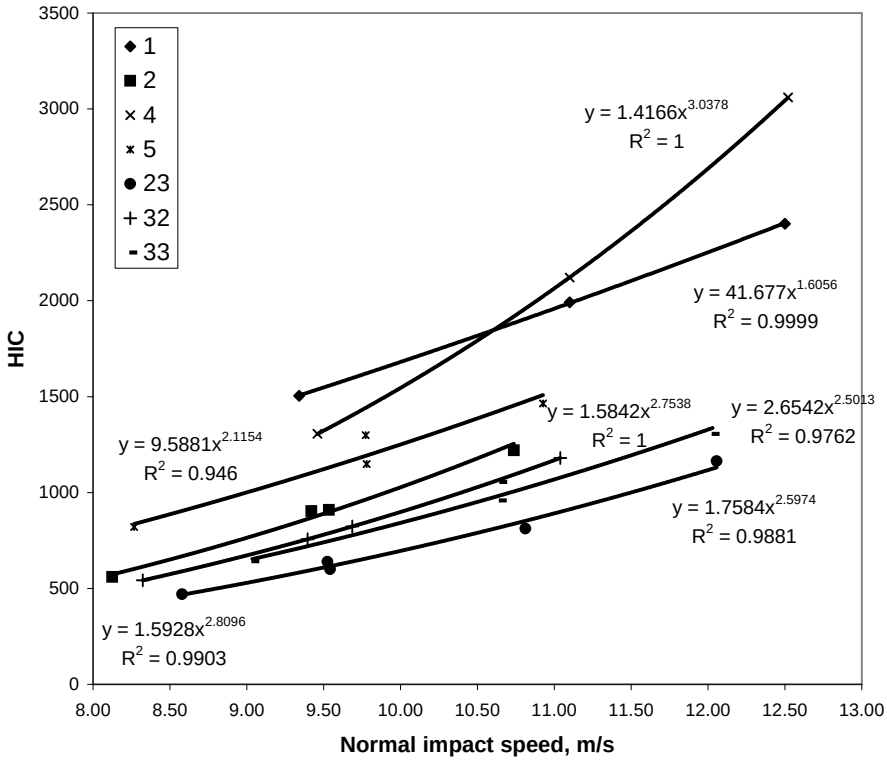

Figure 5.2: HIC versus normal impact speed for test locations in Set A, linear scale.

Equation 5.7, using SPSS. The regression results gave a value for b of 2.491 (95% CI = 2.221–2.760, R^2 = 0.983). This indicated that the theoretical value of 2.5 obtained from the linear spring model was close to the average effect of normal impact speed on HIC in these data.

5.2.2 Effect of normal impact speed on peak displacement

The effect of normal impact speed on peak displacement was analysed in a similar fashion to its effect on HIC (in the previous section).

Figure 5.3 is a plot of peak displacement and normal impact speed on a logarithmic scale. Again, the coefficients for x on each trendline in Figure 5.3 indicate an estimate of β for that impact location. The linear fit appears to be appropriate, indicating that a power relationship between peak displacement and normal impact speed is reasonable. The R^2 values are generally close to one, however two locations have R^2 values of around 0.8, indicating a poorer fit.

Figure 5.4 illustrates the same data but on a linear scale, with fitted power functions for each impact location. In this case, the exponents of x are the estimates for β, and correspond to the trendline coefficients in Figure 5.3. The power functions are close to linear, indicating that the estimate of β is close to one.

Except for one location, the coefficients shown in Figure 5.3 are all lower than the theoretical value of 1.0 given by the linear spring model.

This result was confirmed by performing a multiple regression on the data in Set A. The regression results gave a value for β of 0.799 (95% CI = 0.648–0.950, R^2 = 0.968). The upper 95% confidence limit for β was 0.950, so the linear spring value of 1.0 lay outside the 95% confidence interval.

This indicates that the effect of impact speed on peak displacement was slightly weaker than what is predicted by the linear spring model. Using the damped Hertz contact model, the effect of increasing n and/or c was to decrease the value of β. This indicates that for more complex contact models, a lower value of β can be expected and this might explain the variation in the results. The same variations on the contact model had both a positive and negative effect on b, which could explain why the empirical

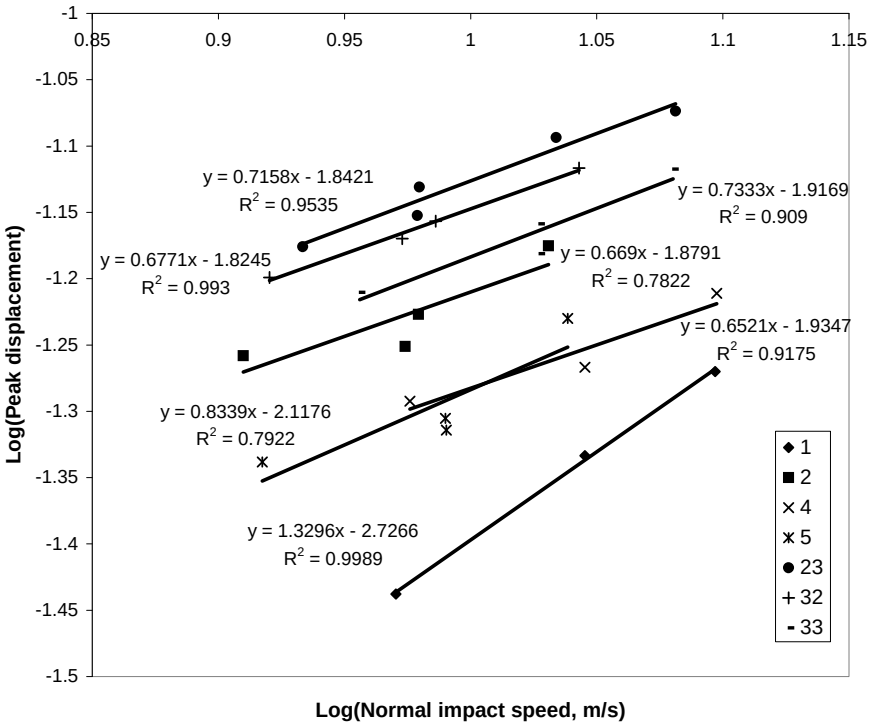

Figure 5.3: Peak displacement versus normal impact speed for test locations in Set A, logarithmic scale.

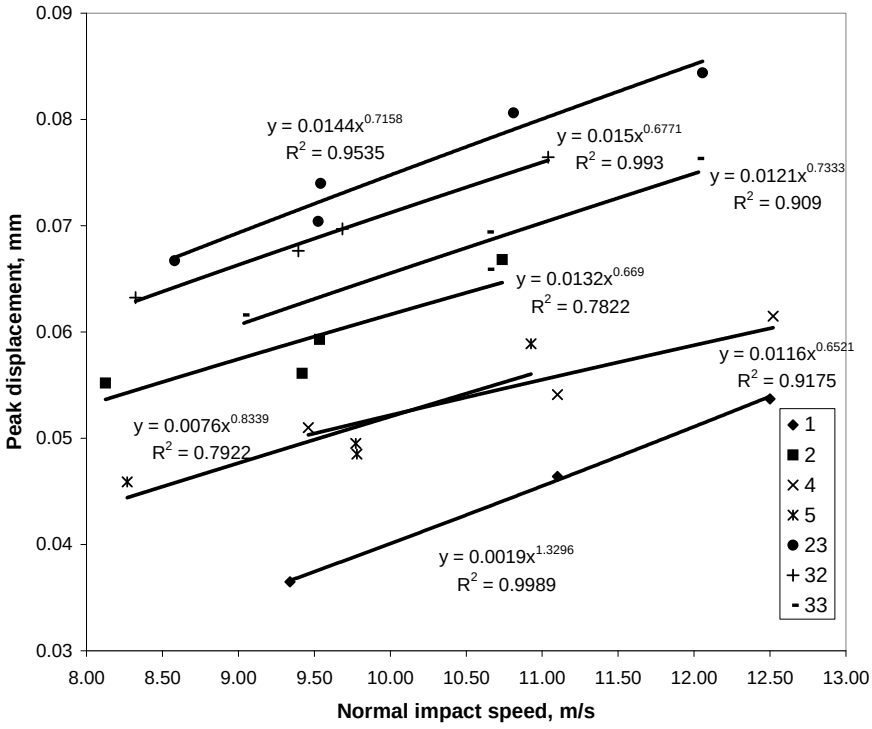

Figure 5.4: Peak displacement versus normal impact speed for test locations in Set A, linear scale.

value of b is still close to the value obtained using the linear spring.

The regression result indicates that a value of 0.8 for β may be a reasonable estimate of the average influence of normal impact speed on peak displacement.

5.2.3 Effect of headform mass and diameter on HIC

A similar analysis was performed on the data in Set B, to examine the effect of headform mass and diameter on HIC. In this data set, the normal impact speed for each location was relatively constant for each location (within 0.2 m/s), but different headforms were used for each test on the same location. The HIC and peak displacement values were adjusted based on a standardised normal impact speed v_{adj} for each location, using the method described in Section 5.1.3.

There were four different headform masses used in Set B: 2.5 kg, 3.5 kg, 4.5 kg and 4.8 kg. The 2.5 kg headform had a diameter of 130mm, while the three other headforms had a diameter of 165mm.

Figure 5.5 shows the relationship between headform mass and HIC for test locations in Set B. Locations with only a 4.5 and 4.8 kg headform test were excluded from this figure. Tests performed with a 2.5 kg headform were also excluded from this figure, to ignore any influence of diameter. For each location, a linear trendline was fitted. The equation for each trendline is shown, and the coefficients for x are the estimated values of a for each location. The linear spring model predicted a value for a of -0.75.

The results in Figure 5.5 imply that the value of a may vary substantially depending on the test location, and the theoretical value of -0.75 may not be an appropriate choice for all scenarios.

The theoretical models explored in Chapter 3 were derived for linear one-dimensional impacts and as such these models did not contain a prediction for the effect of diameter. For the test locations that were tested with a 2.5 kg and a 3.5 kg headform, there was a change in headform mass as well as a change in diameter. These test locations are shown in Figure 5.6. The values for a are given by the coefficients of x in each trendline equation, and are generally higher in magnitude compared with those in Figure 5.5. This

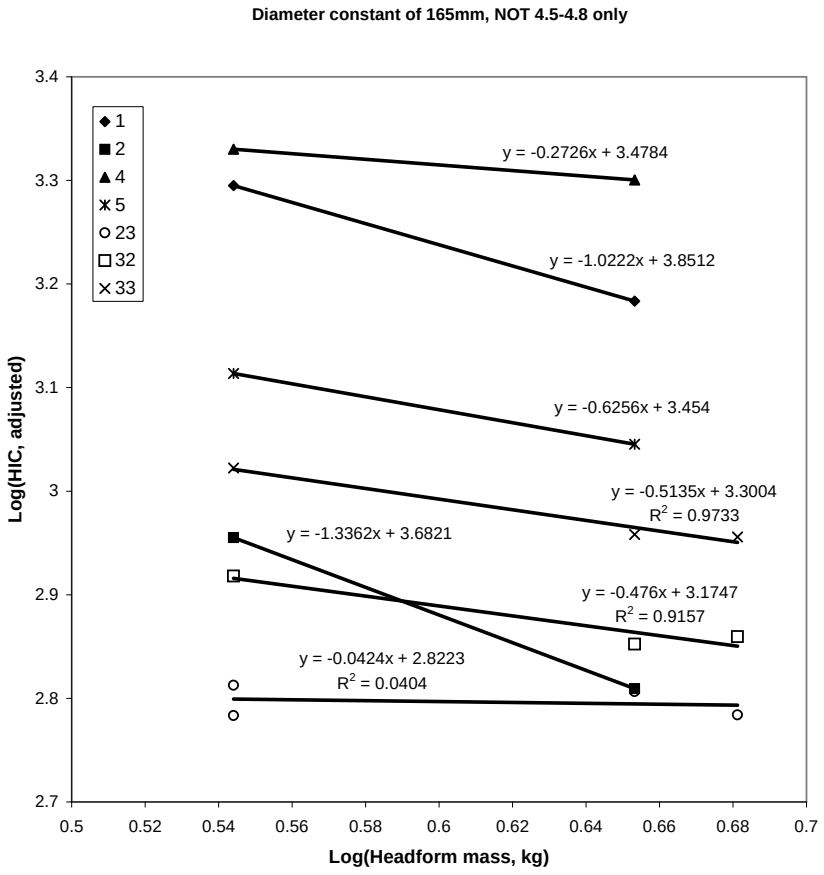

Figure 5.5: HIC versus headform mass for test locations in Set B, 165mm headforms only.

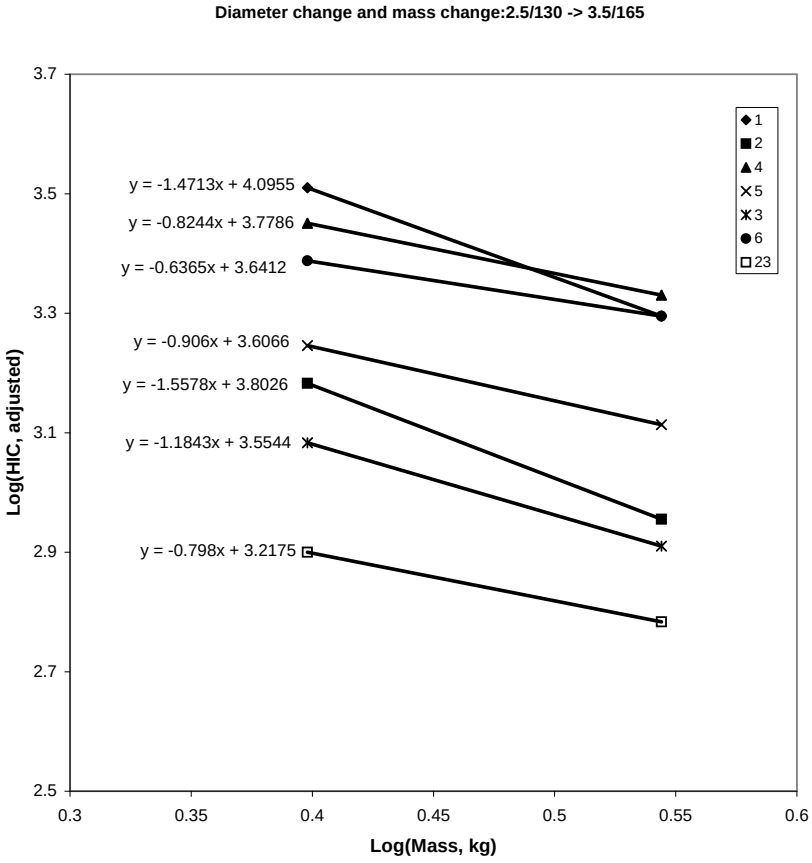

Figure 5.6: HIC versus headform mass for test locations in Set B, 2.5 kg (130mm) and 3.5 kg (165mm) headforms.

indicates that when the diameter and mass both increased, the reduction in HIC was greater.

The data from Set B, including all locations and test results, were used in a multiple regression in SPSS; the regression equation was Equation 5.12. The value for a found by the regression was -0.540 (Standard error = 0.165, $R^2 = 0.98$), with a 95% confidence interval of (-0.882, -0.197). The value for d_{165} was -0.076 (Standard error = 0.037), with a 95% confidence interval of (-0.153, 0.001).

The average effect of headform mass alone, given by a, was less than what the theoretical linear spring model predicted. However, the theoretical value of $a = -0.75$ was included in the 95% confidence interval. The damped-Hertz model predicted lower values of a for increasing values of n, which

might explain why the empirical value of a was lower than the value predicted by the linear spring model. The size of the confidence interval implies that there is some uncertainty in the empirical value of a.

The value of d_{165} implies that moving from a diameter of 130mm to 165mm generally resulted in lower HIC values. However, the 95% confidence intervals for this value included zero, indicating some uncertainty in this result and a large potential variation.

The regression was also performed excluding all 2.5 kg headform tests. As such, the diameter term could be left out of the model. The value of a found in this regression was -0.528 (Standard error = 0.124, $R^2 = 0.98$), with a 95% confidence interval of (-0.792, -0.264). This value is consistent with the result that included the 2.5 kg headform tests and the 95% confidence interval includes the theoretical value of -0.75.

5.2.4 Effect of headform mass and diameter on peak displacement

The data in Set B were also used to investigate the effect of headform mass and diameter on peak displacement. The adjusted value of peak displacement was used for each test, as described in Section 5.1.3.

Figure 5.7 shows the relationship between peak displacement and headform mass for the locations in Set B. This plot excludes tests conducted with a 2.5 kg headform, and thus only shows tests conducted with a 165mm headform. Locations with only a 4.5 kg and 4.8 kg test were also excluded from his plot for clarity.

Figure 5.8 shows the relationship between peak displacement and headform mass, but includes the effect of a change in diameter. Only tests performed with a 2.5 kg or 3.5 kg headform are shown, which also includes a change in diameter from 130mm to 165mm.

The coefficients of x for each trendline give an estimate for α. The theoretical value of α for the linear spring model is 0.5.

The estimated values of α from Figure 5.8 were generally higher than those in Figure 5.7. This indicates that the effect of a change in diameter had an additional positive effect on the peak displacement that is not captured

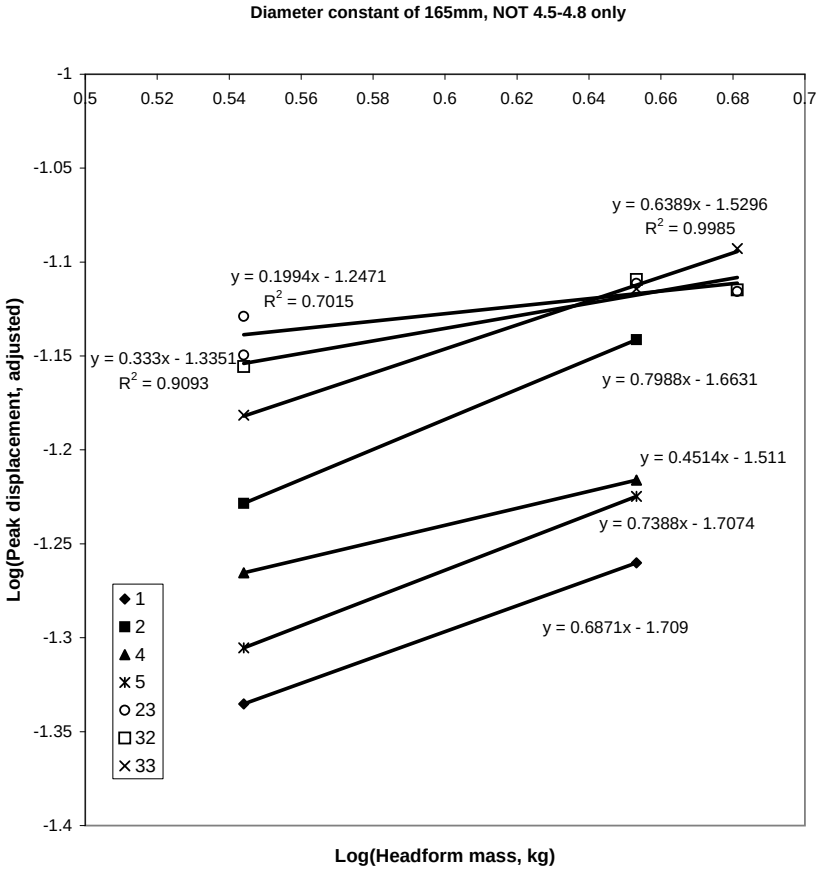

Figure 5.7: Peak displacement versus headform mass for test locations in Set B, 165mm headforms only.

in the theoretical models.

A regression analysis was performed on the data in Set B, based on Equation 5.13. All of the test results in Set B were included, and the adjusted peak displacement values were used.

The regression gave a value for α of 0.475 (95% CI = 0.273–0.676, R^2 = 0.97), which was close to theoretical value of 0.5 predicted by the linear spring model. The same regression gave a value for δ_{165} of 0.075 (95% CI = 0.030–0.120). This confirmed that a change in headform diameter from 130 mm to 165 mm had an additional positive effect on the peak displacement.

The regression was also performed excluding the 2.5 kg headform tests from Set B. The remaining tests had a constant headform diameter of 165mm and so the diameter term could be removed from the regression equation.

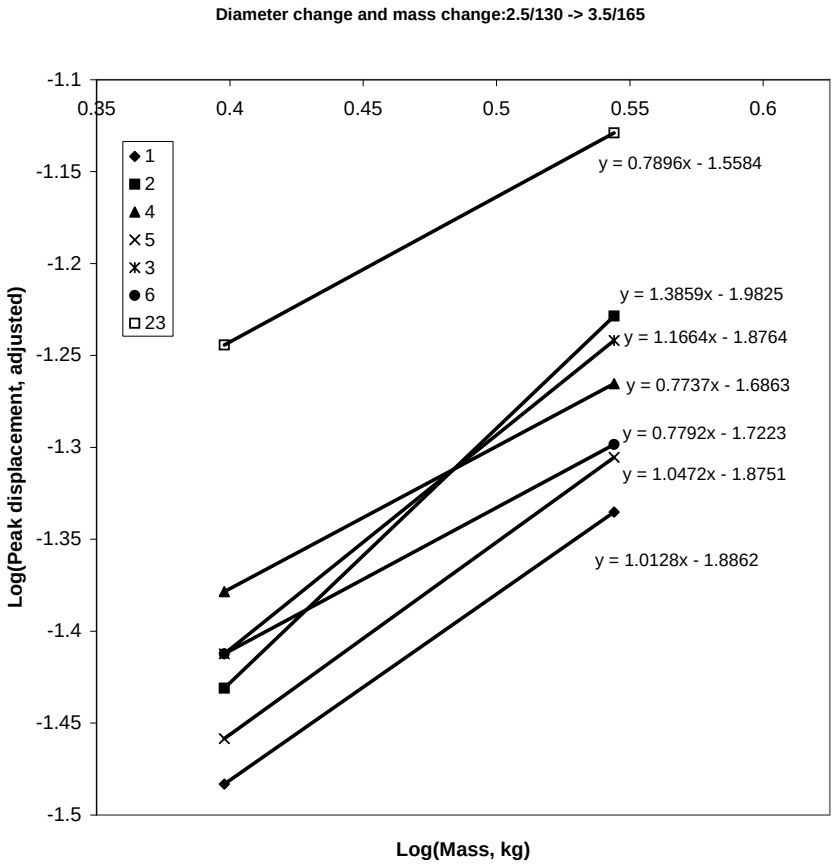

Figure 5.8: Peak displacement versus headform mass for test locations in Set B, 2.5 kg (130mm) and 3.5 kg (165mm) headforms.

The resulting value for α was 0.478 (95% CI = 0.332–0.625, R^2 = 0.97), which was consistent with the result that included the 2.5 kg headform tests.

These results indicate that the theoretical value of α obtained from the linear spring model was a good estimate for the average effect of headform mass on peak displacement. The peak displacement was also postively affected by the headform diameter.

5.2.5 Combined effects

Set A and Set B were combined in a regression for the effects of normal impact speed, headform mass and diameter on HIC. This was based on the general regression model as given by Equation 5.3. A similar regression for peak displacement was performed, based on Equation 5.6. The reason for doing this was to confirm that the combined data would not produce a different result to the two sets being considered individually.

The original normal impact speed from each test was used in this regression, not the adjusted values that were used in the regression for mass and diameter only. Thus, the effect of any minor speed variations in Set B would also be captured in the results.

Some test results were included in both data sets, so the total number of tests in Set AB was not equal to the sum of the number of tests in each set. The combined Set AB consisted of 59 tests on 15 test locations across three vehicle models.

The distribution of headform masses and normal impact speeds in Set AB is shown in Figure 5.9. This plot shows that the majority of tests were conducted with the 3.5 kg headform, and this headform was used for the widest range of normal impact speeds.

The results from the regression for HIC are given in Table 5.1, and the results from the regression for peak displacement are given in Table 5.2. Both regressions were repeated with the 130 mm (2.5 kg) diameter headform excluded, with no meaningful change in the results.

The results in Table 5.1 and 5.2 were consistent with the results of the regressions that considered Sets A and B separately. One difference is that

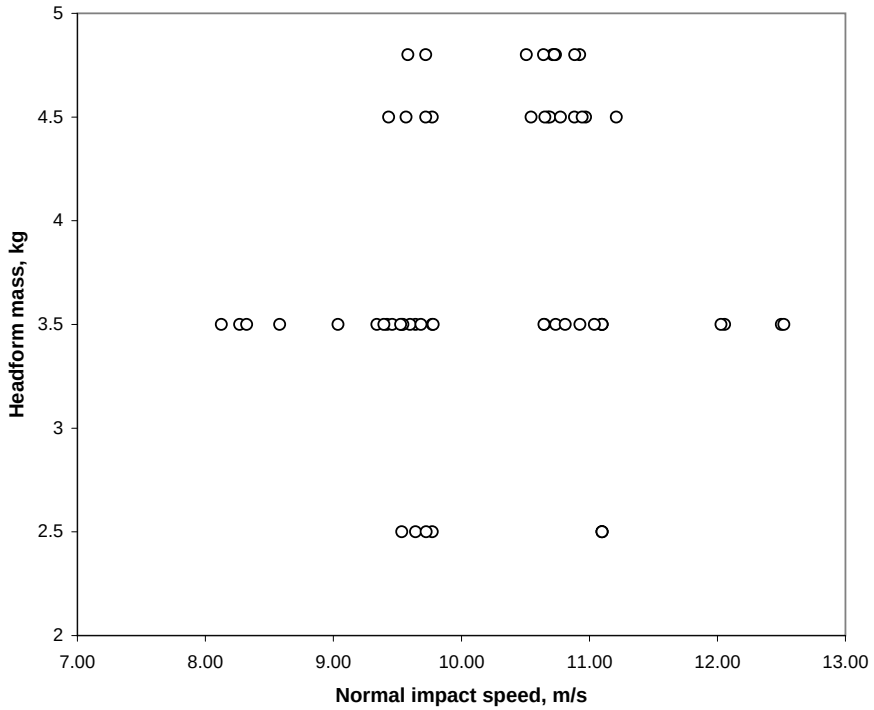

Figure 5.9: Distribution of normal impact speed and headform mass in combined Set AB.

Result	Value	95% CI	
a	-0.439	-0.682	-0.197
b	2.489	2.170	2.808
d_{165}	-0.104	-0.157	-0.051
R^2	0.975		

Table 5.1: Multiple regression results for estimating exponents a and b from combined Set AB

Result	Value	95% CI	
α	0.436	0.299	0.572
β	0.801	0.621	0.981
δ_{165}	0.085	0.056	0.115
R^2	0.982		

Table 5.2: Multiple regression results for estimating exponents α and β from combined Set AB

the confidence interval for d_{165} was smaller and did not include zero, which indicates that there was a definite effect of diameter on HIC in these data. The confidence interval for a was also smaller, and did not include the value of -0.75, as predicted by the linear spring model. This indicates that the value of -0.75 is not likely to be an appropriate selection for a, but the large variation in test results also indicates that a single value for a is not always appropriate for all test locations.

5.3 Summary

We can consider two headform impact tests on the same location: the first with normal impact speed v_1 and headform mass m_1, and the second with normal impact speed v_2 and headform mass m_2. If we know that the HIC from the second test is HIC_2 and that the peak displacement is S_2, then we can estimate the values of HIC_1 and S_1 using the following relationships:

$$\text{HIC}_1 = \text{HIC}_2 \left(\frac{m_1}{m_2}\right)^a \left(\frac{v_1}{v_2}\right)^b \tag{5.14}$$

$$S_1 = S_2 \left(\frac{m_1}{m_2}\right)^\alpha \left(\frac{v_1}{v_2}\right)^\beta \tag{5.15}$$

The value of the exponents a, b, α and β were predicted using a linear spring model in Chapter 3. This model suggested values of 2.5, -0.75, 0.5 and 1, respectively. A more complicated damped Hertz model suggested that all of these exponents may vary for more complex contact characteristics.

Data from Set A were used to test the influence of normal impact speed on HIC and peak displacement. The linear spring model was found to be a reasonable representation of the effect of normal impact speed on HIC in these tests. However, the effect of normal impact speed on peak displacement was weaker than what was predicted by the linear spring model.

Data from Set B were used to test the influence of headform mass and diameter on HIC and peak displacement. The influence of headform mass on HIC varied for different test locations, but on average seemed to be weaker than what was predicted by the linear spring model. The influence of headform mass on peak displacement was also found to have a varying

effect depending on the test location, but on average was close to what was predicted by the linear spring model.

A change in headform diameter was found to have an effect on both HIC and peak displacement. This effect was not predicted by the linear spring model, which was only representative of a one-dimensional impact. The effect of headform diameter could not be considered in isolation, as it was not possible to vary the headform diameter without also changing the headform mass. However, the analysis of test data suggested that an increase in headform diameter from 130mm to 165mm caused a reduction in HIC and an increase in peak displacement.

It is worth noting that none of the test results analysed in this chapter included the effect of bottoming out. Results from tests that bottomed out would be unlikely to follow the smooth relationship predicted by the linear spring model, due to the sudden increase in stiffness when contact is made with a harder structure below the bonnet surface. Thus, they would require analysis in two parts: impacts at speeds that do not bottom out, and impacts at speeds high enough to cause bottoming out. Such an analysis would be more complex than what has been done in this chapter, and was considered outside the scope of this thesis. For tests that may potentially bottom out, the relationships developed in this chapter for peak displacement may be used to predict the conditions under which bottoming out would occur. Such a process is described further in the next chapter.

Chapter 6

Conversion of HIC values from Euro NCAP to the GTR

In this chapter, two specific test protocols are considered. The first protocol is Version 4 of the Euro NCAP test protocol, which was used by ANCAP up until 2009 (Euro NCAP, 2008). The second is the test protocol for the GTR on pedestrian safety (UNECE, 2009).

As described in Chapter 2, each of these protocols specifies different test conditions. The GTR protocol specifies a lower impact speed than the Euro NCAP test protocol and while the current version of the Euro NCAP protocol specifies the same headforms as the GTR, they were different under the earlier Version 4.

The purpose of this chapter is to develop a method for converting a test result obtained under the Euro NCAP test procedure to an equivalent GTR test result. The reason for doing this was to form a basis for predicting the performance of vehicles under the GTR, based on their ANCAP test results. The ANCAP test results included in this thesis were obtained using Version 4 of the Euro NCAP test protocol, which is why that protocol is considered here, and not the more recent Version 5 protocol. For the remainder of this chapter, the use of 'Euro NCAP' is intended to indicate Version 4 of the Euro NCAP pedestrian testing protocol. It does not represent Euro

Category	WAD range	ANCAP headform	GTR headform
1	1000 – 1500 mm	Child, 2.5 kg	Child, 3.5 kg
2	1500 – 1700 mm	Adult, 4.8 kg	Child, 3.5 kg
3	1700 – 2100 mm	Adult, 4.8 kg	Adult, 4.5 kg

Table 6.1: Categories of test location by wrap around distance (WAD).

NCAP as an organisation, all of the physical test results were from testing conducted by ANCAP.

Each headform test location was classified into one of three categories, depending upon its wrap around distance (WAD) measurement. Category one included locations in the WAD range of 1000–1500mm, which would be tested with a child headform under both the Euro NCAP and GTR test protocols. Category two included locations in the WAD range of 1500–1700mm, which would be tested with an adult headform under Euro NCAP and a child headform under the GTR test protocol. Category three included locations in the WAD range of 1700–2100mm, which would be tested with an adult headform under both protocols. The three categories are summarised in Table 6.1.

All of the locations in all categories would be expected to lie on the bonnet of the vehicle, and not on the windscreen. The testable area in the GTR protocol does not extend beyond the rear edge of the bonnet; as such there is no reason to compare any test locations that do not lie on the bonnet.

For each category, there were three different methods considered for converting a Euro NCAP HIC value to an equivalent GTR HIC value. The first method was to use the power law that was developed using the linear spring model, with the theoretical values of the exponents a and b. The second method was to use the same power law, but using the exponent values that were found empirically in the previous chapter. The third method was to examine back-to-back results for tests conducted on the same location under both the Euro NCAP and GTR test conditions. Depending on the category of the test location, there were some differences in how each of these methods were applied.

The following three sections discuss the HIC conversion process for each

Condition	Euro NCAP	GTR
Impact speed, m/s	11.1	9.7
Impact angle, °	50	50
Headform mass, kg	2.5	3.5
Headform diameter, mm	130	165

Table 6.2: Test conditions for child Euro NCAP and child GTR locations (Category one).

category seperately. This is followed by a section discussing the predicted changes in peak displacement and how this might affect the HIC conversion process due to 'bottoming out'. The final section of this chapter contains a summary and discussion of the results.

6.1 Category one: child Euro NCAP to child GTR

Locations lying between wrap around distance values of 1000 mm and 1500 mm are tested with a 'child' headform under both the Euro NCAP and GTR testing protocols.

The test conditions under each protocol for locations in this category are summarised in Table 6.2.

For these locations, there are differences in impact speed, headform mass and headform diameter between the two test protocols.

6.1.1 Estimated HIC ratio using theoretical exponents

In Chapter 4, the effect of impact speed on HIC was predicted using a linear spring model and this effect closely matched the test results in Sets A and B. The effect of headform mass on HIC was also predicted using the linear spring model, however this effect did not closely match all of the test results in Sets A and B. An effect of headform diameter on HIC was not modelled analytically, but an effect was found to be present in the test data.

Excluding the effect of headform diameter, the theoretical change in HIC for these locations was estimated using Equation 5.14. The values for v_1, v_2, m_1 and m_2 were taken from Table 6.2 for the GTR and Euro NCAP test conditions. Using these values, the theoretical ratio of the GTR HIC to the

Euro NCAP HIC was given by the following equation:

$$\frac{\text{HIC}_G}{\text{HIC}_E} = \left(\frac{3.5}{2.5}\right)^a \left(\frac{9.7}{11.1}\right)^b \tag{6.1}$$

Note the subscript 'G' for the GTR value and the subscript 'E' for the Euro NCAP value. The impact angle is constant between the two protocols, so the ratio of normal impact speeds was the same as the ratio of total impact speeds.

Initially, this expression was evaluated using the values of a and b obtained from the linear spring model, which were -0.75 and 2.5 respectively. Using those values, the resulting HIC ratio is 0.555. However, this result neglects any effect of the change in headform diameter.

6.1.2 Estimated HIC ratio using empirical exponents and the effect of diameter

The linear regression in Chapter 5 was used to estimate a value for d_{165}, which was a coefficient for a binary variable that was set to one when the diameter of the headform was 165 mm and zero for a diameter of 130 mm. The value of d_{165} was include in Equation 6.1 as follows:

$$\frac{\text{HIC}_G}{\text{HIC}_E} = 10^{(d165)} \left(\frac{3.5}{2.5}\right)^a \left(\frac{9.7}{11.1}\right)^b \tag{6.2}$$

The values for a, b and d_{165} were taken from the combined regression results in Table 5.1 and were -0.439, 2.489 and -0.104, respectively. Using these values, the predicted HIC ratio is 0.485. This value is less than the value obtained using the theoretical linear spring relationship; this is expected, as the linear spring relationship makes no allowance for the decrease in headform diameter, which was shown to cause a reduction in HIC in the test data.

6.1.3 Analysis of data in Set C

A more direct estimate of the HIC ratio was made using the test results from the 14 locations in Set C. At each location, a Euro NCAP child test and a GTR child test had been performed. Using these data it was possible

to make a direct comparison of the HIC values obtained under each set of test conditions.

The test speed was as close to the specified impact speed as possible for each test (within ±0.2 m/s). To correct for any minor variation in test speed, the adjustment method detailed in Section 5.1.3 was used to adjust the HIC values:

$$\mathrm{HIC}_{adj} = \mathrm{HIC}_0 \left(\frac{v_{adj}}{v_0} \right)^{2.5} \tag{6.3}$$

The value for v_{adj} was 11.1 m/s for the Euro NCAP test, and 9.7 m/s for the GTR test. The value for v_0 was the original measured impact speed for each test, and the value of HIC_0 was the measured HIC value.

The adjusted HIC values for each test location are shown in Figure 6.1. The line of best fit is based on a linear regression performed using SPSS and has a slope of 0.495 (with a zero intercept). The standard error for this estimate was 0.022 and the 95% confidence interval was (0.447, 0.542). Note that this confidence interval includes the value of 0.485 that was estimated using the Chapter 5 regression results, but does not include the value of 0.555 that was estimated using the linear spring model.

This result indicates that for locations in category one, the HIC obtained in a GTR test is approximately one half of the HIC value obtained in an Euro NCAP test. This is consistent with what was predicted using the regression results from Chapter 5, including the effect of diameter, and slightly lower than what would be expected using the linear spring model, with no allowance for the change in headform diameter.

6.2 Category two: adult Euro NCAP to child GTR

Locations lying between wrap around distance values of 1500 mm and 1700 mm are tested with an 'adult' headform under the Euro NCAP testing protocol, but are tested with a 'child' headform under the GTR testing protocol.

The test conditions under each protocol for locations in this category are summarised in Table 6.3.

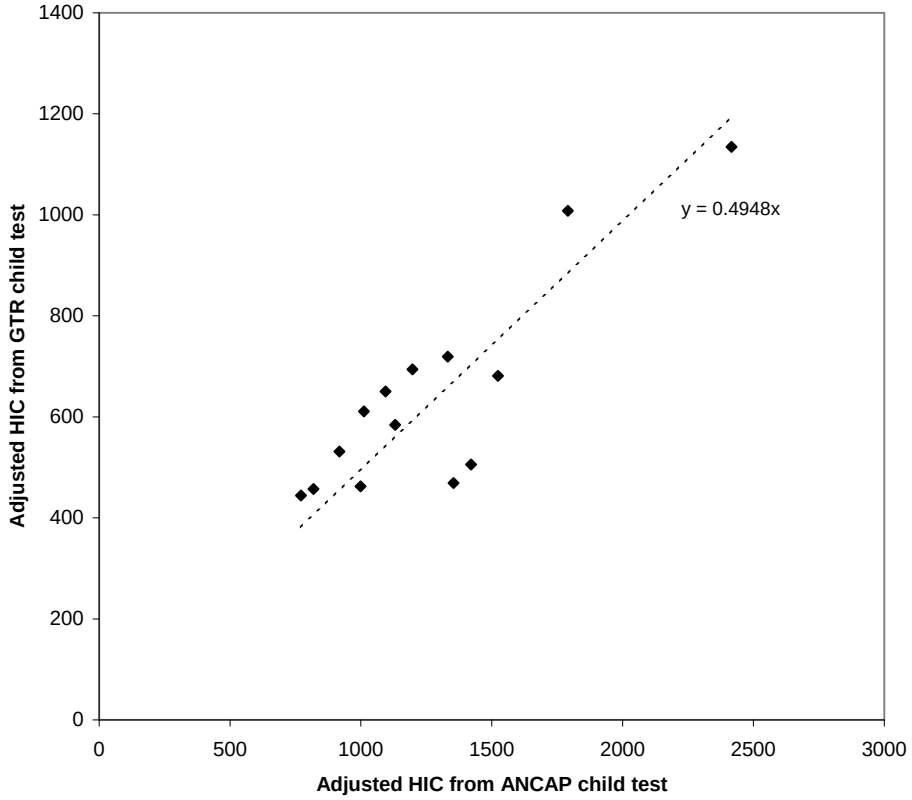

Figure 6.1: Locations tested under Euro NCAP child and GTR child test conditions (Set C).

Condition	Euro NCAP	GTR
Impact speed, m/s	11.1	9.7
Impact angle, °	65	50
Headform mass, kg	4.8	3.5
Headform diameter, mm	165	165

Table 6.3: Test conditions for adult Euro NCAP and child GTR locations (Category two).

6.2.1 Estimated HIC ratio using theoretical and empirical exponents

For locations in category two, there are differences in impact speed, impact angle and headform mass between the two test protocols. The headform diameter is the same for both protocols, which removes some of the uncertainty in predicting the change in HIC between tests.

The theoretical change in HIC for these locations was estimated using Equation 5.14. The values for m_1 and m_2 were taken as listed in Table 6.3 for the GTR and Euro NCAP test conditions. The ratio of the normal impact speeds v_1 and v_2 was dependent on the total impact angle, including both the specified impact angle and the measured bonnet angle. Including those impact angles, the relationship was written as follows:

$$\frac{\text{HIC}_G}{\text{HIC}_E} = \left(\frac{3.5}{4.8}\right)^a \left(\frac{9.7\sin(50^\circ + \theta_b)}{11.1\sin(65^\circ + \theta_b)}\right)^b \tag{6.4}$$

In the above equation, the measured angle of the vehicle bonnet to the ground is represented by θ_b, and the angle between the trajectory of the headform and the ground is included as per the values in Table 6.3. A value of $\theta_b = 0$ would imply a horizontal surface, which would be unlikely to be encountered in practice.

The inclusion of the bonnet angle measurement means that the ratio of normal impact speeds will not be constant for all test locations. Thus, the resulting HIC ratio will not be theoretically constant for all locations either. The HIC ratio will, however, be theoretically constant for a given bonnet angle.

Figure 6.2 shows the variation of the estimated HIC ratio for increasing values of θ_b. Two sets of values for a and b were used to calculate the theoretical HIC ratios: those obtained from the linear spring model ($a = -0.75, b = 2.5$) and those from the combined regression results listed in Table 5.1 ($a = -0.439, b = 2.489$).

As shown in Figure 6.2, the HIC ratio increases with increasing bonnet angle, using both the theoretical and empirical values of a and b. As the bonnet angle increases, both HIC ratios approach one, indicating that the Euro NCAP and GTR HIC values would be expected to be very similar for

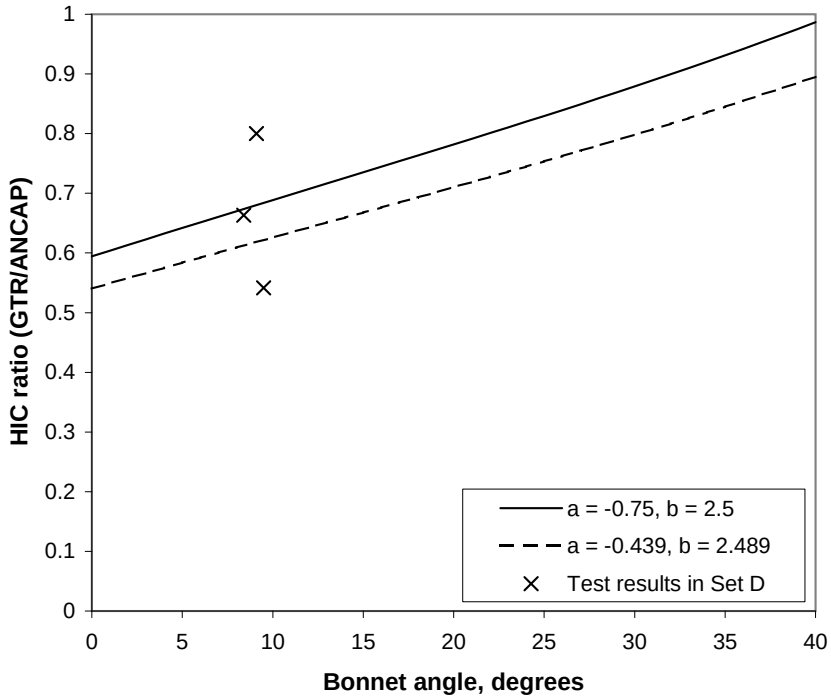

Figure 6.2: Estimated HIC ratio variation with bonnet angle, for locations in category two.

very steep bonnet angles.

In practice, the test locations in category two are most likely to be towards the rear of the bonnet or on the windscreen of the vehicle, which is excluded from the GTR. The bonnet angle at the rear of the bonnet is likely to be relatively flat for a passenger car (less than 15°), implying a HIC in the range of 0.6 to 0.7.

6.2.2 Analysis of data in Set D

The data in Set D consisted of three different test locations, each of which were tested as an adult headform test under Euro NCAP and as a child headform test under the GTR. Each location had a different bonnet angle, and as such the ratio of normal impact speeds was different for each location. As a consequence of this, the predicted HIC ratios were also different for each location.

The measured HIC ratios for each location in Set D were compared to

Location ID	Measured HIC ratio	Predicted using (a, b) (-0.75, 2.5)	(-0.439, 2.489)
14	0.675	0.686	0.624
24	0.772	0.657	0.597
25	0.548	0.692	0.629

Table 6.4: HIC ratios for locations in Set D.

the theoretical ratios predicted using the two choices of values for a and b. This comparison is shown in Table 6.4.

The results from Set D are also shown in Figure 6.2. For consistency, the plotted HIC values from Set D were adjusted using Equation 6.3, with adjusted impact speeds of 9.7 m/s for the GTR tests and 11.1 m/s for the Euro NCAP tests.

As the shown by the values in Table 6.4 and the plotted values in Figure 6.2, there was a large degree of variation in the measured HIC ratios, compared with the two predicted HIC ratios. With such a small sample of data, it was not possible to draw any definite conclusions about which method for predicting the HIC ratio is a more accurate choice.

In this small sample, the variation in the measured HIC ratios was much greater than any variation caused by the selection of a and b in the predicted HIC ratios. For location 14, the measured HIC ratio was between the two predicted HIC ratios. For location 24, the measured HIC ratio was greater than both predictions, and for location 25 the measured HIC ratio was less than both predictions. This indicated that on average, both of the predicted HIC ratios were in an appropriate range.

To summarise, for locations in category two the HIC ratio was dependent upon the bonnet angle. For locations with a bonnet angle of 10°, the GTR HIC value would be expected to be, on average, around 35% lower than the Euro NCAP HIC value. For locations with a bonnet angle of 40°, the GTR HIC would be expected to be very close to the Euro NCAP HIC value, however in practice locations in this category would be unlikely to have a bonnet angle that steep.

Condition	Euro NCAP	GTR
Impact speed, m/s	11.1	9.7
Impact angle, °	65	65
Headform mass, kg	4.8	4.5
Headform diameter, mm	165	165

Table 6.5: Test conditions for adult Euro NCAP and adult GTR locations (Category three).

6.3 Category three: adult Euro NCAP to adult GTR

Locations lying between wrap around distance values of 1700 mm and 2100 mm are tested with an 'adult' headform under both the Euro NCAP and GTR testing protocols.

The test conditions under each protocol for locations in this category are summarised in Table 6.5.

In this case, the impact speed is different between the two test protocols, but the impact angle is the same. The headform mass is slightly lower under the GTR.

There were no data available for a direct comparison of locations in category three.

6.3.1 Estimated HIC ratio using theoretical and empirical exponents

For locations in category three, the change in impact speed was the dominant factor in determining the ratio between the GTR HIC and the Euro NCAP HIC.

Equation 5.14 was used to predict a HIC ratio, using values for m_1 and m_2 from Table 6.5. Because the impact angle was the same under each protocol, the ratio of normal impact speeds was the same as the ratio of the total impact speeds. As such, the values of v_1 and v_2 were also taken from Table 6.5.

Using these values, the relationship for the HIC values obtained under each protocol was:

$$\frac{\text{HIC}_G}{\text{HIC}_E} = \left(\frac{4.5}{4.8}\right)^a \left(\frac{9.7}{11.1}\right)^b \tag{6.5}$$

This expression was firstly evaluated using the values of a and b obtained from the linear spring model (-0.75 and 2.5). Using those values, the estimated HIC ratio is 0.749.

Second, a similar ratio was found using the values of a and b that were obtained from the combined regression. Those values were -0.439 and 2.489 (from Table 5.1). The ratio obtained using those values is 0.735.

In this category, there was only a small variation in headform mass between the two protocols, and as such the effect of the change in impact speed was the dominant factor. Since there was virtually no difference in the theoretical and empirical values of the impact speed exponent b, the resulting HIC ratios were very similar.

There were no back-to-back test results available for a direct comparison of adult Euro NCAP test results to adult GTR test results. However, it is reasonable to expect that because the only significant difference in the test protocols is the impact speed, any such comparison would give a similar result to that obtained using the power law relationship.

Hence, the indication was that locations in category three would have a GTR HIC value that was approximately 25% lower, on average, than the Euro NCAP HIC value.

6.4 Peak displacement and 'bottoming out'

In some headform tests, the outer bonnet surface deforms sufficiently that it comes into contact with a much stiffer structure beneath. An example of this is if the centre of the bonnet deforms enough that it comes into contact with the engine block. As mentioned previously, this test phenomenon is referred to as 'bottoming out'.

The occurrence of bottoming out tends to lead to a dramatic increase in acceleration due to the presence of the stiffer structure, and this typically leads to a higher HIC value than what would be expected if bottoming out did not occur. Figure 6.3 shows an example of a test acceleration pulse in

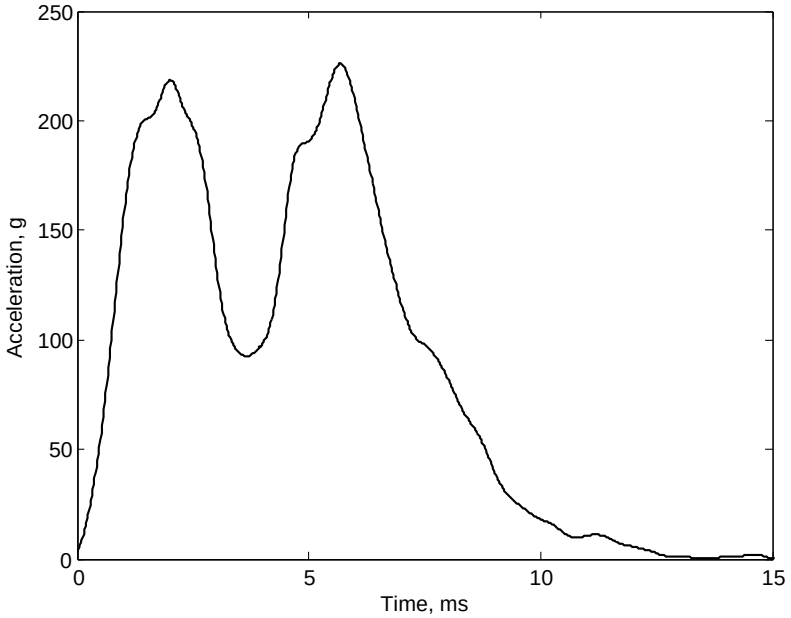

Figure 6.3: Example of bottoming out in an ANCAP child headform test, due to contact with a suspension bolt.

which bottoming out has occurred. In this example, the second 'peak' is due to contact between the bonnet and an exposed suspension bolt.

The linear spring model that was presented in Chapter 4 does not include any effect of bottoming out. In that model, it was assumed that the vehicle structure may deform as much as necessary to absorb the energy of the headform. Furthermore, the data that was analysed in Chapter 5 did not contain results with significant bottoming out. As such, if bottoming out does have a significant effect in real world tests, this effect would not be present in the test results considered in Chapter 5.

Thus, when converting a HIC value from one set of test conditions to another using these methods, the potential for bottoming out introduces some uncertainty. The problem arises when the estimated peak displacement under one set of conditions is higher than it would be under the other set of test conditions. The test with a higher peak displacement would be more likely to bottom out, which may lead to an underestimation of its HIC result, or an overestimation of the other HIC result.

When converting a HIC value from a Euro NCAP test into an equivalent

GTR HIC value, it is important to have an idea of which test would be likely to have a higher peak displacement value. If the Euro NCAP test has a higher peak displacement, then bottoming out would be more likely to occur than in the equivalent GTR test, and as such the GTR HIC value may be overestimated. Conversely, if the Euro NCAP test has a lower peak displacement value, then bottoming out would be less likely to occur than in the equivalent GTR test, and the GTR HIC value may be underestimated.

6.4.1 Rate of occurrence of bottoming out

A random inspection of test results was conducted to gain a rough idea of how many test locations are potentially affected by bottoming out.

Ten vehicles were randomnly selected that had been tested by ANCAP under the Euro NCAP protocol. For each of these vehicles, the test results were examined for locations lying on the bonnet surface. Bottoming out was said to occur if there was a hard structure beneath that bonnet that was engaged due to deformation of the bonnet. This was determined by examining acceleration data from each test, as well as overhead photographs of the structures beneath each test location.

In some cases, the bonnet was resting on a hard structure – for these cases, the hard structure would be engaged regardless of how far the bonnet deformed, and so it was not considered as bottoming out.

Over the ten vehicles that were examined, there were 109 test locations lying on the bonnet, and of those 21 (19%) were determined to be affected by bottoming out. This result suggests that bottoming out may occur at around a fifth of test locations on the bonnet selected for testing by ANCAP.

Despite this, the power function suggested by the linear spring model may be still be a valid approximation of the change in HIC with impact speed and headform mass for locations that include bottoming out. If bottoming out is expected to occur under both sets of test conditions, the power function might represent an average effect, with the effective stiffness in the test including the effect of harder structure beneath the bonnet. Unfortunately a full analysis of the bottoming out problem, including theory and data, was outside the scope of this thesis.

6.4.2 Estimating the change in peak displacement

For each of the location categories, the ratio of peak displacement values under the two protocols was estimated using the relationship presented in Chapter 3:

$$\frac{S_G}{S_E} = \left(\frac{m_G}{m_E}\right)^{\alpha} \left(\frac{v_G}{v_E}\right)^{\beta} \tag{6.6}$$

There were two sets of values used for α and β. The first set of values were the theoretical values derived from the linear spring model, which were $\alpha = 0.5$ and $\beta = 1$. The second set were taken from the regression results listed in Table 5.2, which were $\alpha = 0.436$ and $\beta = 0.801$.

For category one test locations, the peak displacement ratio that was predicted using the regression results also included the effect of headform diameter. This was included by multiplying the peak displacement ratio by 10 raised to the power of $\delta_{165} = 0.085$, which was taken from Table 5.2. This suggested a peak displacement ratio of 1.264. When the theoretical values of α and β were used, with no allowance for diameter, the peak displacement ratio was 1.034.

The back-to-back test results in Set C were also analysed to estimate the peak displacement ratio for locations in category one. This was performed in a similar fashion to the HIC ratio analysis in Section 6.1. This analysis suggested a peak displacement ratio of 1.176 (95% CI: 1.129–1.222).

For category two test locations, a bonnet angle of 10° was used to calculate the peak displacement ratio. As in the case of the HIC ratio, this ratio would be expected to vary depending upon the bonnet angle. For a bonnet angle of up to 40°, the ratio was less than one using both calculation methods. However, the bonnet in this area would be expected to be relatively close to horizontal, so 10° was considered an appropriate choice for gaining a rough idea of whether bottoming out would be more or less likely to occur.

The results of these calculations are listed in Table 6.6. From these results, it was possible to predict whether the peak displacement would be likely to be higher or lower in the GTR test, for each category of test location.

	Using (α, β)		Back-to-back
	Linear spring	Regression	data analysis
Category	(0.5, 1)	(0.436, 0.801)	
1 (WAD 1000–1500 mm)	1.034[a]	1.264[b]	1.176
2 (WAD 1500–1700 mm)	0.669[c]	0.717[c]	-
3 (WAD 1700–2100 mm)	0.846	0.872	-

[a] Does not account for change in headform diameter.
[b] Includes the effect of headform diameter predicted using $\delta_{165} = 0.085$.
[c] Using a bonnet angle of 10°.

Table 6.6: Peak displacement ratios (GTR/Euro NCAP) for each category, using three different methods.

The results in Table 6.6 suggest that locations in categories two and three would experience lower peak displacements under the GTR compared with Euro NCAP, by around 30% and 15%, respectively. Thus, for these locations we would expect the Euro NCAP test to be more likely to experience bottoming out. This implies that the method used to convert Euro NCAP HIC values may overestimate the GTR HIC values for some locations in categories two and three.

There was some variation in the peak displacement ratios for test locations in category one. The ratio calculated using $\alpha = 1$ and $\beta = 0.5$ suggested that the peak displacement values would be approximately equal under both protocols. However, this ratio did not include any effect of headform diameter, which was shown to have an effect in the test data in Chapter 5. The ratio calculated using the regression values and the ratio calculated from the data in Set C suggest that the peak displacement would be around 20–25% higher under the GTR. These estimates include an effect of headform diameter.

Given this, it is reasonable to expect that for locations in category one, the peak displacement would be higher under the GTR compared with Euro NCAP. Thus, for these locations we would expect the GTR test to be more likely to experience bottoming out. This implies that the method used to convert Euro NCAP HIC values may underestimate the GTR HIC values for some locations in category one.

To summarise, GTR HIC values estimated from Euro NCAP test results

are subject to to the following qualifications:

- Category one: some GTR HIC values may be underestimated (20–25% higher peak displacement)
- Category two: some GTR HIC values may be overestimated (30% lower peak displacement)
- Category three: some GTR HIC values may be overestimated (15% lower peak displacement)

If bottoming out is present, its effect on HIC may be difficult to quantify. In the conversion of HIC values between the two test protocols, the occurrence of bottoming out is a potential source of error.

6.5 Summary and discussion

In this chapter, three methods were used to calculate multiplying factors that can be used to convert a HIC value obtained under the Euro NCAP test protocol to an equivalent estimated HIC value under the GTR test protocol. These methods were applied to three different categories of test location, each of which had its own conversion factors based on the test conditions used under the GTR and Euro NCAP test protocols.

The conversion factors for each category, calculated using each method, are listed in Table 6.7.

The first two methods used the power law relationship that was developed from the linear spring model in Chapter 3:

$$\frac{\mathrm{HIC}_G}{\mathrm{HIC}_E} = \left(\frac{m_G}{m_E}\right)^a \left(\frac{v_G}{v_E}\right)^b \tag{6.7}$$

In each of these two methods a different selection of a and b was used. In the first method, the values of a and b were taken from the linear spring model, and were -0.75 and 2.5. In the second method, the values of a and b were taken from the regression results in Chapter 5, as listed in Table 5.1. These values were -0.439 and 2.489.

	Using (a, b)		Back-to-back
	Linear spring	Regression	data analysis
Category	(-0.75, 2.5)	(-0.439, 2.489)	
1 (WAD 1000–1500 mm)	0.555[a]	0.485[b]	0.495
2 (WAD 1500–1700 mm)	0.689[c]	0.626[c]	-
3 (WAD 1700–2100 mm)	0.749	0.735	-

[a] Does not account for change in headform diameter.
[b] Includes the effect of headform diameter predicted using $d_{165} = -0.104$.
[c] Using a bonnet angle of 10°.

Table 6.7: HIC conversion factors (Euro NCAP to GTR) for each category, using three different methods.

The values of b used in each of the first two methods were almost identical, so the selection of b did not substantially affect the conversion factors. However, the two values of a were substantially different and this difference was responsible for the difference in the conversion factors listed for categories two and three, and for some of the difference in the first two conversion factors listed for category one.

In Chapter 5, the final regression on the combined data in Set AB gave a 95% confidence interval for a that did not include the value of a predicted by the linear spring model (-0.75). The results of the regression suggested that the magnitude of a was lower, implying a reduced effect of mass compared with the linear spring model. In Chapter 5, the Hertz contact model also suggested that a lower value for a was appropriate for non-linear contact models.

Given this, it would seem appropriate to use a value of a that is closer to the regression result of -0.439. For the practical purpose of estimating vehicle performance under the GTR from Euro NCAP test results, this would be likely to give a more accurate result.

For tests in category one, the remaining difference between the first two conversion factors was due to the consideration of headform diameter. The first method, using the linear spring model, did not include an effect of headform diameter. However, when using the regression results from Chapter 5, the effect of headform diameter was included using the value of d_{165} listed in Table 5.1. This value caused an additional reduction in

magnitude of the conversion factor. Given that headform diameter was shown to have an effect on HIC in Chapter 4, it would seem reasonable to include that effect in the selection of a Euro NCAP-to-GTR conversion factor.

Due to the resulting level of uncertainty in the conversion factors for category one, the data in Set C were also analysed. This data set consisted of back-to-back Euro NCAP child and GTR child headform tests on the same locations. The average ratio of GTR and Euro NCAP HIC values for locations in this set was 0.495, a value which lies close to that predicted using the Chapter 5 regression results. For the purposes of calculating a conversion factor to convert Euro NCAP HIC values to GTR HIC values, this would appear to be the most reasonable method.

It is worth noting again that these results are for predicting GTR performance from tests performed under Version 4 of the Euro NCAP test protocol. The more recent Version 5 of the Euro NCAP protocol specifies the same headforms as the GTR protocol. Thus, if the estimations were based on Version 5 test results, then any uncertainty arising from the difference in headform mass and diameter would not be present. Instead, only the difference in test speed would need to be considered, the effect of which was similar in the linear spring model and the empirical results. At the time of this study, only results from tests conducted under Version 4 were available.

Finally, the presence of bottoming out must be considered as a source of error in the conversion of HIC values. Bottoming out was found to be a factor in about 20% of ANCAP test locations on the bonnet. Due to the likely differences in peak displacement between the two test protocols, bottoming out may be more or less likely to occur under the GTR, which may lead to an overestimate or underestimate of GTR HIC values from Euro NCAP (ANCAP) results. Locations in category one were more likely to bottom out in the GTR test, so their GTR HIC values may be underestimated in some cases. Conversely, locations in categories two and three were more likely to contain bottoming out in their Euro NCAP test, so in some cases their GTR HIC values may be overestimated.

Chapter 7

Estimating vehicle compliance with the GTR from ANCAP test results

In this chapter, the focus moves from the individual test locations to the overall performance of the vehicle. The compliance of vehicles with the GTR on pedestrian safety is predicted using their results from ANCAP testing. This was done by estimating a new HIC value for each location tested by ANCAP, under the conditions of the GTR. The method for estimating the change in HIC for each location is based on the results in Chapter 6.

A series of assumptions were made about the performance of each area of the bonnet. Under these assumptions, a best case and worst case performance estimate can be made for each vehicle, against the different criteria of the GTR.

The reason for doing this was to estimate what proportion of vehicle models would be expected to pass the GTR on pedestrian safety if it were to be adopted in Australia as an Australian Design Rule. Furthermore, the results give an idea of what sort of issues vehicle designers might need to address in order to meet the requirements of the GTR on pedestrian safety.

7.1 Vehicle data source

Since the inclusion of pedestrian testing in the Australasian New Car Assessment Program in 1997, over 100 vehicles have been tested at the Centre for Automotive Safety Research impact laboratory. In 2002 the Euro NCAP pedestrian testing protocol was heavily revised by the EEVC Working Group 17, with the introduction of Version 3 of the pedestrian testing protocol. Version 4 was later adopted, which was similar to Version 3, with only minor changes (Ponte, 2004). Version 5 of the Euro NCAP pedestrian testing protocol was adopted in 2010, which contains significant changes to the headforms that are used.

For the purposes of this study, vehicles were only included that were tested by ANCAP using Version 3 or 4 of the Euro NCAP pedestrian testing protocol. This was due to the large volume of vehicle test data that were available for vehicles tested under these protocols. For the remainder of this chapter, any reference to the Euro NCAP test protocol will refer to Versions 3 and 4 of the Euro NCAP pedestrian testing protocol.

Under the GTR, vehicles of categories M1 and N1 are tested (UNECE, 2009). Category M1 includes passenger vehicles with up to eight seats in addition to the driver. Category N1 vehicles are those designed for the carriage of goods, with a maximum mass of 3.5 tonnes - this would include most utilities and vans. However, the GTR excludes any N1 vehicles, or M1 vehicles weighing more than 2.5 tonnes that have been derived from N1 vehicles, that have an 'R-point' ahead of the front axle, or less than 1100mm behind the front axle. In the absence of such measurements, any vans were excluded from this study. All passenger vehicles and utilities were included.

There were six vehicles tested by ANCAP that were not included in the study, due to there being an insufficient number of tests performed in the GTR testable area.

After these exclusions, there were 60 vehicles remaining that were included in the study.

The manufacturing year for these vehicles ranged from 2002 until 2009. Of the 60 vehicle models, 33 were regarded as 'current'. These were available to be purchased new as of November 2009. Currency was determined by

Category	WAD range	Euro NCAP headform	GTR headform
1	1000 – 1500 mm	Child, 2.5 kg	Child, 3.5 kg
2	1500 – 1700 mm	Adult, 4.8 kg	Child, 3.5 kg
3	1700 – 2100 mm	Adult, 4.8 kg	Adult, 4.5 kg

Table 7.1: Categories of test location by wrap around distance (WAD).

visiting manufacturer websites.

The number of individual impact test results included was 523, across all 60 vehicles. Of those, 275 were child headform tests, and 248 were adult headform tests. Including symmetrical test locations, and locations that were not tested due to a default pass or default fail, a total of 1115 ANCAP test locations were included.

Of the impact tests included, the highest HIC recorded was 8722, the lowest was 373. The mean HIC from the impact tests was 1709.

7.2 Method

The method for estimating each vehicles' GTR performance was a two part process. Firstly, the HIC values from each ANCAP test location were converted into equivalent GTR HIC values, using a method based on the results in Chapter 6. Secondly, these results were assembled to produce best and worst case estimates of each vehicle's performance under the GTR.

7.2.1 Conversion of HIC values

The method that was used to convert ANCAP HIC values into estimated GTR HIC values depended upon which category the location fell into, based upon its wrap around distance (WAD). These categories were described in detail in Chapter 6, and are summarised again in Table 7.1.

For locations in category one, the ANCAP HIC was first adjusted to an impact speed of 11.1 m/s, using Equation 6.3. The adjusted HIC value was multiplied by a constant factor of 0.495 in order to estimate the equivalent GTR HIC value. This mutiplying factor was based on the analysis of back-to-back test data in Set C.

For locations in categories two and three, the theoretical equation for

HIC ratio was used to predict the HIC values under the GTR, from the HIC values obtained by ANCAP under the Euro NCAP protocol:

$$\mathrm{HIC}_G = \mathrm{HIC}_E \left(\frac{m_G}{m_E}\right)^a \left(\frac{v_G}{v_E}\right)^b \tag{7.1}$$

The values of the exponents were taken from the regression results listed in Table 5.1. These values were -0.439 and 2.489 for a and b respectively. This value of a was found to more closely represent the average effect of the change in headform mass (see Chapter 6), and the value of b was consistent with what was predicted by the linear spring model.

The Euro NCAP headform mass m_E was 4.8 kg for locations in both categories two and three. The GTR headform mass m_G was 3.5 kg for locations in category two and 4.5 kg for locations in category three.

For locations in category two, the impact speeds v_E and v_G were taken from the measured normal impact speed in the ANCAP test, and the desired normal impact speed of the GTR test. To calculate these values, the measured bonnet angle for each test location had to be taken into account. The desired total impact speed for the GTR test was 9.7 m/s.

In a limited number of cases, the bonnet angle was not available, as it had not been recorded during the test. The average bonnet angle was taken from locations in category two that were on the bonnet and had a known bonnet angle (total of 89). The average bonnet angle from these locations was 8.9°, and so this was used in cases where the bonnet angle was not known.

For locations in category three, the impact speed v_E was taken from the measured total impact speed of the ANCAP test. The GTR impact speed v_G was 9.7 m/s. The measured bonnet angle did not need to be taken into account for these test locations, due to the constant impact angle between the two protocols.

Using this methodology, a GTR HIC value could be predicted from the existing ANCAP test results for each location.

7.2.2 Method for estimating results for each vehicle

The HIC scaling method presented in the previous section was applied to every test result for the included vehicles.

A computer program was written that took the list of results from the ANCAP tests and calculated the 'best case' and 'worst case' estimates of GTR performance for each vehicle. The program was written and run using Matlab Version 7.5[1].

In the following description of the program logic, the term 'zone' refers to one of the six numbered adult zones, or six numbered child zones. The term 'subzone' refers to one of the four lettered areas within each zone (for reference, see Figure 2.2).

For the purposes of this estimate, the Euro NCAP subzone divisions were used as the smallest units of area. The GTR does not use any area divisions aside from the division between the adult and child test areas, and allows a non-structured definition of the relaxation zone. However, any attempt to divide the testable area into smaller quanta than the Euro NCAP subzones would have been difficult and inaccurate.

As described in Section 2.2.1, under the Euro NCAP protocol, one test location is selected by ANCAP for every zone (the 'ANCAP test'). The vehicle manufacturer then has the option of nominating one or more of the remaining three subzones, which will, hopefully for the manufacturer, perform better than the ANCAP test location. One location is selected within the manufacturer nominated subzones for an additional test (the 'manufacturer test').

Thus, within each zone there was at least one subzone that contained a test result, the ANCAP test. There may or may not have been an additional subzone that also contained a test result, the manufacturer test. The remaining two or three subzones did not contain test results, but some knowledge was assumed regarding those remaining subzones.

- If there were no manufacturer nominated subzones, then it was assumed that the ANCAP tested subzone was the worst of all four. Thus, the three non-tested subzones would perform the same as the

[1]The Mathworks, Natick, Massachusetts

ANCAP test in the worst possible case, and in the best possible case would pass any requirement (i.e. they would have a notional HIC of less than 1000).

- If there were one or more manufacturer nominated subzones, then it was assumed that the subzone that was tested was the worst performing out of those nominated.
  - If the ANCAP test performed worse than the manufacturer test (as expected), then:
    - The remaining manufacturer nominated subzones, that were not tested, would perform the same as the manufacturer test in the worst possible case, and in the best possible case would pass any requirement (i.e. they would have a notional HIC of less than 1000).
    - Any subzones that were not nominated by the manufacturer and were not tested, would perform the same as the ANCAP test in the worst possible case, and in the best possible case would perform the same as the manufacturer test.
  - Otherwise, if the manufacturer test performed worse than the ANCAP test (unexpected, but occurred in some cases), then:
    - All non-tested subzones would perform the same as the ANCAP test location in the worst possible case, and in the best possible case would pass any requirement (i.e. they would have a notional HIC of less than 1000).

Using the logic outlined above, any non-tested subzones were given an upper and lower estimate of the HIC, or performance, which could be expected.

Two additional factors also had to be taken into account:

1. In each of the ANCAP adult zones, subzones C and D were divided into two, at the WAD of 1700 mm. Two appropriate HIC values were calculated for these subzones, one corresponding to a GTR child test (category two) and one corresponding to a GTR adult test (category

three). The lower 2/3 of the subzone was counted as part of the GTR child test area, and the upper 1/3 was counted as part of the GTR adult test area.

2. The GTR test area does not extend beyond the rear edge of the bonnet. As such, a manual inspection of photos of each vehicle was carried out. The approximate number of subzones to be included was estimated for each vehicle. Any subzones not on the bonnet area did not contribute towards the GTR performance estimate. If the rear edge of the bonnet roughly bisected a series of subzones, then those subzones were only counted as half of an area unit.

Once an upper and lower HIC limit had been established for all of the subzones included within the GTR test area, an overall best case and worst case estimate could be made against the three criteria of the GTR. These three criteria were:

1. No more than 1/3 of the testable area could exceed a HIC of 1000 (the 'relaxation' area).

2. No more than 1/2 of the child test area could exceed a HIC of 1000 (the 'relaxation' area).

3. No test could exceed a HIC of 1700.

For each of these criteria, an upper and lower estimate was made using the assumptions outlined above. In the cases of criteria 1 and 2, an upper and lower estimate of the required relaxation area was made, relative to the total area and total child test area. For criterion 3, an upper and lower estimate was made of the number of subzones exceeding a HIC of 1700.

This procedure would be adaptable if other HIC limits were written into the GTR procedure, or if other criteria were introduced. For example, if the upper HIC limit for the relaxation zone were changed to 2000 and the remainder 800, then a different performance estimate could be calculated using those figures. If the limit of 1/3 in the first criteria were, for example, reduced to 1/4, then this could also be taken into account. For the purposes of this thesis, none of these theoretical scenarios were considered.

7.3 Results

7.3.1 Results for all vehicles

The results for all 60 vehicles are listed in Table 7.3. For each vehicle, upper and lower estimates are given for the three criteria of the GTR. Vehicles marked with a star (*) were current in November 2009. The upper estimate was the worst case scenario, and the lower estimate was the best case scenario, based on the scaled ANCAP test results.

Of all of the vehicles, seven were estimated to pass all criteria in both their best case and worst case scenarios, and six of those were current vehicles. The seven vehicles that were estimated to pass were:

- Nissan Tiida (2006)
- Honda Odyssey (2006)
- Hyundai Accent (2006, not current)
- Hyundai Elantra (2007)
- Holden Barina (2008)
- Kia Cerato (2009)
- Honda City (2009)

There was only one vehicle that was estimated to fail all three criteria in its best and worst case scenario. This was the Holden Cruze (2002, not current).

The results for all vehicles are presented graphically in Figure 7.1, Figure 7.2 and Figure 7.3. In each plot, the vehicles are sorted by their worst case estimate. Vehicles that were estimated to pass that GTR criterion under both cases (best and worse) are marked with a solid line and dot. Vehicles that passed that GTR criterion under their best case estimate, but did not pass in their worst case estimate, are marked with a dashed line and cross. Vehicles that were estimated to fail that GTR criterion under both cases (best and worse) are marked with a solid line and cross.

	% of total area HIC > 1000		% of child area HIC > 1000		No. of subzones HIC > 1700	
Vehicle name	Upper	Lower	Upper	Lower	Upper	Lower
Mazda Tribute	54.39	12.28	45.83	10.42	6.67	1.00
Subaru Forester	27.78	16.67	27.08	14.58	2.00	0.00
Toyota RAV4	44.44	19.44	46.88	20.83	2.00	0.00
Holden VY Commodore	55.56	5.56	50.00	6.25	18.67	2.00
Ford Falcon BA	49.07	12.04	46.88	13.54	9.00	1.00
Toyota Camry	52.78	19.44	50.00	18.75	6.00	0.00
Hyundai Getz	83.33	20.83	83.33	20.83	8.00	2.00
Holden Cruze	87.50	62.50	87.50	62.50	6.00	2.00
Honda Jazz VTi	41.67	41.67	41.67	41.67	2.00	0.00
Mitsubishi Magna ES	48.15	12.04	41.67	10.42	12.00	2.00
Daewoo Kalos	100.00	25.00	100.00	25.00	8.00	2.00
Mitsubishi Lancer	26.67	6.67	26.67	6.67	8.00	2.00
Holden Monaro CV8	48.15	12.96	41.67	10.42	12.00	2.00
Toyota Echo	45.83	12.50	45.83	12.50	8.00	2.00
Mitsubishi Outlander	51.85	24.07	52.08	22.92	8.00	4.00
Subaru Liberty MY 04	33.33	22.22	31.25	18.75	2.00	0.00
Hyundai Accent	48.15	12.96	41.67	10.42	4.00	0.00
Mazda Mazda3	36.67	13.33	36.67	13.33	2.00	0.00
Toyota Landcruiser 100	66.67	18.75	79.17	22.92	14.67	3.67
Lexus RX330	69.44	16.67	73.96	18.75	4.00	0.00
Nissan Patrol*	33.33	8.33	33.33	10.42	8.00	2.00
Ford Courier	38.10	7.14	38.10	7.14	0.00	0.00
Holden Rodeo LX	52.38	11.90	58.33	12.50	14.00	3.00
Toyota Hilux*	63.89	18.75	70.83	18.75	5.33	2.00
Nissan Patrol C/C*	66.67	16.67	83.33	18.75	16.00	4.00
Mitsubishi 380	55.56	16.67	50.00	14.58	12.67	2.33
Toyota Landcruiser C/C	68.75	25.00	80.21	28.13	25.00	7.00
Holden Viva	57.41	12.04	58.33	12.50	12.00	2.00
Nissan Tiida*	0.00	0.00	0.00	0.00	0.00	0.00
Nissan Maxima	47.22	11.11	43.75	10.42	9.00	2.00
Honda Odyssey*	0.00	0.00	0.00	0.00	0.00	0.00
Holden Commodore VE*	38.89	8.33	37.50	8.33	4.00	0.00
Hyundai Accent	33.33	8.33	33.33	8.33	0.00	0.00
Toyota Camry*	27.78	16.67	27.08	14.58	4.00	1.33
Mitsubishi Triton*	80.16	32.14	79.17	28.13	26.00	7.00
Toyota Aurion*	27.78	5.56	27.08	6.25	4.00	0.00
Subaru Tribeca*	50.00	16.67	54.17	18.75	2.00	0.00
Holden Epica*	11.11	0.00	8.33	0.00	4.00	0.00
Subaru Impreza*	5.56	0.00	4.17	0.00	2.00	0.00
Toyota Kluger*	42.86	16.67	47.92	18.75	4.00	1.00
Mazda CX-7*	44.44	11.11	43.75	12.50	10.00	2.00
Mazda BT-50*	58.33	20.83	58.33	18.75	9.33	4.00
Hyundai Elantra*	0.00	0.00	0.00	0.00	0.00	0.00
Mahindra Pik-Up*	50.00	16.67	58.33	18.75	24.00	8.00
Subaru Forester*	9.52	2.38	4.17	0.00	4.00	1.00
Mitsubishi Lancer*	12.96	0.00	10.42	0.00	4.00	0.00
Ford Falcon*	36.11	16.67	33.33	14.58	2.67	0.00
Nissan Navara*	49.12	19.30	41.67	14.58	12.67	4.00
Honda Jazz GLi*	16.67	0.00	16.67	0.00	2.00	0.00
Holden Barina*	33.33	8.33	33.33	8.33	0.00	0.00
Suzuki APV*	66.67	16.67	66.67	16.67	8.00	2.00
Kia Cerato*	0.00	0.00	0.00	0.00	0.00	0.00
Hyundai iLoad*	83.33	25.00	83.33	25.00	8.00	2.00
Subaru Liberty*	5.56	0.00	4.17	0.00	2.00	0.00
Subaru Outback*	5.56	0.00	4.17	0.00	2.00	0.00
Proton Jumbuck*	46.67	13.33	46.67	13.33	12.00	3.00
Great Wall SA220*	66.67	16.67	83.33	18.75	16.00	4.00
Honda City*	0.00	0.00	0.00	0.00	0.00	0.00
Hyundai Santa Fe*	24.07	6.48	20.83	6.25	4.00	0.00
Subaru Exiga*	5.56	0.00	4.17	0.00	2.00	0.00

Table 7.3: Upper and lower estimates of performance against three criteria of the GTR.

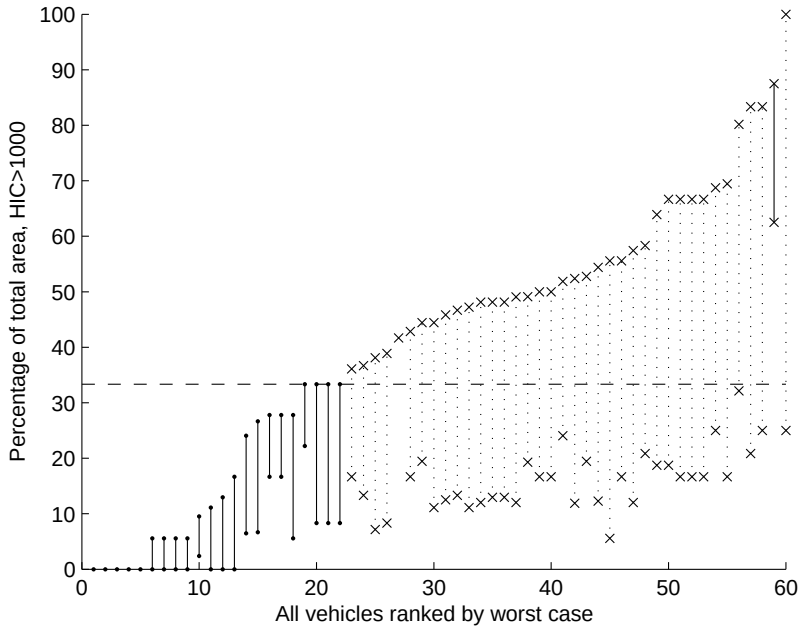

Figure 7.1: Upper and lower estimates of percentage of total test area with HIC over 1000 (limit 33.3% for relaxation zone).

Figure 7.1 shows that 22 vehicles were estimated to pass the requirement that a maximum of 1/3 of the test area may exceed a HIC of 1000. The majority of vehicles were estimated to potentially pass or fail this requirement, depending on whether their best case or worst case scenario was met. Just two vehicles were estimated to fail this requirement in both the best and worse cases (one is ranked 27th and may be difficult to spot in the figure).

Figure 7.2 shows that a large proportion of the vehicles, 42 out of 60, were estimated to pass the requirement that a maximum of 1/2 of the child test area may exceed a HIC of 1000. Just one vehicle was estimated to fail this requirement in both the best and worse cases. The remaining vehicles were estimated to pass this requirement in the best case but fail in the worst case, so their result was uncertain.

Figure 7.3 shows that eight vehicles were estimated to pass the requirement that no test exceed a HIC of 1700. A further 20 vehicles may or may not pass this requirement, depending on whether their best case or worst case estimate was met. The remaining 32 vehicles were estimated to fail this

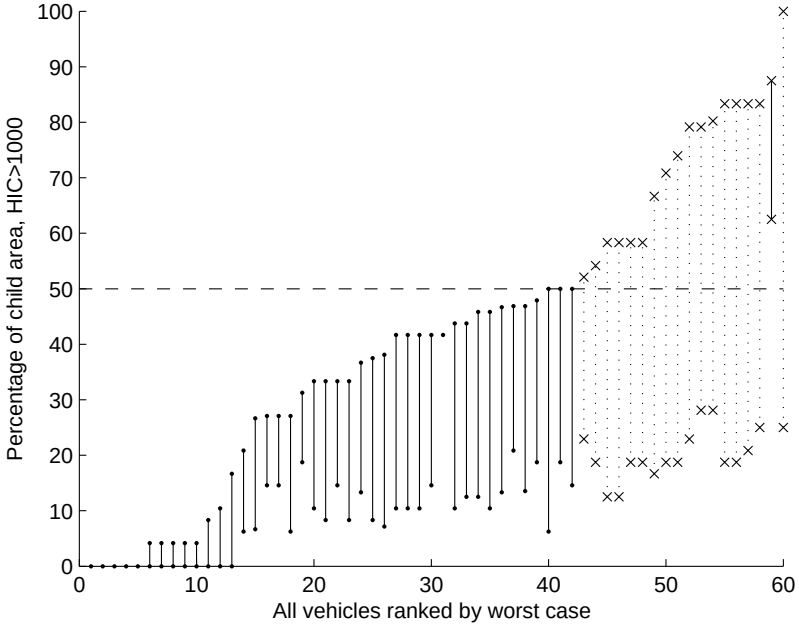

Figure 7.2: Upper and lower estimates of percentage of child test area with HIC over 1000 (limit 50% for relaxation zone).

requirement in both the best and worse cases.

7.3.2 Results for current vehicles only

Figure 7.4, Figure 7.5 and Figure 7.6 show the results for the 33 currently available vehicles only (as of November 2009).

The results for the current vehicles exhibit similar trends to those for all vehicles. Proportionally, slightly more current vehicles were estimated to pass the requirement that no more than 1/3 of the testable area exceeds a HIC of 1000 (Figure 7.4), compared with all vehicles (Figure 7.1). None of the current vehicles were estimated to fail either of the relaxation zone criteria under their best case estimate, but 15 were estimated to exceed the maximum HIC of 1700 in both their best and worst case scenarios.

If we consider only the criteria relating to the relaxation zone, we can see that the requirement that the relaxation zone does not exceed 1/3 of the total test area is the limiting factor for overall vehicle performance. In fact, in all cases where the relaxation zone passed the requirement that it

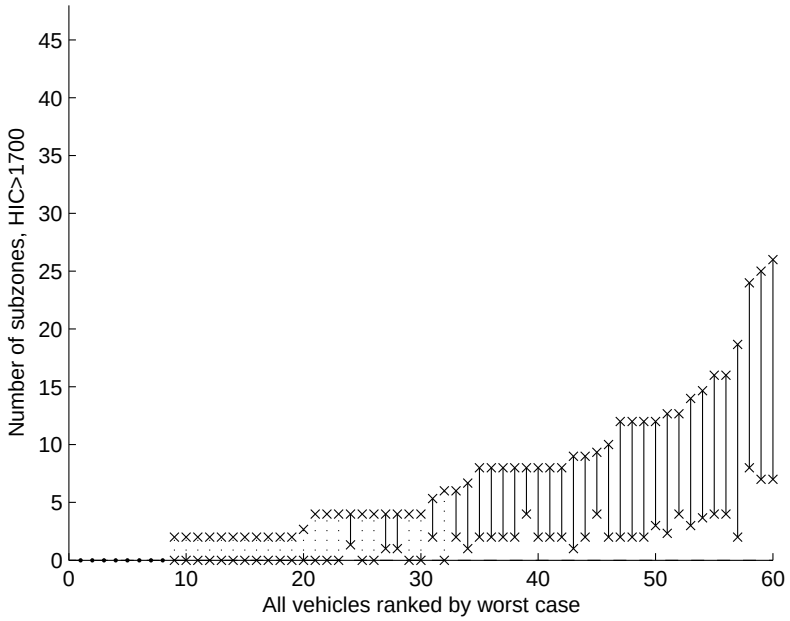

Figure 7.3: Upper and lower estimates of number of subzones exceeding HIC 1700 (limit is zero).

was less than 1/3 of the total test area, the vehicle was also estimated to pass the requirement that the relaxation zone was less than 1/2 of the child test area. Hence, the child area requirement of the relaxation zone was not a limiting factor as to whether to the entire vehicle was estimated to pass or fail the GTR requirements.

For simplicity, from here onwards the requirement that the relaxation zone is less than 1/3 of the total test area will be referred to as the 'HIC1000' criterion and the requirement that no test exceeds a HIC of 1700 will be referred to as the 'HIC1700' criterion.

It is of interest to examine the relationship between a vehicle's performance in the HIC1000 criterion, against their performance in the HIC1700 criterion. These results are given in Table 7.4 and Table 7.5 for all vehicles and current vehicles only, respectively. Vehicles counted under 'Pass' were those that passed under both their best case and worst case estimates, and those counted 'Fail' were those that failed under both their best case and worst case estimates. Vehicles counted under 'Uncertain' were those

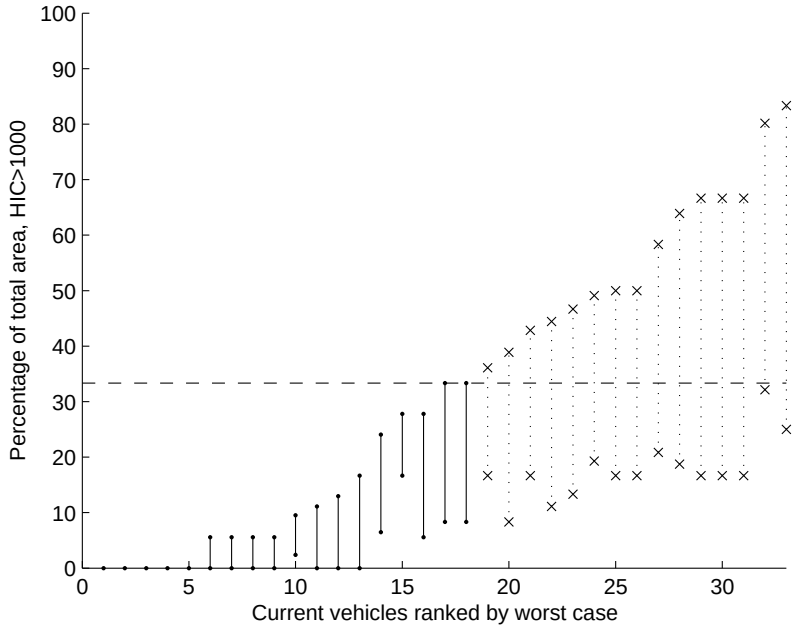

Figure 7.4: Upper and lower estimates of percentage of total test area with HIC over 1000, for current vehicles as of Nov 2009 (limit 33.3% for relaxation zone).

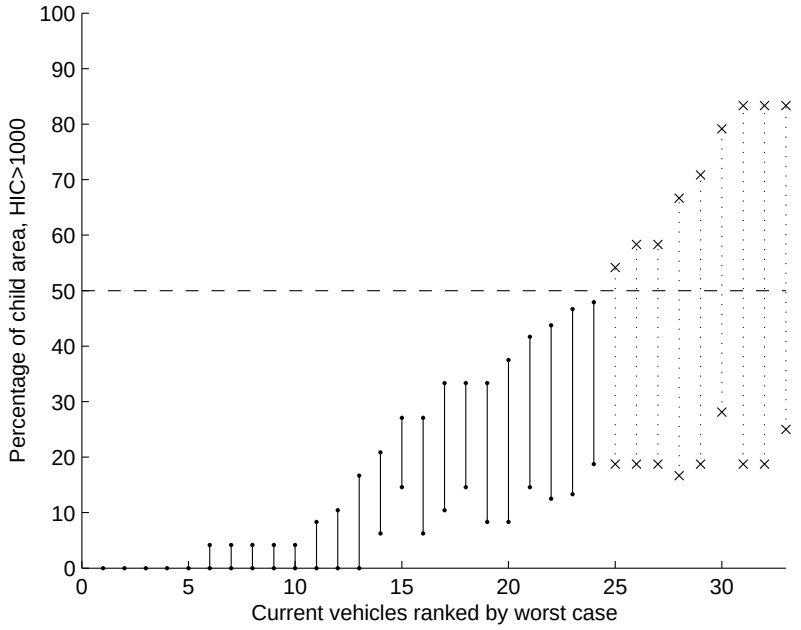

Figure 7.5: Upper and lower estimates of percentage of child test area with HIC over 1000, for current vehicles as of Nov 2009 (limit 50% for relaxation zone).

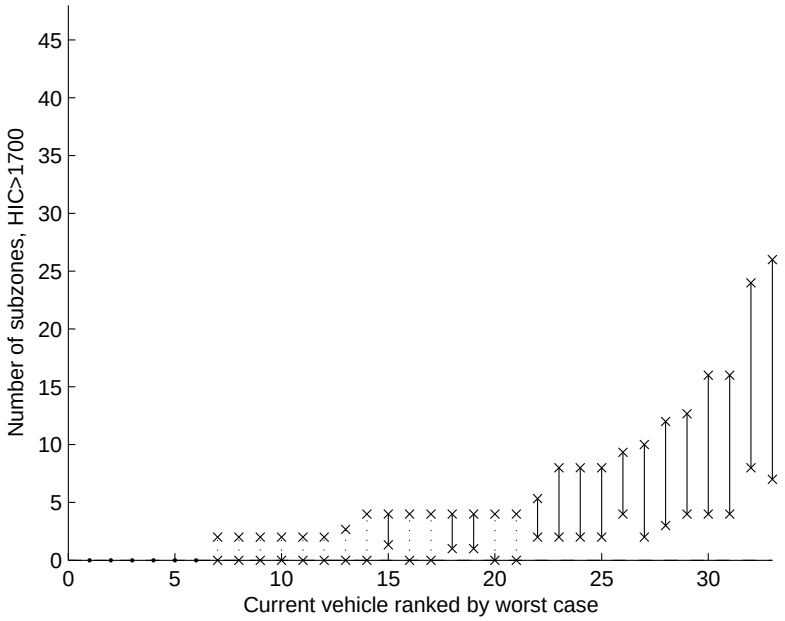

Figure 7.6: Upper and lower estimates of number of subzones exceeding HIC 1700, for current vehicles as of Nov 2009 (limit is zero).

which passed under their best case estimate, but failed under their worst case estimate.

The results in Table 7.4 and Table 7.5 show the relationship between results under the two criteria for all vehicles and for current vehicles only. The upper left corner of each table shows the number of vehicles that were estimated to pass both criteria in the best and worst cases, as stated earlier, this includes 7 vehicles in total, 6 of which were current.

Additionally, there were 11 vehicles, 9 of which were current, that were estimated to pass the HIC1000 criterion and but had an uncertain result in

	HIC1000 criterion		
HIC1700 criterion	Pass	Uncertain	Fail
Pass	7	1	0
Uncertain	11	8	1
Fail	4	27	1

Table 7.4: Estimated performance in the HIC1000 criterion compared with performance in the HIC1700 criterion, all vehicles.

	HIC1000 criterion		
HIC1700 criterion	Pass	Uncertain	Fail
Pass	6	0	0
Uncertain	9	3	0
Fail	3	12	0

Table 7.5: Estimated performance in the HIC1000 criterion compared with performance in the HIC1700 criterion, current vehicles as of Nov 2009.

the HIC1700 criterion. Upon closer inspection, each of these vehicles had a maximum of four subzones that might fail the HIC1700 criterion (Figure 7.3). For these vehicles, it would be reasonable to expect that only minor modifications would be needed in order to make them pass both criteria. In fact, many of these vehicles might pass the HIC1700 criterion without any modification, if their best case estimate were correct.

The results suggest that the HIC1700 criterion is the most difficult to pass – 32 out of the total 60 vehicles (and 15 out of 33 current vehicles) were estimated to fail this criterion in both their best and worst cases. The implication of this result is that the most dangerous locations on the vehicle bonnet are most likely to cause failure in the GTR. The HIC1000 criterion reflects the overall design of the bonnet, and this criterion was not as likely to be a problem for the vehicles that were examined.

7.3.3 Comparison between ANCAP and GTR performance

Finally, the ANCAP performance of vehicles was compared with their performance against the GTR criteria. The ANCAP head score is scored out of a maximum of 24 points, with two points available for each head testing zone. Table 7.6 gives the mean ANCAP head score for all vehicles, categorised by their estimated compliance with the HIC1000 and HIC1700 criteria.

The highest average ANCAP head test scores were for vehicles that were estimated to pass the HIC1000 criterion, regardless of their estimated performance against the HIC1700 criterion. This suggests that vehicles that passed the HIC1000 criterion were more likely to perform well across the majority of the bonnet surface, regardless of whether one or more locations

	HIC1000 criterion		
HIC1700 criterion	Pass	Uncertain	Fail
Pass	10.6	1.2	-
Uncertain	12.0	7.6	9.0
Fail	12.2	4.9	5.2

Table 7.6: Mean ANCAP head score (out of 24), for all vehicles. Performance against the HIC1000 criterion compared with performance against the HIC1700 criterion.

were particularly dangerous. In fact, the highest scoring vehicles under ANCAP were those estimated to pass the HIC1000 criterion, and fail the HIC1700 criterion. Under the Euro NCAP protocol, a vehicles' overall performance is dependent on most of the vehicle surface performing well, and the presence of one or two very dangerous locations will not lead to the entire vehicle failing.

In this respect, the GTR and the Euro NCAP procedures do not produce a similar evaluation of a vehicle's performance: a vehicle that fails the HIC1700 criterion of the GTR may still score relatively highly under ANCAP/Euro NCAP. The HIC1000 criterion of the GTR is more likely to reflect the ANCAP/Euro NCAP performance of a vehicle.

The results in Table 7.6 suggest that a vehicle that passes the GTR head testing requirements is likely to recieve an ANCAP head test score of around 10 to 12 points. The vehicle's overall ANCAP score would also include the upper and full leg testing results. The GTR does not include an upper leg test but does include a full leg test, with almost identical requirements to the Euro NCAP full leg test. Thus, we could assume that a vehicle that passes the GTR legform testing requirements would score the full 6 points available in the Euro NCAP full legform tests. With these 6 points, as well as 10–12 points for the head tests, the entire vehicle would recieve somewhere around 16–18 points in total. This is about the upper limit for a 'Marginal' result, and close to the minimum requirement of 18.5 points for an 'Acceptable' result under ANCAP. Thus, in terms of an ANCAP rating, a GTR compliant vehicle would be expected to recieve either an 'Acceptable' or 'Marginal' result.

7.4 Summary

Sixty vehicles that were tested by ANCAP between 2002 and 2009 were evaluated under the GTR on pedestrian safety. This evalulation was performed by taking the ANCAP test results for each test location on each vehicle and converting them to equivalent GTR test results, using the methods outlined in Chapter 6. By making certain assumptions about the ANCAP test location selection process, a best case and worst case estimate was made for each of the three test criteria of the GTR.

The criterion that was most likely to be failed was exceeding the maximum allowable HIC of 1700. The other two criteria were related to the size of the 'relaxation zone', the area in which the HIC was allowed to exceed 1000, but still had to be less than 1700. The first of these criteria was that the relaxation zone could not exceed 1/3 of the total test area, and the second of these criteria was that the relaxation zone could not exceed 1/2 of the child test area. The first of these was found to be the limiting factor: in all cases that it was passed, the second criterion was also passed, but not vice versa.

Performance under the two relaxation zone criteria was uncertain for many of the vehicles: in the best case scenario they would pass, and in the worst case scenario they would fail. Just one vehicle was estimated to fail these criteria.

When only current vehicles were considered, then around half of those tested by ANCAP were estimated to pass the GTR with little or no modification. The majority of the remaining vehicles were estimated to exceed a HIC of 1700 in at least one location, and may or may not have passed the relaxation zone (they would pass in their best case scenario, and fail in their worst case scenario).

Vehicles that performed well under the two relaxation zone criteria were more likely to have a high ANCAP head score, regardless of whether one or more tests exceeded the maximum allowable HIC of 1700. This illustrates a key difference between the two test protocols. The Euro NCAP protocol (used by ANCAP) rewards a high average performance, while the GTR protocol ensures that no locations are extremely dangerous.

7.4.1 Sources of Error

The estimates of each vehicle's performance under the GTR were based on a location-by-location conversion of HIC values obtained by ANCAP. This conversion method was based on the methods and results presented in Chapter 6. The conversion method assumed that for a given pair of test conditions there was a constant multiplier value that could be used to convert one HIC value to another. The conversion method was based on a combination of the theoretical linear spring model, the regression results obtained in Chapter 5, and a direct comparison of ANCAP and GTR test results.

On average, we could expect that this conversion method would give reasonable estimates for HIC values under the GTR. However, the results in Chapters 5 and 6 suggest that for a given test location, there may be variation from the HIC that would be obtained if the test was performed directly.

One factor that was not taken into account by the conversion method was the effect of 'bottoming out'. This was discussed in detail in Chapter 6 (Section 6.4). The presence of bottoming out may lead to an underestimate or overestimate of HIC values under the GTR, depending on the test location.

The overall GTR performance estimates for each vehicle were based on the maximum and minimum possible HICs for each zone, but this was done on the basis of some assumptions. The uncertainty in the results due to these assumptions may overwhelm any uncertainty in the HIC conversion process.

The first assumption was that the test result from a specific location applies to the entire subzone in which it appears. In reality, it is likely that the rest of the subzone would score differently. Because of this, the area estimations may be slightly overestimated.

The second assumption was that the ANCAP selected test location was in fact the worst location (or subzone) of the entire zone, and that the manufacturer test location was in fact the worst location (or subzone) of those nominated. If the worst location was not selected by ANCAP, this

will tend to underestimate potential HIC values under the GTR.

The third assumption was that the manufacturer nominated subzones would all perform better than those which were not nominated. In cases where the manufacturer location has actually turned out to be worse than the ANCAP location, it was assumed that that subzone was the worst.

These assumptions may not be valid, as the test location selection process is subjective, and is based on the test house's experience and judgement as to which test location will result in the highest HIC value. Additionally, these assumptions rely on the manufacturer having some knowledge of which subzones are likely to perform better than others. Clearly this is not always the case, as on occasion the manufacturer nominates subzones which end up performing worse than the originally nominated ANCAP subzone. However, in the majority of cases these assumptions would be expected to reflect reality.

Chapter 8

Relationship of test conditions to outcomes at real crash speeds

This chapter estimates the relative performance of different test protocols in the context of real world crash speeds. The test protocols considered were those that have relevance to Australia. Four theoretical structures are considered, which exactly meet the requirements of each of four test criteria: the Euro NCAP pass criterion, the GTR full pass criterion, the GTR relaxation area pass criterion, and the AS 4876.1 pass criterion.

A HIC of 1000 is often considered a 'safe' limit for pedestrian head testing protocols. Two of the four structures give a HIC of 1000 at their tested speed, thus the test speed could be called their maximum 'safe' speed. For the other two test criteria that specify an acceptable HIC limit greater than 1000, an equivalent 'safe speed' is calculated, at which a HIC of 1000 would be expected for the structure that just meets that criterion.

In addition to this, a real crash speed distribution was obtained from in-depth crash investigations. This is used to derive a distribution of HIC values for each of the four theoretical structures, across the distribution of real crash speeds. The resulting distributions indicate what proportion of real crash speeds would be likely to meet a given level of performance. This distribution is also used to calculate a theoretical overall injury risk for each

structure.

Current test protocols evaluate the tested structure at a single test speed. The methods used in this chapter demonstrate a different way of assessing a vehicle structure, across the range of speeds experienced in real crashes.

8.1 Equivalent 'safe speed'

In Chapter 2, Section 2.2, three pedestrian testing protocols were described that have relevance in Australia. The first of these was the Euro NCAP pedestrian testing protocol, which is used by ANCAP for the assessment of new cars for consumer information purposes. The second was the GTR testing protocol, which may be adopted in Australia as an Australian Design Rule (ADR). The third protocol was the Australian Standard AS 4876.1, which is a non-compulsory standard for bull bars.

Considering these three protocols, there are four test criteria which are used to determine whether a particular structure is acceptable:

1. The Euro NCAP pass criteria of HIC = 1000 at 40 km/h
2. The GTR full pass criteria of HIC = 1000 at 35 km/h
3. The GTR relaxation zone pass criteria of HIC = 1700 at 35 km/h
4. The AS 4876.1 pass criteria of HIC = 1500 at 30 km/h

There are two pass criteria which set an acceptable HIC limit of 1000 (1 and 2), and two pass criteria which set an acceptable HIC limit that is greater than 1000 (3 and 4).

Depending on the test protocol, and the location being tested, different headforms may be used to meet each of the test criteria listed above. The mass and diameter of these headforms will vary.

While headform mass, and possibly diameter, could be considered in the same way as speed, for the purposes of this chapter it was assumed that the headform choices were appropriate in each protocol and would be representative of a real head impact. Thus, the only consideration was the comparison between the test speed and the proposed 'safe speed'. Taking this into account, Equation 5.14 was rewritten as:

$$\mathrm{HIC}_1 = \mathrm{HIC}_2 \left(\frac{v_1}{v_2} \right)^b \tag{8.1}$$

From the linear spring model and the analysis of empirical test data in Chapter 4, a value of $b = 2.5$ was found to be an appropriate choice. The empirical data that was analysed in Chapter 5 was from headform tests performed on vehicle bonnets, it was assumed that a bull bar might also conform to a similar relationship.

Consider a structure that just passes one of the criteria given in the list above. For each criterion, at least one such structure would exist – these structures may be considered to be those that just satisfy the design requirements implied by each criterion. For example, for criterion 1, a structure will exist that scores a HIC of exactly 1000 when struck at 40 km/h with the appropriate headform: i.e. with a child headform for WAD 1000 – 1500 mm or an adult headform for WAD 1500 – 2100 mm.

Equation 8.1 was used to estimate the HIC over a range of speeds, for each of these four theoretical structures. The value of HIC_2 was the allowable HIC value given by each criterion, and v_2 was the test speed used in each protocol. The values of v_1 represented a range of impact speeds that might be encountered in an actual impact. The resulting values of HIC_1 were those that would result from impacts at different impact speeds. Figure 8.1 shows the resulting dependence of HIC on impact speed, for each of these four theoretical structures.

A HIC of 1000 is often regarded as the 'safe' limit for a head impact in pedestrian testing protocols (Euro NCAP, 2009; UNECE, 2009). In this respect, the two pass criteria with higher limits than 1000 should have a 'safe' impact speed at which a structure designed to meet that criteria will score a HIC of 1000. For the other two criteria, the 'safe speed' would be the speed of the impact test itself: i.e. 40 km/h for the Euro NCAP test, and 35 km/h for the GTR full pass criteria.

Table 8.1 lists the 'safe speeds' for each of these structures. A structure that is designed to exactly meet the GTR relaxation area requirements could be considered 'safe' for impact speeds below 28.3 km/h, assuming that 'safe' corresponds to a HIC of 1000. Similarly, a bull bar designed to exactly meet

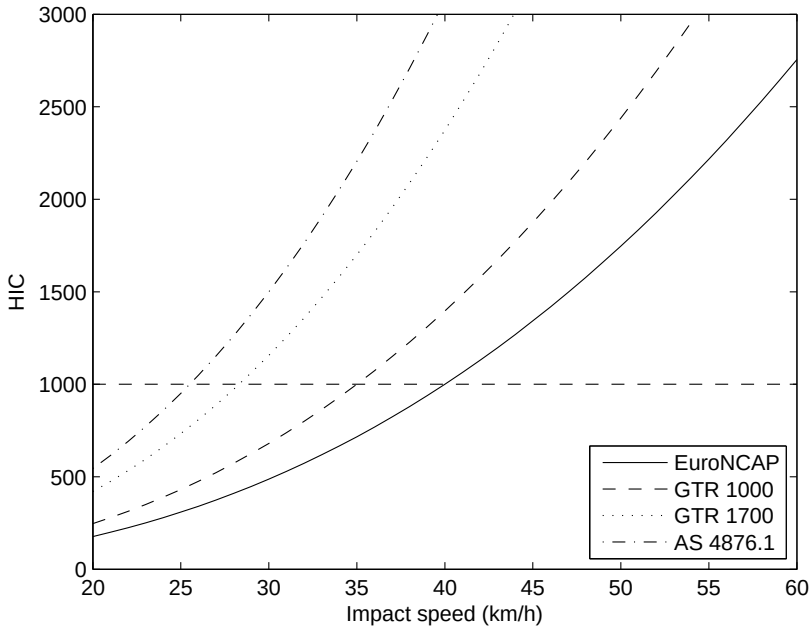

Figure 8.1: Estimated HIC for different impact speeds, for structures designed to meet four different pass criteria.

the requirements of AS 4876.1 could be considered 'safe' for impact speeds below 25.5 km/h, assuming that 'safe' corresponds to a HIC of 1000.

8.2 HIC distribution for real crash speeds

In the real world, pedestrian crashes occur at a range of vehicle impact speeds. The distribution of crash speeds tells us what proportion of crashes occur at a given speed, and the proportion of crashes that occur below or above a given speed.

	Pass criteria			
	Euro NCAP	GTR all	GTR relax.	AS 4876.1
Test speed, km/h	40	35	35	30
Required HIC	1000	1000	1700	1500
'Safe speed', km/h	40	35	28.3	25.5

Table 8.1: Maximum 'safe speed' values for structures that comply with four alternate pass criteria.

A speed distribution from real world crashes implies a limiting distribution of HIC values for any set of test specifications. For example, if a structure just meets the GTR pass criteria, the expected HIC values for any speed can be calculated using Equation 8.1. A real crash speed distribution can then be used to calculate the proportion of real crash speeds that would fall beneath certain HIC levels for that structure.

In this section, a distribution of real crash speeds was used to calculate an equivalent distribution of HIC values, for each of the four theoretical structures. An impact speed distribution was needed that was, as much as possible, representative of a wide range of injury severities. Mass crash data collected via police reports was not useful for this purpose as it would not contain reliable estimates of impact speed in pedestrian crashes, or sufficient detail of injury severity. Instead a crash speed distribution was obtained from in-depth crash investigation studies.

8.2.1 Crash speed distribution

Mizuno (2003) presented a dataset compiled by the International Harmonised Research Activities (IHRA) working group on pedestrian safety. The dataset consisted of just over 1600 pedestrian crash cases investigated in Australia, Japan, Germany, and the USA. The Australian data consisted of 64 cases investigated by the Centre for Automotive Safety Research (then known as the Road Accident Research Unit) in metropolitan Adelaide between 1999 and 2000, the Japanese data consisted of 240 cases investigated from 1987 to 1988, the German data consisted of 783 cases investigated between 1985 and 1998, and the US data consisted of 521 cases investigated between 1994 and 1999.

The IHRA dataset was used for this study; however, cases were only included where the list of pedestrian injuries included a head injury with an Abbreviated Injury Scale (AIS) score greater than one. This meant that any cases were excluded where the pedestrian received no head injury, or minor head injury only. These cases were excluded as the pedestrian testing protocols are not principally aimed at addressing minor head impacts.

After these exclusions, a sample of 498 crashes was available, 21 of which

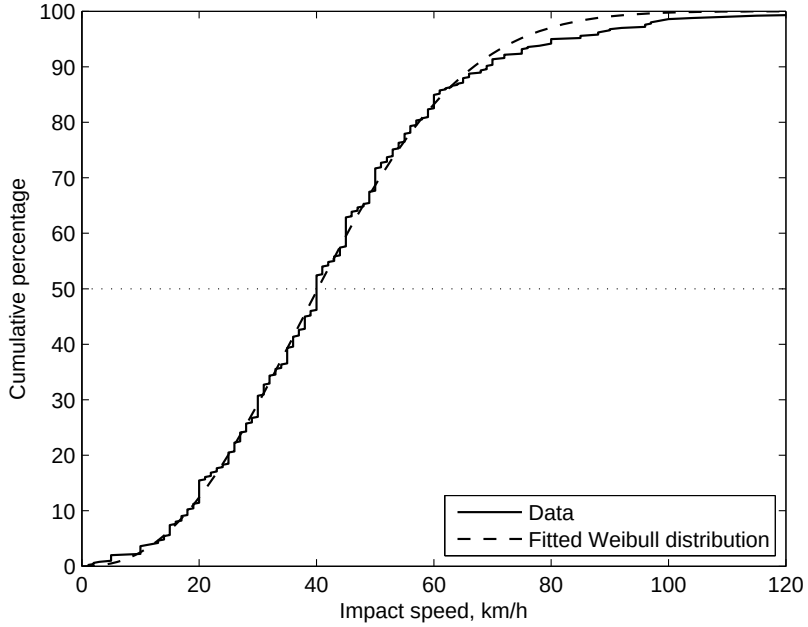

Figure 8.2: Cumulative impact speed distribution of IHRA pedestrian data (Head AIS > 1; from Mizuno (2003)) and the fitted Weibull distribution.

were from Australia.

To simplify the analysis, a Weibull statistical distribution was fitted to the crash speed data. The distribution was fitted using least-squares regression on the Weibull cumulative distribution function. The resulting Weibull scale parameter was 46.97 and the shape parameter was 2.37.

Figure 8.2 shows the cumulative distribution of crash speeds for the data and for the fitted Weibull distribution.

8.2.2 HIC distribution

The cumulative distribution shown in Figure 8.2 was used to generate equivalent cumulative HIC distributions corresponding to each of the four theoretical structures described in Section 8.1. For the purposes of this analysis, it was assumed that the head impact speed was equal to the vehicle collision speed. Previous studies have shown that the head impact speed may be above or below the crash speed (Harris, 1976; Lawrence et al., 2006), the

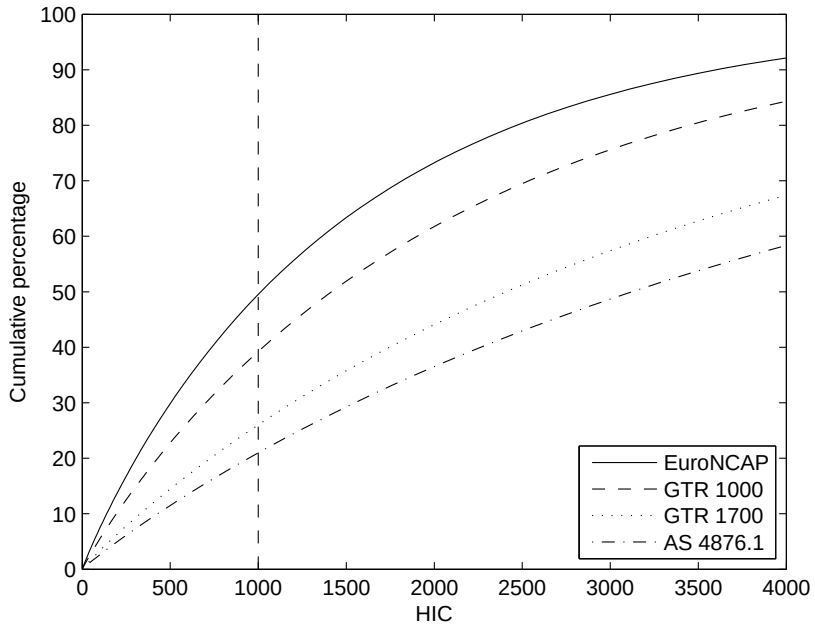

Figure 8.3: Cumulative distributions of HIC values for real crash speeds, for structures that exactly meet the requirements of four different test criteria.

assumption of equality was taken for simplicity.

Equation 8.1 was used to calculate the HIC distribution. The variable HIC_2 was set to the allowable HIC value given by each pass criteria, and v_2 was the test speed used for the corresponding test. The fitted Weibull speed distribution in Figure 8.2 described values for v_1. The resulting values of HIC_1 were used to generate a cumulative distribution of HIC values for each theoretical structure. These cumulative distributions are shown in Figure 8.3.

As shown in Figure 8.3, a structure that exactly meets the Euro NCAP requirements could be expected to give a HIC of less than 1000 for 50% of real crash speeds. A structure that meets the GTR base criteria could be expected to give a HIC of less than 1000 for 39% of real crash speeds, while a structure that meets the GTR relaxation criteria could be expected to give a HIC of less than 1000 for 26% of real crash speeds. Finally, a structure that meets the AS 4876.1 test criteria could be expected to give a HIC of

less than 1000 for 21% of real crash speeds.

For higher HIC values, the cumulative distributions for each theoretical structure are relatively closer. The Euro NCAP structure meets a HIC of 1000 for 2.4 times as many crash speeds as the AS 4876.1 structure. But if we consider a HIC of 3500, the Euro NCAP structure meets this value for 1.6 times as many crash speeds as the AS 4876.1. Thus, the differences in the performance of each structure are greater when considering lower HIC values.

8.2.3 Head injury risk distribution

An underlying assumption in all pedestrian headform testing is that higher HIC values imply a greater risk of head injury. If the relationship between HIC and head injury risk is known, then the distribution of HIC values for real crash speeds can also be related to the risk of receiving a head injury. Thus, an overall head injury risk can be calculated for each of the four theoretical structures.

Prasad and Mertz (1985) examined the relationship between HIC and head injury risk. The authors assembled results from three different studies on cadavers where the HIC could be related to some indicator of head injury. The two indicators of head injury considered were skull fracture and arterial rupture. The presence of arterial rupture was measured by pressurising the brain with an ink or dye before the test. This made it possible to detect any ruptures in a post test autopsy, which was equated with an AIS level of 4 and higher. The authors noted that the absence of arterial rupture did not imply an absence of brain injury, as there are forms of brain injury that could not be examined in the cadaver tests (e.g. damage to the veinous system and Diffuse Axonal Injury). The presence of skull fracture was determined by inspection in the post test autopsy.

Prasad and Mertz used this data to generate a curve for HIC versus skull fracture risk, and a curve for HIC versus AIS 4+ head injury risk. The curves were generated by fitting a normal cumulative distribution to the HIC and injury data from the cadaver testing. These curves were also presented in Mertz (2003) on a linearised scale. In Prasad and Mertz (1985), the authors

state that the skull fracture data were judged to be more reliable.

The purpose of this section is to demonstrate a method for relating a HIC distribution to an injury risk, and as such a relationship between HIC and injury risk is needed. The curves generated by Prasad and Mertz are the most widely referenced, but the method could be equally applied to other injury risk curves, including the MTBI curves presented by Funk et al. (2007), the injury risk curves developed by Marjoux et al. (2008) or the expanded Prasad and Mertz curves generated by NHTSA for AIS levels 1 to 6 (NHTSA, 1995). For the purposes of this section, the skull fracture risk curve presented by Prasad and Mertz (1985) alone was used, given its apparent increased reliability over Prasad and Mertz's AIS 4+ curve and its applicability to the HIC levels commonly encountered in pedestrian impact tests.

The skull fracture risk curve is shown in Figure 8.4. The curve was constructed using a cumulative normal distribution function, using the values $\mu = 1500$ and $\sigma = 488$, given by Mertz (2003). Note that the 'safe' HIC value of 1000 corresponds to a 15% risk of skull fracture. The greatest increase in skull fracture risk occurs just after this value, with a HIC of 2000 corresponding to an 85% risk of skull fracture.

The crash speeds extracted from the IHRA data set, as shown in Figure 8.2, were used to calculate equivalent HIC values for each of the four theoretical structures. The risk of skull fracture associated with each HIC value was then calculated from the relationship illustrated in Figure 8.4. The result of this calculation was a distribution of skull fracture risk values, corresponding to the real crash speed distribution. The mean of these values was equivalent to the 'total' skull fracture risk for a given structure, across the crash speed distribution. This 'total' value represented the risk of sustaining a skull fracture, if struck by a vehicle whose speed was randomnly selected from the distribution of real crash speeds.

Using this method, a total skull fracture risk value was calculated for each theoretical structure. These values are listed in Table 8.2 along with the risk relative to that of the Euro NCAP structure.

The results suggest that a pedestrian struck by a bull bar that exactly meets AS 4876.1 would be almost twice as likely to sustain a skull fracture

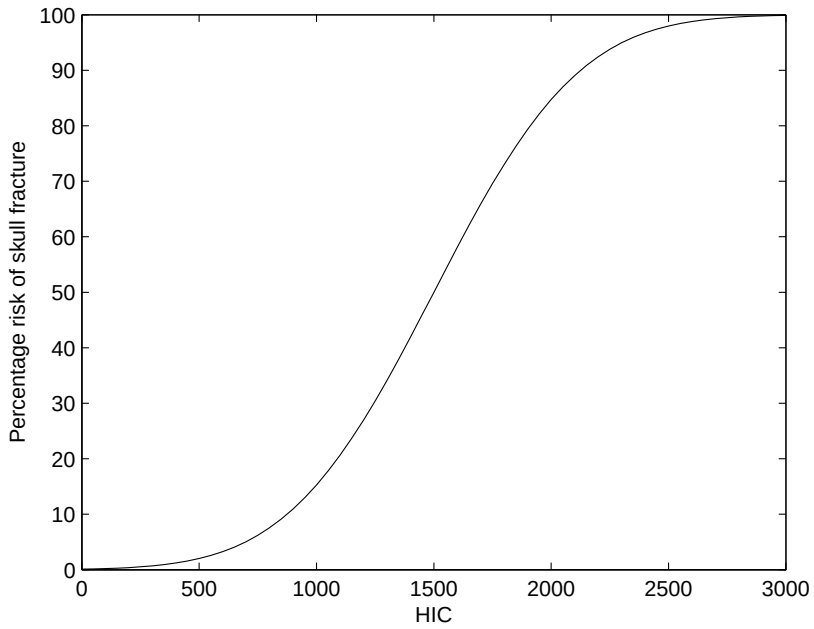

Figure 8.4: Risk of skull fracture versus HIC (derived from Mertz (2003)).

Criterion met by the structure	Total SFR	Relative SFR
Euro NCAP	38%	1.00
GTR (HIC 1000)	50%	1.30
GTR (HIC 1700)	66%	1.72
AS 4876.1	72%	1.87

Table 8.2: Total and relative skull fracture risk (SFR), for structures that exactly meet the requirements of four different test criteria.

(72%) compared with being struck by a vehicle that exactly meets the requirements of the Euro NCAP protocol (38%). The structure that exactly meets the GTR 'base' requirement of HIC=1000 would be likely to cause a skull fracture in half of all cases, while the structure in the relaxation zone would be likely to cause a skull fracture in about two thirds of cases.

The figures in Table 8.2 indicate what percentage of pedestrians in real crashes would sustain a skull fracture, assuming that: (a) the distribution of crash speeds is true, (b) the crash speed is equal to the head impact speed, (c) the test headform mass and diameter are representative of a real head, and (d) the HIC and skull fracture risk relationship is representative of the true relationship. If any of these assumptions are not true, or need to be modified, then the values in Table 8.2 would also need to be updated. The risk for each structure relative to Euro NCAP is also sensitive to these assumptions.

The method used to obtain the total skull fracture risk values is a demonstration of how the severity of different test protocols can be compared with each other in the context of real world injury risk. A relatively large amount of information regarding real crash speeds, and the risk of head injury, can be summarised by a single value. This method can also be used to quantify the effect of changes to a test protocol, in terms of the effect on overall injury risk.

8.2.4 Limitations

Assumption of equal crash and head impact speeds

The results presented above were based on the assumption that the head impact speed was equal to the crash speed. However, this assumption may introduce an error if results were sensitive to it.

When the GTR was developed, the goal was to design for a vehicle crash speed of 40 km/h, and the test speed of 35 km/h would appear to be have been chosen to represent the resulting speed of the head, according to UNECE meeting minutes (UNECE, 2003). This implies a ratio of 0.875 between the crash speed and head impact speed.

To test the sensitivity of the results, the alternate assumption under-

pinning the GTR was used and the results were recalculated. The speed distribution used above was scaled by 0.875, and the total skull fracture risk values were recalculated using the new speed distribution. The new values for each structure were lower than those presented in Table 8.2, and were as follows: (1) 27%, (2) 38%, (3) 56% and (4) 64%. The values relative to the Euro NCAP value were also affected, such that the AS 4876.1 structure had a relative skull fracture risk value of 2.32, compared with 1.87 using the original speed distribution. The relative values for the GTR structures were similarly affected.

Thus, the total and relative skull fracture risk values were sensitive to the assumption of equal crash and head impact speeds. This limitation could be addressed through further research into the true head impact speed distribution for real crashes.

Effect of 'bottoming out'

As for the previous chapter, the possibility of 'bottoming out' must also be taken into account. Bottoming out occurs when a much stiffer structure exists beneath the outer surface of the structure being tested, for example, the engine block underneath the bonnet. If the outer surface deforms sufficiently during the impact that it comes into contact with the much stiffer structure, then the acceleration on the headform rises, and higher HIC values can be expected.

In the model used to predict the change in HIC, it was assumed that the structure could deform as much as necessary without encountering any bottoming out. However, in a real vehicle structure, bottoming out can be expected to occur eventually as the impact energy increases. As the impact speed rises, so too does the amount of deformation, and eventually bottoming out will occur.

Generally speaking, if significant bottoming out does occur, the resulting HIC values are sufficiently high that the structure being tested will not pass whichever test criteria it is being tested against. Thus, for the theoretical structures used to generate Figure 8.3, it was assumed that no bottoming out would occur at the passing test criteria. However, at higher impact

speeds the possibility of bottoming out remains. Hence, the numerical HIC values above the pass level given in Figure 8.3 should be considered a lower estimate.

Crash speed data

The crash speed distribution was based on predominantly international data. It is possible that that the Australian distribution of pedestrian crash speeds may differ from this distribution. As such, the values produced by this speed distribution may not be truly indicative of real crash speeds in Australia. Note that the crash speeds in the Australian contribution to this data were not substantially different from the overall distribution of crash speeds. The method could be easily applied to a more comprehensive set of Australian crash speed data, if it were obtained in the future.

Head injury risk curve

The skull fracture risk curve (Figure 8.4) was derived from the values of μ and σ presented in Mertz (2003), which were based on the analysis of cadaver testing. Mertz notes that the curve was based on testing of adult cadavers, and is not necessarily representative of a child's injury risk. The curve itself may not reflect reality, as there may be significant differences between the tissue and bone strength of a cadaver and a live human.

The results listed in Table 8.2 can only be seen as an estimate that is representative of adult skull fracture risk at the most, and not as a general result. There are several assumptions at play, which have been discussed earlier. The main goal of these results is to demonstrate a method for comparing existing test protocols, or modifications to existing test protocols, in the context of real world crash speeds and injury.

8.3 Summary

The goal of this chapter was to examine the effect of test conditions and acceptable HIC limits in the context of real world crash speeds. Three test protocols were considered that are relevant in Australia: the Euro NCAP

pedestrian testing protocol, the GTR pedestrian testing protocol, and AS 4876.1 on Motor Vehicle Frontal Protection Systems (bull bars).

The real world safety effects were estimated for four different theoretical structures. These structures were defined to meet each of four different test criteria: (1) the Euro NCAP pass criteria, (2) the GTR pass criteria, (3) the GTR relaxation area pass criteria and (4) the AS 4876.1 pass criteria.

For criteria (3) and (4), the acceptable HIC was higher than 1000, and so an equivalent 'safe' impact speed was calculated, which would correspond to a HIC of 1000. These 'safe' speeds were 28 km/h and 26 km/h, respectively. For criteria (1) and (2), the 'safe' speed would be the actual test speeds, i.e. 40 km/h and 35 km/h, respectively.

A distribution of real pedestrian crash speeds was used to derive an equivalent distribution of HIC values for each of these four theoretical structures. For each of the four structures, it was possible to estimate the percentage of real crash speeds for which the HIC would be less than 1000. These percentages were: (1) 50%, (2) 39%, (3) 26% and (4) 21%. For these estimates, the head impact speed was assumed to be equal to the crash speed.

The HIC distribution for real crash speeds was also used to calculate an overall skull fracture risk value for each theoretical structure. This was done using the head injury risk curves published by Prasad and Mertz (1985) and Mertz (2003). The resulting overall skull fracture risk values were (1) 38%, (2) 50%, (3) 66% and (4) 72%. The values are based on many assumptions, but present a new method for summarising the relative safety of structures that meet different test protocols.

While real crash speeds were used for these estimates, care must be taken in extrapolating these results to apply to the 'real world'. If these results were to apply to real crashes, then the headform mass and impact angle must be assumed to be biofidelic.

For example, the distribution of HIC values for the structure that meets the Euro NCAP requirements would only apply to the 'real world' if in a real crash the effective head mass of the struck pedestrian was the same as the applicable Euro NCAP headform mass, and if their head was struck at the same speed and impact angle as the test. This may not always be

the case. So, while the Euro NCAP structure may score a HIC of less than 1000 for 50% of the real crash speeds considered, it may be faulty reasoning to extrapolate this result to suggest, for example, that such a structure was 'safe for 50% of struck pedestrians'. Instead, the results may be best interpreted as a comparison between the requirements of different testing protocols, in the context of real crash speeds. Additionally, the results provide a qualitative estimate of the distribution of HIC values that might be expected for each of the four theoretical structures, but for the reasons just outlined, the true quantitative distributions may vary from these. This is evident in that when the head impact speed was assumed to be less than the crash speed, the proportion of crashes deemed 'safe' differed. However, the relative performance of the test protocols was less affected by this assumption.

Putting this into a broader context, we can consider the development of the protocols as discussed in Chapter 2. For the Euro NCAP and GTR test protocols (which have evolved from the work of EEVC WG10 and ISO), the emphasis was on selecting the most biofidelic conditions to represent a pedestrian crash that occurs at 40 km/h. The head impact speed of 35 km/h in the GTR was selected as it was said to be representative of the head impact speed in a real crash that occurs at 40 km/h. The impact angles were similarly selected based on simulations of 40 km/h impacts, and the headform masses were based on what was thought to be the effective head mass of a pedestrian in these collisions. The implication of this is that both protocols are intended to represent the same thing (a pedestrian crash at 40 km/h), however when we compare their requirements we find that one is a much stricter test than the other. Thus, the decisions made on the basis of biofidelity will inherently affect the resulting real-world injury risk for a structure that meets the requirements of either of those protocols.

The end goal of any test protocol should be to encourage designs that produce the minimal level of risk to a struck pedestrian. The methodology used in this chapter provides a means for evaluating this risk across the range of impact speeds encountered in the field. As such, test conditions and HIC limits can be selected that produce a particular minimum standard of risk for a structure that meets the requirements.

Chapter 9

Discussion

This chapter presents a summary of the results presented in this thesis, followed by a discussion of some specific issues. Following this is a more general discussion, and recommendations for future work and applications in the area.

9.1 Summary

The central theme of this thesis has been the effect of test conditions on the measured severity of pedestrian headform impact tests. These tests are carried out using dummy headforms that are fired into the front surface of a test vehicle. The acceleration of the headform is measured and is used to calculate the Head Injury Criterion (HIC), an indication of the severity of the impact. The test conditions include the speed and angle of the headform upon impact, and the mass and diameter of the headform.

Figure 9.1 is a flow chart describing the procedural inputs and outcomes of a headform impact test. The dotted box at the top specifies the test conditions. These are usually specified by the protocol being used for the test. The solid box to the left represents the mechanical characteristics of the location being tested, which determine how dangerous that location is in a collision, relative to others. The dotted box at the bottom indicates the parameters that can be measured from the results of the test.

The test outputs (HIC and peak displacement) are dependent on the test

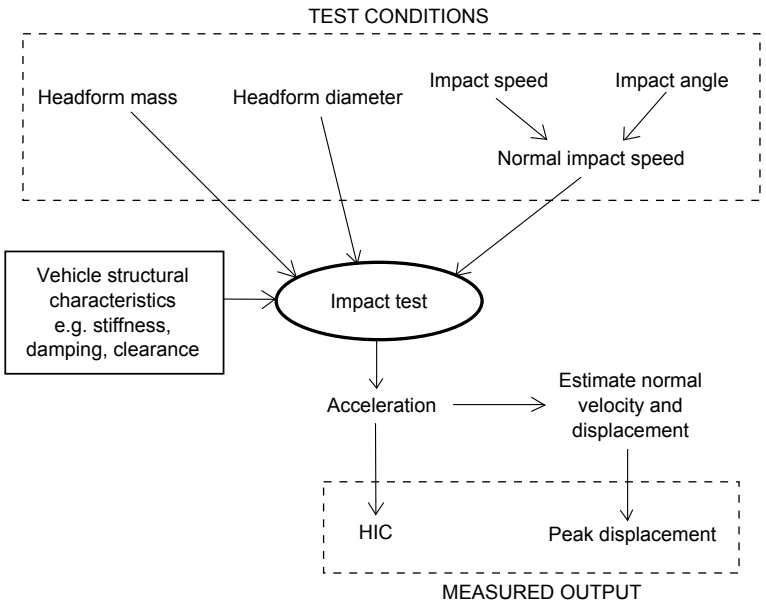

Figure 9.1: Flow chart of headform impact test.

conditions and the mechanical characteristics of the location being tested. The concepts explored in this thesis consider the test conditions only, with the mechanical characteristics being constant for a given test location. That is, a change in test output is measured or predicted for a given change in test conditions, for multiple tests performed on the same test location.

The relationship between HIC and the test conditions was first explored in Chapter 3 using a theoretical model of a mass and a linear spring, with the mass representing the headform and the spring representing the structure being tested. This model produces an acceleration pulse which is a half-sine wave. The results of Chou and Nyquist (1974), combined with the energy balance of the mass-spring system, were used to derive an expression for HIC in terms of the spring stiffness, impact speed and headform mass. When taking the ratio of the HIC values from two impact tests performed on the same structure, the stiffness value is cancelled out. To the author's knowledge, this exact derivation has not been published before, but it can also be found by simplifying others' results.

Thus, the ratio of the HIC values is dependent, via a power function, on the ratio of impact speeds and the ratio of headform masses in the two impact tests. The theoretical relationship for a linear spring is as follows:

$$\frac{\mathrm{HIC}_1}{\mathrm{HIC}_2} = \left(\frac{m_1}{m_2}\right)^{-3/4} \left(\frac{v_1}{v_2}\right)^{5/2} \tag{9.1}$$

This relationship is theoretically valid for a linear spring, when there is sufficient space for the structure of the vehicle to deform without coming into contact with a harder structure below (i.e. no bottoming out occurs).

In a real impact test, one set of test conditions may produce bottoming out, while the other does not. Thus, in order to predict whether bottoming out will occur, the theoretical model was also used to derive a relationship for predicting the change in peak displacement between two sets of test conditions. In a similar way to HIC, the ratio of two peak displacement values (S_1 and S_2) can be expressed for a linear spring as follows:

$$\frac{S_1}{S_2} = \left(\frac{m_1}{m_2}\right)^{1/2} \left(\frac{v_1}{v_2}\right) \tag{9.2}$$

Using the above equation, it is possible to estimate whether or not bottoming out will occur under a new set of test conditions, where the clearance in known.

These two theoretical relationships were examined using data obtained from back-to-back tests on various locations on several different vehicles. Multiple tests were performed on the same test locations, varying the impact speed or headform mass. Chapter 4 describes these tests and the method used for estimating peak displacement from the acceleration measurements.

Chapter 5 describes the analyses of these data. Graphical analysis and linear regression were used to examine the values of a, b, α and β in the following generalised equations:

$$\frac{\mathrm{HIC}_1}{\mathrm{HIC}_2} = \left(\frac{m_1}{m_2}\right)^{a} \left(\frac{v_1}{v_2}\right)^{b}$$

$$\frac{S_1}{S_2} = \left(\frac{m_1}{m_2}\right)^{\alpha} \left(\frac{v_1}{v_2}\right)^{\beta}$$

These power laws for HIC and peak displacement were assumed based on the theoretical linear spring model. The results of the regression for the HIC relationship were consistent with the theoretical value of $b = 2.5$, however

they suggested that the value of a was lower in magnitude than the theoretical value of -0.75. In the case of the relationship for peak displacement, the empirical data suggested values slightly lower in magnitude for α and β, but they were close to their theoretical values of 0.5 and 1, respectively.

The data analysis also showed that a change in headform diameter had an effect on both HIC and peak displacement. An increase in headform diameter caused a reduction in HIC and an increase in peak displacement. The exact effect was difficult to quantify from the empirical data available, as it was not possible to test different diameter headforms independently from headform mass.

In Chapter 6, the relationships derived in earlier chapters were used to estimate the difference in test outcomes for a location tested under the Euro NCAP and GTR test protocols. The current version the Euro NCAP test protocol is Version 5, however the Euro NCAP Version 4 test protocol was used for Chapter 6, due to the availability of a large volume of existing test results performed under that version of the protocol, and the similar Version 3.

The Euro NCAP and GTR test protocols differ in respect of impact speed, with the GTR protocol specifying a test speed of 35 km/h and the Euro NCAP test protocol specifying a test speed of 40 km/h. The protocols also differ in respect of the size and mass of the headforms used. The GTR specifies a 3.5 kg child and a 4.5 kg adult headform that are both 165 mm in diameter. The current Euro NCAP protocol specifies the same headforms as the GTR, however Version 4 of the Euro NCAP protocol specified a 2.5 kg child headform that is 130 mm in diameter and a 4.8 kg adult headform that is 165 mm in diameter. While the 2.5 and 4.8 kg headforms are now defunct, they are useful for examining the influence of headform mass and diameter.

In order to estimate the differences in HIC produced by the two test protocols, the test locations were split into different categories based on their wrap-around-distance (WAD) measurement. The WAD dividing the adult and child test areas was different for the two test protocols – the GTR uses 1700 mm as the dividing line, however the Euro NCAP Version 4 protocol uses 1500 mm. Thus, the test locations were split into three

WAD range (mm)	GTR headform	Euro NCAP headform	HIC ratio	Peak disp. ratio
1000–1500	Child	Child	0.50	1.20
1500–1700	Child	Adult	0.65	0.70
1700–2100	Adult	Adult	0.75	0.85

Table 9.1: Summary of approximate estimated ratios of HIC and peak displacement between the GTR and Euro NCAP (Versions 3–4) test protocols.

categories based on their WAD values (see Table 9.1).

For each of these categories of test location, the estimated difference in HIC between the two test protocols was calculated. There were three methods potentially available to estimate a multiplying factor to convert Euro NCAP HIC values to an equivalent GTR value. The first method was to use the theoretical power law relationship for HIC ratio (Equation 9.1). The second method was to use the power law, but to use the values for a and b that were obtained from the regression analysis of back-to-back test results. The second method also took into account the change in headform diameter in the WAD 1000–1500 mm region by using the regression coefficient for diameter change. The third method was to use a multiplying factor based on a direct comparison of results from back-to-back tests performed under the two relevant sets of test conditions.

Through a combination of these methods, it was possible to give an estimate of the difference in HIC that could be expected for test locations in each category. Similar methods were used to estimate the difference in peak displacement that could be expected, which gave an indication of how more or less likely it was that bottoming out would occur (a source of error in the estimation process). Table 9.1 summarises the expected differences in HIC and peak displacement for each location category. The values in this table have been approximated based on the different methods available for their calculation.

The values in Table 9.1 show that in the first category (WAD 1000–1500 mm), HIC values from a GTR test would be expected to be about half of what they would be under ANCAP, in the absence of any bottoming out. However, the GTR test would be slightly more likely to bottom out, with

about 20% more peak displacement expected. If the GTR test bottomed out and the ANCAP test did not, then the GTR HIC value would most likely be greater than half of the ANCAP value.

The HIC values from a GTR test would be expected to be about 35% lower for WAD 1500–1700 mm, and 25% lower for WAD 1700–2100 mm. In both of these cases the peak displacement would be expected to be lower for the GTR test, so bottoming out would be less likely to occur.

It is interesting to note that the HIC ratios in Table 9.1 increase with WAD. Since the difference in total impact speed is the same in all cases, this trend is an effect of the differences in headform mass ratio for each WAD range, as well as the change in impact angle for locations in the WAD range 1500–1700 mm. This trend is approximately reversed for the peak displacement ratios for the same reasons; the inversion is because peak displacement increases with headform mass, while HIC decreases.

This approach to converting HIC values from one test protocol to another was used in Chapter 7 to estimate the compliance of vehicles with the GTR, based on their ANCAP test results. This was performed for sixty vehicles that had been previously tested under Versions 3 and 4 of the Euro NCAP pedestrian testing protocol.

The method for estimating vehicles' GTR performance was based on some assumptions regarding the location selection. Generally, each test location was selected because it was the worst location in a given region. By assuming that this was always the case, it was possible to put an upper and lower limit on the HIC values that would be obtained for the untested regions.

Using these upper and lower HIC limits, a worst case and best case performance estimate was made for each vehicle. These performance estimates were made against the three head test criteria of the GTR: (1) that two thirds of the total test area does not exceed a HIC of 1000, (2) that half of the child test area does not exceed a HIC of 1000, and (3) that the remaining area does not exceed a HIC of 1700.

Using the vehicle performance estimates, criterion (2) was found to be irrelevant if criterion (1) was passed – in all situations that criterion (1) was satisfied, criterion (2) was also satisfied. Vehicles were most likely to

perform poorly against criterion (3), and this appeared to be the weak point for most. However, in cases where the vehicle only failed criterion (3), but passed (1) and (2), it appeared that only a small number of problematic test locations would need to be addressed in order for the whole vehicle to be made passable.

Finally, in Chapter 8, the relationship between test speeds and real crash speeds was investigated. Three test protocols were considered: the Euro NCAP pedestrian testing protocol (used by ANCAP), the GTR test protocol and AS 4876.1, the Australian Standard for bull bar safety (which also specifies a headform test speed and HIC limit). From these three test protocols, there were four test criteria for consideration. Using roman numerals to distinguish from previous criteria, these were: (i) the Euro NCAP pass criterion of HIC = 1000 at 40 km/h, (ii) the GTR pass criterion of HIC = 1000 at 35 km/h, (iii) the GTR relaxation zone pass criterion of HIC = 1700 at 35 km/h and (iv) the AS 4876.1 pass criterion of HIC = 1500 at 30 km/h.

Four theoretical structures were considered, each of which exactly met one of the criteria (i)–(iv). For example, structure (i) would give a HIC of 1000 when tested at 40 km/h. For the purposes of this theoretical analysis, it was assumed that the headform and impact angle were representative of a real impact. Test criteria (iii) and (iv) have a passing HIC value of greater than 1000, and theoretical 'safe speeds' were calculated, at which a structure that exactly meets those criteria would give a HIC of 1000, indicating an equivalent risk to criteria (i) and (ii). For criterion (iii) the 'safe speed' was 28 km/h and for criterion (iv) it was 26 km/h. For criteria (i) and (ii), the 'safe speed's were the test speeds themselves, or 40 km/h and 35 km/h, respectively.

Following this, a published crash speed distribution was used to derive the corresponding distribution of HIC values that would exist for each structure. To do this, the head impact speed was assumed to be equal to the vehicle crash speed. This process enabled the requirements of the test protocols to be compared on a common ground – that is, the proportion of real crash speeds at which the structure would meet a given level of HIC. The results demonstrated that the Euro NCAP test protocol was the most strict,

and for real crash speeds, would result in twice as many impacts that meet a HIC limit of 1000 compared to the AS 4876.1 bull bar standard.

A skull fracture risk distribution derived by Prasad and Mertz (1985) was used in conjuction with the crash speed distribution to calculate an overall, or average, skull fracture risk for each theoretical structure. The resulting risk values for each structure were were (i) 38%, (ii) 50%, (iii) 66% and (iv) 72%. These values are based on many assumptions, but demonstrate a method for summarising the performance of structures that meet the requirements of different test protocols, in a real-world context.

9.2 Discussion of specific issues

9.2.1 Choice of theoretical model

As described in the previous section, a theoretical impact model of a mass impacting a linear spring was used to derive a relationship between HIC, headform mass and impact speed. The same model was also used to derive a relationship between peak displacement, headform mass and impact speed. The linear spring model was a single-parameter model, in that the mechanical behaviour of the structure being impacted was characterised by a single value, the stiffness k.

The relationships for HIC and peak displacement were then generalised in terms of the exponents of headform mass and impact speed. A more complicated impact model, the damped Hertz model, was used to examine how those exponents might vary. The damped Hertz model was a three parameter model, including the stiffness k, displacement exponent n and damping c. Because of the multiple parameters, it was not possible to derive explicit relationships for HIC and peak displacement, in the same way that was done for the linear spring. Instead, a numerical method was used to simulate impacts and derive the exponents.

The damped Hertz model showed that the stiffness value k had no effect on the value of the exponents. With zero damping, the value of n affected all exponents. As n was increased to be greater than one: the effect of headform mass on HIC and peak displacement became weaker, the effect of

impact speed on HIC became stronger, and the effect of impact speed on peak displacement became weaker. Damping was introduced by setting c to values greater than zero. As c was increased the effect of headform mass on HIC and peak displacement was unaffected. However, an increase in c lead to an initial decrease, then increase, in the effect of impact speed on HIC, and a decrease in the effect of impact speed on peak displacement.

There are many other impact models or pulse shapes that were not considered. The linear spring model was used because an analytical solution already existed for HIC and when linked with the energy balance involving headform mass, the relationship between HIC, headform mass and impact speed could be derived. The relationship of the test conditions to peak displacement could also be easily derived for the linear spring model.

It would have been possible to consider more complicated contact models that take into account headform diameter, or the three dimensional nature of the impact. Any of these contact models would have required the use of finite-element techniques to generate results. Instead, the approach taken in this thesis was to examine empirical data in the light of results obtained using a simple theoretical model.

When compared to acceleration measurements from real tests, the linear spring model does not produce 'realistic' pulse shapes. This is particularly evident when viewing the force versus displacement plot. This difference also holds true for the damped Hertz model, although to a lesser extent. Despite these differences in pulse shape, the relationship of HIC to headform mass and impact speed is similar in real impacts to what is predicted by the linear spring model.

9.2.2 Bottoming out

The relationship suggested by the linear spring model assumes a continuous smooth relationship between HIC and impact speed and headform mass in pedestrian headform tests. In reality, many test locations will eventually 'bottom out' at a particular speed or with a greater headform mass. This occurs when the outer structure deforms sufficiently that it comes into contact with a much stiffer structure underneath, or when the stiffness otherwise

becomes highly nonlinear.

The test data used in Chapter 5 for the regression analysis did not contain any test results that bottomed out. This tells us that the results of the regression, which largely conformed to the power law predicted by the linear spring model, can only be assumed to be valid where no bottoming out occurs.

As a means of addressing this limitation, the relationship between peak displacement and the test conditions was also developed, and this can be used as a guide for determining the speed (or mass) at which bottoming out will occur. Once bottoming out does occur, the HIC would be expected to rise, however the relationship at this point may no longer conform to what is predicted by the linear spring model.

If the relationship between HIC and the test conditions were being used to extrapolate a HIC value from a test to a higher impact energy, then it would be advisable to calculate the conditions under which bottoming out would occur. This could be done by measuring the clearance available to any stiffer structures beneath the test location in question, and by measuring the peak normal displacement during the test. By rearranging Equation 9.2, it is possible calculate a critical speed and/or mass at which the peak displacement will be equal to the available clearance distance. Thus, these values allow us to predict the conditions necessary for bottoming out at a particular test location. Any such extrapolation should not be extended beyond these critical values, or it could be assumed that the HIC would rise very rapidly at that point.

9.2.3 Comparison with other published results

Earlier, Section 2.3 described several existing studies which had briefly looked at the relationship between HIC and impact speed and headform mass. The results in some of these studies do not agree with what was found in this thesis, although their investigations were not as complete.

Oh et al. (2008) used MADYMO simulations to derive a relationship in which HIC was proportional to impact velocity raised to the power of 2.28. This is close to the theoretical and empirical value of 2.5 found in this thesis.

However, the results presented by Oh et al. were based on simulations of a full-body dummy being struck by a vehicle, and as such they may have limited applicability to a pedestrian headform test. Similar MADYMO studies of fully-body dummies by Liu et al. (2002) and Svoboda et al. (2003) suggested exponents for impact speed of 1.68 and 1.39 respectively (these exponents were estimated based on the data presented in the papers, as described in Section 2.3).

Two finite element studies (Liu et al., 2010; Youn et al., 2005) presented results for HIC and impact speed but did not derive any relationship between the two. Both of these studies involved simulating pedestrian headform tests, the first on the windshield, and the second on the bonnet. In Section 2.3.1, the data from these studies were used to fit power functions. The resulting power functions suggested that HIC was proportional to impact speed raised to an exponent of around 1.7. This is less than what was suggested by the theoretical model and the empirical data presented in this thesis. In the case of Liu et al. (2010), their simulation was of windscreen impacts, and so their results might not be expected to align with results from impacts on metal structures such as the bonnet. However, the simulations performed by Youn et al. (2005) were of an impact with the bonnet and so this discrepancy is harder to explain. In the absence of additional information, it can only be assumed that the characteristics of their finite element model do not reflect the same relationship between HIC and impact speed that was found from impacts with real structures.

Mizuno and Kajzer (2000) performed a small number of headform tests at three different test speeds, striking both the windscreen and the bonnet. The resulting HIC values in this paper suggest a linear relationship (implying an exponent of one in a power function). Again, the discrepancy with the results found in this thesis cannot be easily explained in the absence of further knowledge. It is possible that the particular test location used by Mizuno and Kajzer (2000) behaved significantly different from the test locations used in this thesis.

The headform test data presented by Pereira (2010) would appear to agree with the results presented in this thesis. This study compared the HIC obtained at test speeds of 35 km/h and 40 km/h, as used in the GTR

and Euro NCAP. Using an exponent of 2.5 for the speed ratio, the ratio of HIC values from a 35 km/h test and a 40 km/h test would be 0.716. This is close to the result of 0.729 obtained from a line of best fit through the combined adult and child headform test data presented in Pereira (2010).

The HIC adjustment formula that was suggested by Kahane and Tarbet (2006) (see Equation 2.8) suggests an identical relationship to the theoretical linear spring model. That is, that HIC is proportional to impact speed raised to the power of 2.5. Unfortunately, that publication contained no details on how this formula was derived. The power of 2.5 can also be found in two other derivations for impact models that used a linear spring as a basis (Bicchi and Tonietti, 2004; Martin, 1990).

The effect of headform mass on HIC was shown in the results of finite-element analysis of headform tests presented by Youn et al. (2005). Those results suggested that the 3.5 kg headform produced HIC values that were 0.80 of those obtained using the 2.5 kg headform. Using the theoretical value of $a = -0.75$ in the power law, the predicted HIC ratio is 0.777. However, it was not clear whether the headform diameter was different for the two headform masses in the simulation, but it is likely that there was a difference. Using the values obtained from the regression analysis in Chapter 5 ($a = -0.439$, $d_{165} = -0.104$), the HIC ratio for 3.5 kg and 2.5 kg headforms is 0.679. If the effect of diameter is not included, then the HIC ratio is 0.863. Thus, the results presented by Youn et al. (2005) for headform mass suggest a relationship for headform mass to HIC that is similar to what was found in this thesis.

In general, the data presented in previous studies that compare HIC with headform mass and impact speed have been limited either in the number of results or the applicability of their model to a real headform test. Some of the previously published results and relationships agree with what has been presented in this thesis, and some of them do not. It is worth noting that none of these studies have set out to systematically investigate and quantify the relationship between test conditions and HIC, or relate the results to a theoretical model of impact. Instead, the relationship of HIC to the test conditions was incidental to the main goal of the study. The work contained in this thesis contains a more complete investigation of these relationships.

9.3 General discussion

This thesis has examined the influence of test conditions on the measured severity of pedestrian headform tests. These test conditions include the impact speed, headform mass, headform diameter and the impact angle. By altering any of these values, the severity of the impact, measured through HIC, will be likely to change. The relevance of the test conditions has been examined, mostly in the context of comparing different test protocols, particularly the Euro NCAP and GTR test protocols. This was done on the basis of comparing individual tests, the overall vehicle assessment, and the performance of compliant structures over the range of real world crash speeds.

The work presented in Chapters 6 and 7 showed that the GTR test protocol, in general, will produce lower HIC values than the Euro NCAP protocol. This difference is strongest in the child test area. Child test locations under Version 4 of the Euro NCAP protocol would score a HIC that is approximately twice the HIC they would receive in the equivalent GTR test. This might mean, for example, that a particular child test location that scored zero points in the Version 4 Euro NCAP assessment (e.g. HIC=1800) could pass the GTR requirements (HIC=900). In the adult test area these differences in HIC are less pronounced. The differences would also be less pronounced when considering the current version of the Euro NCAP protocol, in which both the adult and child headform mass and diameter are the same as those in the GTR, and the test speed is the only significant difference. For the current Euro NCAP protocol, both the child and adult test locations would be expected to score HIC values that are around 40% higher than their equivalent GTR value (computed using test speeds of 35 and 40 km/h, with an impact speed exponent of 2.5).

On a whole-vehicle basis, the differences in test outcomes between the GTR and Euro NCAP were analysed in Chapter 7. The results in that chapter suggested that the GTR requirement of no test exceeding a HIC of 1700 would be the most difficult to pass. Interestingly, vehicle compliance with this criterion did not appear to correlate to a higher Euro NCAP head score. The Euro NCAP head score appeared to be more closely related to

the vehicle's compliance with the 'HIC1000' criterion (that locations in two thirds of the test area score a HIC <1000). These findings are indicative of how the two protocols assess the overall vehicle performance. The GTR specifies an absolute limit: if a single test exceeds a HIC of 1700 then the entire vehicle is non-compliant, even if every other test results in a HIC under 1000. However, under the Euro NCAP protocol, a single bad result does not mean the vehicle will necessarily recieve a poor score, if the rest of the tests perform well. A vehicle that scores HICs in excess of 1000 for over 1/3 of the GTR test area will fail the HIC1000 criterion, and would also be likely to perform poorly under Euro NCAP, because those locations would score zero Euro NCAP points. This is more in line with what Euro NCAP aims to assess, as failing the HIC1000 criterion of the GTR hints at a more systematic design failure.

These predictions allow us to see general trends in vehicle performance, but it would be unreasonable to suggest that the HIC scaling method presented in this thesis could be used as a replacement for physical testing in these protocols. For example, the Euro NCAP results for a particular vehicle, with appropriate scaling for speed and headform mass, could not reasonably be used as evidence of GTR compliance. There is sufficient uncertainty in the experimental data in Chapter 5 that a test which might actually pass the requirements could be predicted to fail, and vice versa. The method for predicting GTR (or Euro NCAP) performance may be of more use to vehicle manufacturers, who may only wish to test at a single speed during prototype development. The method may also be of use to vehicle design legislators, when considering the implications of changing a condition in a regulatory test protocol.

The results in Chapter 8 illustrated the differences in the requirements of different test protocols. These differences may be explained by the goals, or purpose, of those test protocols. The purpose of the GTR is to set a minimum standard of performance that all vehicles must meet before they are allowed on the market. The bull bar test standard, AS 4876.1, falls into the same category as the GTR in this respect, in that its purpose is to set a minimum standard for performance (although this standard is not mandatory in Australia). The Euro NCAP protocol is different: its goal is

to assess the relative level of safety of different vehicles. It is expected that the requirements of the Euro NCAP protocol will not be met by all vehicles. If every vehicle received the maximum score in all of the Euro NCAP tests, then every vehicle would be ranked as highly as possible, and there would no way to discriminate among them. This difference in goals explains why the GTR and AS 4876.1 have weaker requirements than the Euro NCAP protocol, and thus exhibit a different HIC profile for real crash speeds. Given the more stringent requirements, it is expected that structures that meet the Euro NCAP/ANCAP requirements are 'safe' for a much larger proportion of real crashes.

While there are differences in how each test protocol assesses a particular vehicle, each of these protocols was developed in a similar way. A test speed is chosen that represents a certain proportion of crashes, taking into account the feasibility of designing a structure to perform well at that speed. Following this, the other conditions of the test (including the impact angle and headform mass) are chosen on the basis of biofidelity; the goal is to replicate the conditions of a typical real crash as best as possible. There is a potential flaw in this method, however. The danger is that vehicle manufacturers will optimise their design for this test speed, while neglecting performance at other speeds. For example, the clearance between the hood and the engine may be designed so that a headform will not bottom out during a regulation test, but at a slightly higher impact speed or headform mass, bottoming out will occur, with a much larger HIC as a result.

Another potential flaw that exists in current testing protocols is the use of set upper and lower limits for HIC. For example, under Euro NCAP, a test location that scores a HIC of 900 is ranked the same as a location that scores a HIC of 500; both receive the maximum points score available. However, at the higher impact speed of 50 km/h, the same locations would score HICs of 1570 and 870 (based on the HIC scaling relationship with an exponent of 2.5). Thus at the higher speed, one location still scores a HIC that would be considered acceptable, while the other scores a HIC that exceeds 1350 and would thus be unacceptable. Many pedestrian impacts, particularly those that are injurious, occur at 50 km/h or higher, so the equal rating of these two hypothetical test locations is questionable. The

use of set HIC limits may discourage manufacturers from further improving the performance of a test location, if it already scores under the set limit. Similarly, manufacturers may be discouraged from redesigning a location that scores a very high HIC value to achieve a lower HIC that still exceeds the set upper limit. For example, if a test location scores a HIC of 3000 in a 40 km/h Euro NCAP test, the scaling relationship implies that the HIC would be 1460 at 30 km/h. If the same location were redesigned to give a HIC of 2000 in the Euro NCAP test, then it would score a HIC of 970 at 30 km/h. Such a test location would fail the Euro NCAP requirements in both cases, but the redesigned version would be considered acceptable at 30 km/h, while the original would not. With the current upper limit of 1350 for failure, there is no incentive to redesign this location in such a way, despite the benefits that may exist at lower speeds.

An alternate approach could mean that the selection of test speed is more arbitrary: the test result can then be used to predict the performance across all speeds using the HIC scaling relationship, which would then be weighted by an appropriate crash speed distribution. Bottoming out could be taken into account by measuring clearance and using the peak displacement relationship to predict when contact with a harder structure will occur. An overall injury risk can be calculated if a relationship between HIC and injury is assumed. Such an approach can easily integrate the effect of active safety devices such as Brake Assist, which would simply modify the crash speed distribution and the HIC values would then be redistributed accordingly. This method for calculating an overall injury risk value, as demonstrated in Chapter 8, is dependent on many assumptions. These assumptions allow several pieces of data to be linked together: the HIC values at all crash speeds, the vehicle crash speed distribution and an injury risk curve. Because of the level of assumptions required, the final overall risk values might not be an accurate representation of real world performance. However, using the overall injury risk to compare test locations may prove to be a more valid basis for comparing test outcomes than what is currently used. Using such an approach would overcome the aforementioned limitations of the present methods for assessing pedestrian head protection.

9.4 Conclusions

In Section 2.4, the goals of this thesis were stated. This section concludes the discussion by revisiting these goals and how they have been addressed.

The primary goal was *"to investigate the relationship between HIC and the test conditions, that is, the impact speed, headform mass and impact angle"*. Through the theoretical models developed in Chapter 3 and the test results explored in Chapter 5, such a relationship has been examined. The theoretical model of a linear spring suggests that HIC is related to impact speed and headform mass through a power function. The impact data were consistent with such a relationship, although some results suggested that the relationship was not universal for all locations. In non-perpendicular impacts, the normal component of the impact speed was used, which meant that the impact angle also had an effect on HIC, if it differed between impacts.

In summary, for two tests on the same location, the ratio of HIC values was found to be proportional to:

- The ratio of normal impact speeds, raised to the power 2.5. This was predicted by the linear spring model, and was consistent with the average effect in the test data.

- The ratio of headform masses raised to the power of -0.75. This was predicted by the linear spring model, however the test data suggested that the exponent value may vary from this in real tests.

The second goal of this thesis was *"to predict the performance of vehicles under the GTR based on their ANCAP test result"*. This goal was addressed firstly on a location-by-location basis in Chapter 6, and then on a vehicle-by-vehicle basis in Chapter 7. The results suggested that lower HIC values could be expected under the GTR in all cases, particularly for those in the ANCAP child test area. For the overall performance of vehicles, most of those tested by ANCAP were estimated to fail the GTR requirements, primarily due to exceeding the maximum allowable HIC of 1700. In general, the results suggested that many vehicles could be redesigned to pass the GTR

by addressing a small number of test locations, that posed a particularly high level of risk to a struck pedestrian.

Finally, the third goal of this thesis was *"to use real pedestrian crash speeds to examine different selections of test speed and HIC limits used in pedestrian testing protocols"*. This was achieved in Chapter 8 using a real crash speed distribution, in conjunction with a relationship between HIC and head injury risk (the skull fracture risk curves developed by Prasad and Mertz (1985)). Three pedestrian testing protocols were compared by considering hypothetical structures that exactly met the requirements of those protocols. Using the speed distribution and injury risk function, the overall risk posed by these structures could be evaluated.

The final results showed that a structure meeting the least strict protocol (AS 4876.1) posed almost twice the risk to a struck pedestrian compared with a structure meeting the most strict protocol (Euro NCAP). The structures meeting the GTR requirements both posed additional risk compared with the Euro NCAP structure: the base GTR requirement posed about 30% more risk and the relaxation zone structure posed about 75% more risk. These results indicated that the selection of test speed and HIC requirements in a test protocol has a strong effect on the real world performance of vehicles that are designed to meet that protocol. By averaging performance over a distribution of real crash speeds, the minimum level of average risk implied by each protocol can be compared.

9.5 Future work and applications

The work in this thesis has presented a relationship and methodology for estimating changes in HIC, for a given change in test conditions. Those test conditions include impact speed, impact angle, headform mass and headform diameter. This relationship was used for two applications. The first application was to examine the difference between two test protocols, and the second was to compare multiple test protocols on the basis of real world crash speeds.

In the future, it would be useful to perform more headform testing to further test the applicability of the relationship. The empirical test data

used in this thesis was obtained exclusively from tests on the bonnets of various vehicles. Future test programs could begin with testing a very simple structure (e.g. a flat sheet of steel) and then begin to move towards more complicated structures to examine how and when the relationship can be applied. These complicated structures may involve bottoming out, or might consist of several structures that are engaged throughout the impact. By extending the relationship to more complex structures, the accuracy of the HIC estimations could potentially be improved.

As described earlier, the relationships presented in this thesis may be used as the basis for new methods of evaluating vehicle pedestrian protection. Existing test protocols evaluate a vehicle's performance at one test speed and have fixed limits that determine the acceptability of a particular test result. If the test conditions can be related to real-world conditions (through speed distributions, effective mass distributions, etc), then the performance of a vehicle can be evaluated in the context of real conditions. The advantage of such an approach would be that vehicle manufacturers would be encouraged to consider performance across the range of impact conditions experienced in real crashes, instead of focusing on one particular scenario.

A further application of the relationship between HIC and test conditions is the use of pedestrian headform testing to reconstruct real pedestrian accidents. A test may be performed on a vehicle at the location which struck the pedestrian in the accident being reconstructed. The resulting HIC value can later be adjusted for different impact speeds, angles or masses, based on simulations of the accident. Using this method, it would not be necessary to exactly match the conditions of the real accident for the headform test. Often the impact characteristics of the vehicle are used as feedback to refine multibody simulations of the accident; as the conditions in the simulation are updated, the HIC scaling relationship could be used to estimate the HIC under the new conditions.

The relationships for HIC and peak displacement that have been presented in this thesis may have a broader application than just pedestrian headform testing. It would be of interest to investigate the applicability of the results to other head impact tests. For example, testing of helmets, vehicle interior testing, or playground surface testing.

Finally, the relationships and methodologies developed in this thesis may be used when modifying or designing pedestrian headform test protocols. The selection of test conditions, coupled with a set limit of impact severity, determine the level of performance that considered acceptable in a test protocol. If vehicles are to be designed to meet a particular test protocol, then test conditions that lead to a more severe impact will generally encourage higher levels of safety performance, and test conditions that lead to less severe impacts will encourage vehicle designs that do not perform as well. The relationships developed in this thesis may be used as a guide for estimating the relative levels of severity of different test conditions in pedestrian head testing protocols.

Appendices

Appendix A

Test result listing

This appendix contains the full listing of test results included in data sets A, B, C and D.

In each table, V(total) refers to the total measured impact speed, in metres per second. For an ANCAP test this would be 11.1 ± 0.2 m/s, and for a GTR test this would be 9.7 ± 0.2 m/s. The following column, headed V(normal), contains the normal impact speed. For a perpendicular test, this would be equal to V(total), otherwise it is equal to the total impact speed multiplied by the sine of the angle between the headform trajectory and the bonnet surface.

The columns labelled M, HIC and S respectively contain the headform mass in kilograms, the HIC (with maximum 15 ms time window) and the peak displacement, in millimetres.

Table A.1 lists the tests in Set A, in which the impact speed was varied and the headform mass was constant for each location. Table A.2 lists the tests in Set B, in which the headform mass was varied, and the normal impact speed was the same for each location.

Table A.3 lists the tests in Set C, in which each location was tested as an ANCAP child test and also as a GTR child test. Table A.4 lists the tests in Set D, in which each location was tested as an ANCAP adult test and also as a GTR child test.

Vehicle	Location ID	V(total)	V(normal)	M	HIC	S
Kluger	1	9.34	9.34	3.5	1505	36.5
Kluger	1	11.1	11.1	3.5	1992	46.4
Kluger	1	12.5	12.5	3.5	2402	53.7
Kluger	2	9.46	8.13	3.5	560	55.2
Kluger	2	11.1	9.53	3.5	910	59.3
Kluger	2	12.5	10.74	3.5	1220	66.8
Kluger	2	9.42	9.42	3.5	903	56.1
Kluger	3	11.1	9.64	3.5	813	57.3
Kluger	3	9.6	9.6	3.5	657	56.8
Kluger	4	9.46	9.46	3.5	1306	51
Kluger	4	11.1	11.1	3.5	2121	54.1
Kluger	4	12.52	12.52	3.5	3060	61.5
Kluger	5	9.39	8.27	3.5	820	45.9
Kluger	5	11.1	9.77	3.5	1299	49.5
Kluger	5	12.41	10.93	3.5	1465	58.9
Kluger	5	9.78	9.78	3.5	1149	48.5
Commodore	23	9.81	8.58	3.5	470	66.7
Commodore	23	11.03	9.54	3.5	600	74
Commodore	23	11.01	9.53	3.5	639	70.4
Commodore	23	12.46	10.81	3.5	812	80.6
Commodore	23	13.88	12.06	3.5	1164	84.4
ix35	32	11	9.69	3.5	823	69.7
ix35	32	9.4	8.32	3.5	542	63.2
ix35	32	12.55	11.04	3.5	1180	76.5
ix35	32	10.65	9.39	3.5	757	67.6
ix35	33	11.1	10.65	3.5	1055	65.9
ix35	33	9.41	9.04	3.5	642	61.6
ix35	33	12.52	12.03	3.5	1305	76.3
ix35	33	11.08	10.65	3.5	958	69.4

Table A.1: Tests in Set A.

Vehicle	Location ID	V(total)	V(normal)	M	HIC	S
Kluger	1	11.1	11.1	2.5	3268	33
Kluger	1	11.1	11.1	3.5	1992	46.4
Kluger	1	10.97	10.97	4.5	1496	54.5
Kluger	2	11.1	9.53	2.5	1537	37.2
Kluger	2	11.1	9.53	3.5	910	59.3
Kluger	2	10.98	9.43	4.5	633	71.7
Kluger	3	11.1	9.64	2.5	1211	38.7
Kluger	3	11.1	9.64	3.5	813	57.3
Kluger	4	11.1	11.1	2.5	2799	41.7
Kluger	4	11.1	11.1	3.5	2121	54.1
Kluger	4	11.21	11.21	4.5	2030	61.2
Kluger	5	11.1	9.77	2.5	1762	34.8
Kluger	5	11.1	9.77	3.5	1299	49.5
Kluger	5	11.1	9.77	4.5	1110	59.6
Kluger	6	11.1	11.1	2.5	2443	38.7
Kluger	6	11.1	11.1	3.5	1972	50.3
Kluger	7	11.09	10.68	4.5	1111	68.4
Kluger	7	11.13	10.71	4.8	1067	66.4
Kluger	8	11.09	10.69	4.5	763	78.4
Kluger	8	10.9	10.51	4.8	697	76.1
Kluger	9	11.1	10.77	4.5	848	77.9
Kluger	9	11.06	10.74	4.8	834	78
Kluger	10	11.11	10.65	4.5	605	85.5
Kluger	10	11.1	10.64	4.8	558	86.4
Kluger	11	11.1	10.88	4.5	1071	78.4
Kluger	11	11.14	10.92	4.8	1079	80.1
Kluger	12	11.1	10.94	4.5	1529	63.8
Kluger	12	11.04	10.89	4.8	1166	72.7
Commodore	23	11.12	9.73	2.5	823	57.8
Commodore	23	11.03	9.54	3.5	600	74
Commodore	23	11.01	9.53	3.5	639	70.4
Commodore	23	11.07	9.57	4.5	637	77.2
Commodore	23	11.02	9.58	4.8	607	76.6
ix35	32	11	9.69	3.5	823	69.7
ix35	32	11.01	9.72	4.5	714	77.9
ix35	32	10.98	9.72	4.8	726	76.9
ix35	33	11.1	10.65	3.5	1055	65.9
ix35	33	11.02	10.54	4.5	888	76.2
ix35	33	11.17	10.73	4.8	922	81.4

Table A.2: Tests in Set B.

Vehicle	Location ID	V(total)	V(normal)	M	HIC	S
Camry	15	10.99	9.55	2.5	974	53.6
Camry	15	9.77	8.49	3.5	471	64
Camry	16	10.99	9.87	2.5	895	56.3
Camry	16	9.79	8.79	3.5	544	66.1
Camry	17	11.13	10.21	2.5	1803	46.7
Camry	17	9.73	8.93	3.5	1016	57.4
Camry	18	11.05	9.88	2.5	1507	39.9
Camry	18	9.67	8.65	3.5	676	52.5
Camry	19	11.02	9.69	2.5	1396	46.3
Camry	19	9.74	8.57	3.5	511	56.3
Commodore	21	11.05	9.54	2.5	1339	53.6
Commodore	21	9.8	8.46	3.5	481	74.9
Commodore	22	11.11	10.13	2.5	1014	55.8
Commodore	22	9.7	8.85	3.5	611	61.5
Commodore	23	11.12	9.73	2.5	823	57.8
Commodore	23	9.81	8.58	3.5	470	66.7
Mazda3	26	11.06	10.14	2.5	2394	42.1
Mazda3	26	9.65	8.85	3.5	1120	51.2
Mazda3	27	11.17	10.33	2.5	1353	43.9
Mazda3	27	9.72	8.99	3.5	723	52.8
Mazda3	28	11.06	9.47	2.5	1084	48.5
Mazda3	28	9.68	8.29	3.5	647	55.5
Mazda3	29	11.04	10.09	2.5	1181	51.4
Mazda3	29	9.8	8.96	3.5	712	58.7
Mazda3	30	11.08	10.27	2.5	1126	57
Mazda3	30	9.81	9.1	3.5	601	64.3
Mazda3	31	11.02	9.88	2.5	757	61.3
Mazda3	31	9.74	8.73	3.5	449	68.4

Table A.3: Tests in Set C.

Vehicle	Location ID	V(total)	V(normal)	M	HIC	S
Camry	14	11.02	10.56	4.8	1001	68.6
Camry	14	9.7	8.26	3.5	676	50.7
Commodore	24	11.27	10.84	4.8	781	89.9
Commodore	24	9.71	8.33	3.5	603	52.1
Mazda3	25	11.13	10.73	4.8	1729	63
Mazda3	25	9.77	8.42	3.5	947	52

Table A.4: Tests in Set D.

Appendix B

Analyses of published data

This appendix contains plots that illustrate the analysis of existing published data.

For each plot below, that data were obtained from tables published in the associated study, or were read from the published graphs. In most cases, a power function has been fitted to HIC and speed data. In the case of Pereira (2010), a linear function has been fitted to results obtained at two different test speeds.

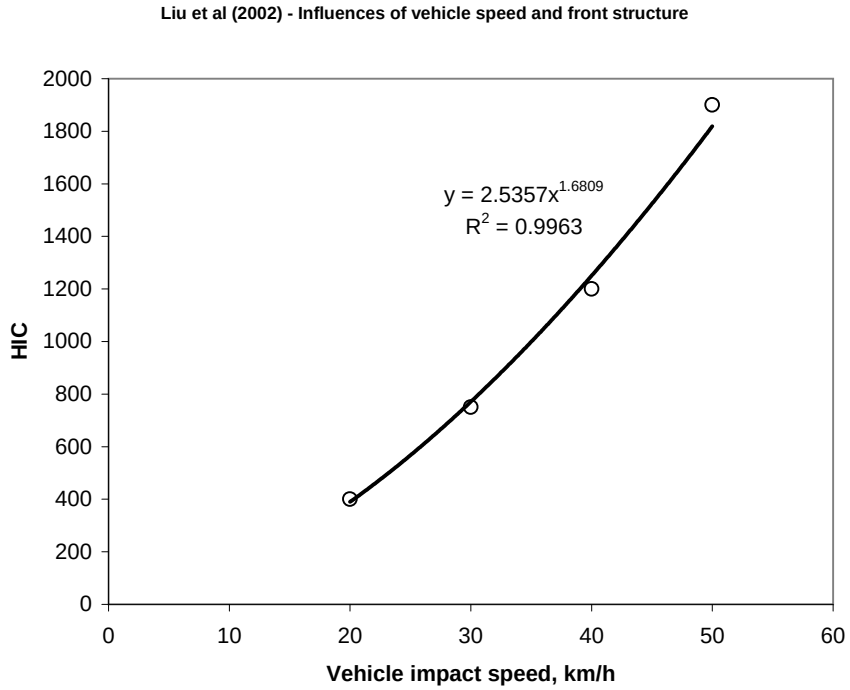

Figure B.1: Power function fitted to data published by Liu et al. (2002).

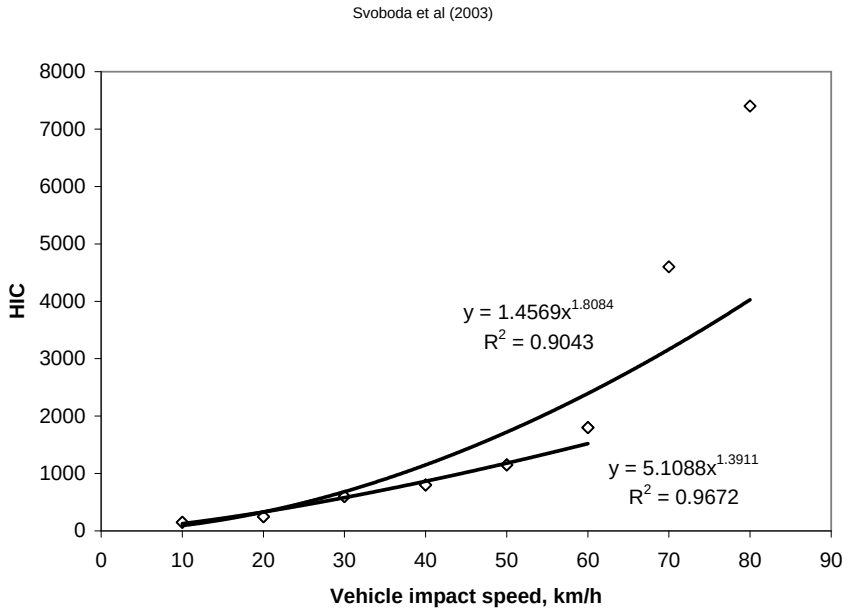

Figure B.2: Power functions fitted to data published by Svoboda et al. (2003).

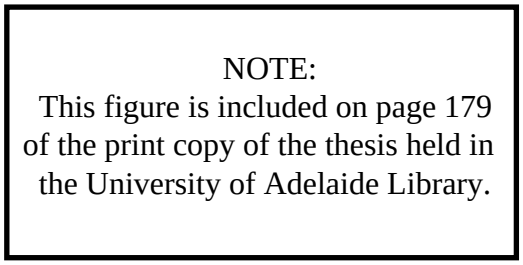

Figure B.3: Power function fitted to data published by Liu et al. (2010).

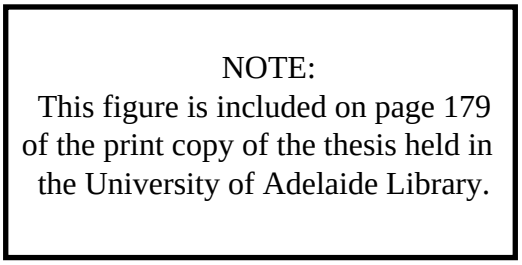

Figure B.4: Linear function fitted to data published by Pereira (2010).

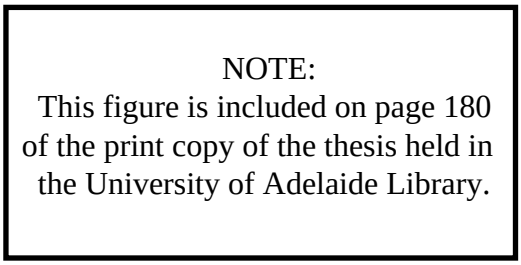

Figure B.5: Power function fitted to data published by Youn et al. (2005), using the total impact speed.

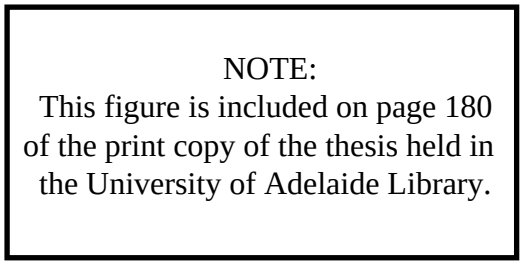

Figure B.6: Power function fitted to data published by Youn et al. (2005), using the normal impact speed.

Appendix C

Numerical simulation of impacts

This appendix describes the method for numerical simulation of impacts using the damped Hertz contact model.

The numerical simulation was performed using Huen's method for solving differential equations numerically. The impact was simulated by stepping through timesteps $i = 1, 2, \cdots, N$, with a time difference of Δt between timesteps. The initial conditions were that the displacement $x_0 = 0$, velocity $\dot{x}_0 = v_0$ and acceleration $\ddot{x}_0 = 0$.

An acceleration function was defined as follows:

$$a(x, \dot{x}) = \frac{-k}{m} x^n (1 + c\dot{x}) \tag{C.1}$$

Huen's method works by first predicting a value for the current timestep, based on the values at the previous timestep.

Firstly, displacement and velocity for the current timestep were predicted, on the assumption that the acceleration and velocity were constant from the previous timestep. Note that the * in the following formulae indicate predicted values.

$$x_i^* = x_{i-1} + \dot{x}_{i-1}\Delta t \tag{C.2}$$

$$\dot{x}_i^* = \dot{x}_{i-1} + \ddot{x}_{i-1}\Delta t \tag{C.3}$$

A predicted value for acceleration was calculated using the predicted values of displacement and velocity:

$$\ddot{x}_i^* = a(x_i^*, \dot{x}_i^*) \tag{C.4}$$

The corrected displacement and velocity for the current timestep were then calculated as follows:

$$x_i = x_{i-1} + \frac{1}{2}(\dot{x}_{i-1} + \dot{x}_i^*)\Delta t \tag{C.5}$$

$$\dot{x}_i = \dot{x}_{i-1} + \frac{1}{2}(\ddot{x}_{i-1} + \ddot{x}_i^*)\Delta t \tag{C.6}$$

Finally, the corrected acceleration was calculated using the corrected displacement and velocity:

$$\ddot{x}_i = a(x_i, \dot{x}_i) \tag{C.7}$$

Using these equations, the impact could be simulated for all timesteps where $x > 0$. When x was less than zero, the impact was considered finished – this represents the point at which the headform leaves the bonnet surface.

Bibliography

Amori, R. T., Armitage, R. R., Chou, C. C., Lim, G. C., Patel, R. N., and Shahab, S. A. (1995). Influence of system variables on interior head impact testing. SAE Technical Paper 950882, Society of Automotive Engineers, Warrendale, USA.

Anderson, R. and Doecke, S. (2011). An analysis of head impact severity in simulations of collisions between pedestrians and SUVs/work utility vehicles, and sedans. *Traffic Injury Prevention*, 12(4):388–397.

Anderson, R., Long, A., and Serre, T. (2009). Phenomenological continuous contact-impact modelling for multi-body simulations of pedestrian-vehicle contact interactions based on experimental data. *Nonlinear Dynamics*, 58(1):199–208.

Anderson, R., Streeter, L., Ponte, G., Van de Griend, M., Lindsay, T., and McLean, J. (2003). Pedestrian subsystem head impact results reflect the severity of pedestrian head injuries. *International Journal of Vehicle Design*, 32(1/2):1–15.

Bicchi, A. and Tonietti, G. (2004). Dealing with the safety-performance trade-off in robot arms design and control: fast and "soft-arm" tactics. *IEEE Robotics and Automation Magazine*, June 2004:22–33.

Chou, C. and Nyquist, G. (1974). Analytical studies of the Head Injury Criterion (HIC). SAE Technical Paper 740082, Society of Automotive Engineers, Warrendale, USA.

EEVC (1982). Pedestrian injury accidents. In *Proceedings of the 9th Interna-*

tional Technical Conference on Experimental Safety Vehicles, Washington DC, USA. National Highway Traffic Safety Administration.

EEVC (1985). Pedestrian injury protection by car design. In *Proceedings of the 10th International Technical Conference on Experimental Safety Vehicles*, Washington DC, USA. National Highway Traffic Safety Administration.

EEVC (1998). Improved test methods to evaluate pedestrian protection afforded by passenger cars. EEVC working group 17 report, European Enhanced Vehicle-safety Committee, Brussels, Belgium.

EEVC (2002). Improved test methods to evaluate pedestrian protection afforded by passenger cars (December 1998 with September 2002 updates). EEVC working group 17 report, European Enhanced Vehicle-safety Committee, Brussels, Belgium.

Euro NCAP (2008). Pedestrian testing protocol. Testing Protocol Version 4.2, European New Car Assessment Programme, Brussels, Belgium.

Euro NCAP (2009). Pedestrian testing protocol. Testing Protocol Version 5.0, European New Car Assessment Programme, Brussels, Belgium.

European Parliament (2009). Regulation (EC) No 78/2009 of the European Parliament and of the Council of 14 January 2009: On the type-approval of motor vehicles with regard to the protection of pedestrians and other vulnerable road users. *Official Journal of the European Union*, L35:1–27.

Funk, J., Duma, S., Manoogian, S., and Rowson, S. (2007). Biomechanical risk estimates for mild traumatic brain injury. In *Association for the Advancement of Automotive Medicine: 51st Annual Proceedings*, Illinois, USA. Association for the Advancement of Automotive Medicine.

Glaeser, K. (1991). Development of a head impact test procedure for pedestrian protection. In *Proceedings of the 13th International Technical Conference on Experimental Safety Vehicles*, Washington DC, USA. National Highway Traffic Safety Administration.

Harris, J. (1976). Research and development towards improved protection for pedestrians struck by cars. In *Proceedings of the 6th International Technical Conference on Experimental Safety Vehicles*, Washington DC, USA. National Highway Traffic Safety Administration.

Harris, J. (1989). A study of test methods to evaluate pedestrian protection for cars. In *Proceedings of the 12th International Technical Conference on Experimental Safety Vehicles*, Washington DC, USA. National Highway Traffic Safety Administration.

Hobbs, C. A. and McDonough, P. J. (1998). Development of the European New Car Assessment Programme (Euro NCAP). In *Proceedings of the 16th International Technical Conference on the Enhanced Safety of Vehicles*, Washington DC, USA. National Highway Traffic Safety Administration.

Hunt, K. and Crossley, F. (1975). Coefficient of restitution interpreted as damping in vibroimpact. *Journal of Applied Mechanics*, 42(E):440–445.

Janssen, E. and Nieboer, J. (1990). Protection of vulnerable road users in the event of a collision with a passenger car: Part 1 – computer simulations. Report 754050002/I, TNO Road-Vehicles Research Institute, Delft, The Netherlands.

Johnson, K. (1985). *Contact mechanics*. Cambridge University Press, Cambridge.

Kahane, C. and Tarbet, M. (2006). HIC test results before and after the 1997–2003 head impact upgrade of FMVSS 201. Technical Report DOT HS 810 739, National Highway Traffic Safety Administration, Washington DC, USA.

Kerkeling, C., Schafer, J., and Thompson, G. (2005). Structural hood and hinge concepts for pedestrian protection. In *Proceedings of the 19th International Technical Conference on the Enhanced Safety of Vehicles*, Washington DC, USA. National Highway Traffic Safety Administration.

King, C. (2011). Pedestrian safety and bull bars. Accessed online July 2011: `http://www.minister.infrastructure.gov.au/ck/releases/2011/February/CK006_2011.aspx`. Media Release, Department of Infrastructure and Transport, Canberra, Australia.

Lawrence, G. J. L. and Hardy, B. J. (1998). Pedestrian safety testing using the EEVC pedestrian impactors. In *Proceedings of the 16th International Technical Conference on the Enhanced Safety of Vehicles*, Washington DC, USA. National Highway Traffic Safety Administration.

Lawrence, G. J. L., Hardy, B. J., Carroll, J. A., Donaldson, W. M. S., Visvikis, C., and Peel, D. A. (2006). A study on the feasibility of measures relating to the protection of pedestrians and other vulnerable road users. Project Report UPR/VE/045/06, TRL Limited, Crowthorne, United Kingdom.

Lim, G., Chou, C., Patel, R., Shahab, S., and Patel, P. (1995). Estimating the minimum space to meet federal interior head impact requirements. SAE Technical Paper 950333, Society of Automotive Engineers, Warrendale, USA.

Liu, B., Zhu, M., Sun, Y., Xu, J., Ge, D., and Li, Y. (2010). Investigation on energy absorption characteristics of PVB laminated windshield subject to human head impact. *Applied Mechanics and Materials*, 34–35:956–960.

Liu, Q., Yong, X., and Zhou, Q. (2009). Friction effects in pedestrian headform impacts with engine hoods. *Tsinghua Science and Technology*, 14(5):631–638.

Liu, X. J., Yang, J., and Lövsund, P. (2002). A study of influences of vehicle speed and front structure on pedestrian impact responses using mathematical models. *Traffic Injury Prevention*, 3(1):31–42.

Marjoux, D., Baumgartner, D., Deck, C., and Willinger, R. (2008). Head injury prediction capability of the HIC, HIP, SIMon and ULP criteria. *Accident Analysis and Prevention*, 40(3):1135–1148.

Martin, R. B. (1990). Problems associated with testing the impact absorption properties of artificial playing surfaces. In Schmidt, R. C., Hoerner, E. F., Milner, E. M., and Morehouse, C. A., editors, *Natural and artificial playing fields: characteristics and safety features*, pages 77–84. American Society for Testing and Materials, Philadelphia, USA.

McLean, A. (2005). Vehicle design for pedestrian protection. CASR Report 037, Centre for Automotive Safety Research, University of Adelaide, Adelaide, Australia.

Melvin, J. and Evans, J. (1971). A strain energy approach to the mechanics of skull fracture. SAE Technical Paper 710871, Society of Automotive Engineers, Warrendale, USA.

Mertz, H. (2003). Injury risk assessments based on dummy responses. In Nahum, A. and Melvin, J., editors, *Accidental injury: biomechanics and prevention*, pages 89–102. Springer, New York, second edition.

Mizuno, K. and Kajzer, J. (2000). Head injuries in vehicle-pedestrian impact. SAE Technical Paper 2000-01-0157, Society for Automotive Engineers, Warrendale, USA.

Mizuno, Y. (2003). Summary of IHRA pedestrian safety WG activities. In *Proceedings of the 18th International Technical Conference on the Enhanced Safety of Vehicles*, Washington DC, USA. National Highway Traffic Safety Administration.

Mizuno, Y. and Ishikawa, H. (2001). Summary of IHRA pedestrian safety WG activities – proposed test methods to evaluate pedestrian protection afforded by passenger cars. In *Proceedings of the 17th International Technical Conference on the Enhanced Safety of Vehicles*, Washington DC, USA. National Highway Traffic Safety Administration.

MLIT (2004). Technical standard for protection of heads of pedestrians. Accessed online March 2011, Attachment 99: `http://www.unece.org/trans/doc/2004/wp29grsp/ps-95.pdf`.

Newman, J. (1980). Head injury criteria in automotive crash testing. SAE Technical Paper 801317, Society of Automotive Engineers, Warrendale, USA.

Newman, J., Shewchenko, N., and Welbourne, E. (2000). A proposed new biomechanical head injury assessment function – the maximum power index. SAE Technical Paper 2000-01-SC16, Society of Automotive Engineers, Warrendale, USA.

NHTSA (1995). FMVSS no. 201 upper interior head protection. Final economic assessment, National Highway Traffic Safety Administration, Washington DC, USA.

Oh, C., Kang, Y., and Kim, W. (2008). Assessing the safety benefits of an advanced vehicular technology for protecting pedestrians. *Accident Analysis and Prevention*, 40(3):935–942.

Okamoto, Y. and Kikuchi, Y. (2006). A study of pedestrian head injury evaluation method. In *Proceedings of the 2006 International IRCOBI Conference on the Biomechanics of Impact*, Zurich, Switzerland. International Research Council on the Biomechanics of Impact.

Pellman, E., Viano, D., Tucker, A., Casson, I., and Waeckerle, J. (2003). Concussion in professional football: reconstruction of game impacts and injuries. *Neurosurgery*, 53(4):799–814.

Pereira, N. (2010). ISO headform pedestrian protection test results comparison at critical bonnet regions. SAE Technical Paper 2010-36-0236, Society of Automotive Engineers, Warrendale, USA.

Ponte, G. (2004). Pedestrian protection in vehicle impacts: further results from the Australian New Car Assessment Program. In *Proceedings of the 2004 Road Safety Research, Policing and Education Conference*, Perth, Australia. Office of Road Safety.

Prasad, P. and Mertz, H. (1985). The position of the United States delegation to the ISO Working Group 6 on the use of HIC in the automotive

environment. SAE Technical Paper 851246, Society of Automotive Engineers, Warrendale, USA.

Robbins, D. (1983). Anthropometric specifications for small female and large male dummies, volume 3. NHTSA Contract DTNH22-80-C-07502, National Highway Traffic Safety Administration, Washington DC, USA.

Ryan, G. and McLean, A. (1965). Pedestrian survival. SAE Technical Paper 650968, Society of Automotive Engineers, Warrendale, USA.

Severy, D. (1963). Auto-pedestrian impact experiments. In *Proceedings of the Seventh Stapp Car Crash Conference*, Detroit, Michigan. Wayne State University Press.

Severy, D. and Brink, H. (1966). Auto-pedestrian collision experiments. SAE Technical Paper 660080, Society of Automotive Engineers, Warrendale, USA.

Simms, C. and Wood, D. (2009). *Pedestrian and cyclist impact: a biomechanical perspective*. Springer, London.

Stammen, J. A. and Saul, R. A. (2001). Pedestrian head impact testing and PCDS reconstructions. In *Proceedings of the 17th International Technical Conference on the Enhanced Safety of Vehicles*, Washington DC, USA. National Highway Traffic Safety Administration.

Standards Australia (2002). Motor vehicle frontal protection systems - part 1: Road user protection. AS 4876.1-2002, Standards Australia, Sydney, Australia.

Svoboda, J., Solc, Z., and Cizek, V. (2003). Analysis of collision between pedestrian and small car. *International Journal of Crashworthiness*, 8(3):269–276.

UNECE (1998). Agreement concerning the establishing of global technical regulations for wheeled vehicles, equipment and parts which can be fitted and/or be used on wheeled vehicles. Accessed online March 2011: `http://www.unece.org/trans/main/wp29/wp29wgs/wp29gen/wp29glob/globale.pdf`.

UNECE (2003). GRSP informal group on pedestrian safety – 6th meeting – draft detailed meeting minutes, GR/PS/64 (Sec 6.5). Accessed online March 2011: http://www.unece.org/trans/doc/2003/wp29grsp/ps-64.doc.

UNECE (2004). Proposed draft global technical regulation (GTR) on pedestrian protection, GR/PS/116. Accessed online February 2012: http://www.unece.org/fileadmin/DAM/trans/doc/2004/wp29grsp/ps-116.doc.

UNECE (2005). GRSP informal group on pedestrian safety – 8th meeting – draft detailed meeting minutes, GR/PS/144 (Sec 5). Accessed online February 2012: http://www.unece.org/fileadmin/DAM/trans/doc/2005/wp29grsp/ps-144r1e.pdf.

UNECE (2009). Draft regulation on pedestrian safety. Accessed online March 2011: http://www.unece.org/trans/doc/2009/wp29grsp/ECE-TRANS-WP29-GRSP-2009-10e.pdf.

Versace, J. (1971). A review of the severity index. SAE Technical Paper 710881, Society of Automotive Engineers, Warrendale, USA.

Youn, Y., Kim, S., Oh, C., Shin, M., and Lee, C. (2005). Research and rule-making activities on pedestrian protection in Korea. In *Proceedings of the 19th International Technical Conference on the Enhanced Safety of Vehicles*, Washington DC, USA. National Highway Traffic Safety Administration.